AD-A032 074 TELEDYNE GEOTECH ALEXANDRIA VA SEISMIC DATA ANALYSIS--ETC F/G 8/11
EXPERIMENTS IN REFINING SEISMIC MAGNITUDE ESTIMATES FOR SEISMIC--ETC(U)
NOV 75 D H VON SEGGERN, P A SOBEL, D W RIVERS F08606-76-C-0004

UNCLASSIFIED SDAC-TR-75-17 NL

1 OF 2
ADA032074

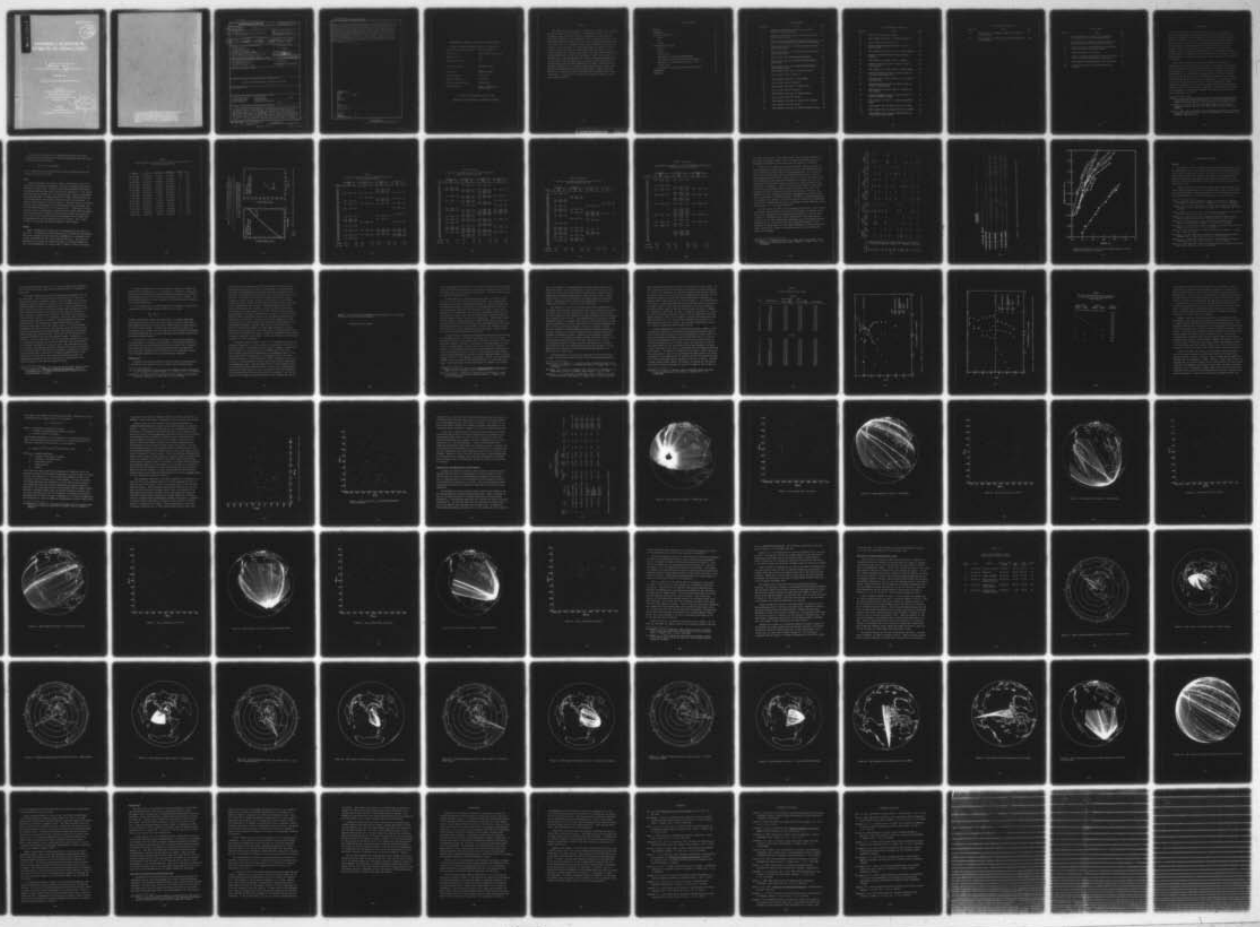

SDAC-TR-75-17

EXPERIMENTS IN REFINING M_s ESTIMATES FOR SEISMIC EVENTS

D.H. von Seggern, P.A. Sobel and D.W. Rivers
Seismic Data Analysis Center
Teledyne Geotech, 314 Montgomery Street, Alexandria, Virginia 22314

11 NOVEMBER 1975

APPROVED FOR PUBLIC RELEASE; DISTRIBUTION UNLIMITED.

Sponsored By
The Defense Advanced Research Projects Agency
Nuclear Monitoring Research Office
1400 Wilson Boulevard, Arlington, Virginia 22209
ARPA Order No. 1620

Monitored By
VELA Seismological Center
312 Montgomery Street, Alexandria, Virginia 22314

Disclaimer: Neither the Defense Advanced Research Projects Agency nor the Air Force Technical Applications Center will be responsible for information contained herein which has been supplied by other organizations or contractors, and this document is subject to later revision as may be necessary. The views and conclusions presented are those of the authors and should not be interpreted as necessarily representing the official policies, either expressed or implied, of the Defense Advanced Research Projects Agency, the Air Force Technical Applications Center, or the US Government.

Unclassified

SECURITY CLASSIFICATION OF THIS PAGE (When Data Entered)

REPORT DOCUMENTATION PAGE

READ INSTRUCTIONS BEFORE COMPLETING FORM

1. REPORT NUMBER: SDAC-TR-75-17
2. GOVT ACCESSION NO.:
3. RECIPIENT'S CATALOG NUMBER:
4. TITLE (and Subtitle): EXPERIMENTS IN REFINING M_S ESTIMATES FOR SEISMIC EVENTS.
5. TYPE OF REPORT & PERIOD COVERED: Technical Rept.
6. PERFORMING ORG. REPORT NUMBER:
7. AUTHOR(s): D. H. von Seggern, P. A. Sobel, and D. W. Rivers
8. CONTRACT OR GRANT NUMBER(s): F08606-76-C-0004
9. PERFORMING ORGANIZATION NAME AND ADDRESS:
   Teledyne Geotech
   314 Montgomery Street
   Alexandria, Virginia 22314
10. PROGRAM ELEMENT, PROJECT, TASK AREA & WORK UNIT NUMBERS: VT/4709
11. CONTROLLING OFFICE NAME AND ADDRESS:
    Defense Advanced Research Projects Agency
    Nuclear Monitoring Research Office
    1400 Wilson Blvd.-Arlington, Virginia 22209
12. REPORT DATE: 11 November 1975
13. NUMBER OF PAGES: 90 (12) 111p.
14. MONITORING AGENCY NAME & ADDRESS (if different from Controlling Office):
    VELA Seismological Center
    312 Montgomery Street
    Alexandria, Virginia 22314
15. SECURITY CLASS. (of this report): Unclassified
15a. DECLASSIFICATION/DOWNGRADING SCHEDULE:
16. DISTRIBUTION STATEMENT (of this Report)

17. DISTRIBUTION STATEMENT (of the abstract entered in Block 20, if different from Report)

APPROVED FOR PUBLIC RELEASE; DISTRIBUTION UNLIMITED.

18. SUPPLEMENTARY NOTES

19. KEY WORDS (Continue on reverse side if necessary and identify by block number)

Seismic Ray Tracing	Ray Intensity
Seismic Magnitude	Rayleigh Waves
Wave Propagation	Surface Wave Dispersion

seismic magnitude

20. ABSTRACT (Continue on reverse side if necessary and identify by block number)

Two experiments were conducted to investigate the possibility of reducing the observed scatter in M_S estimates for seismological events. The first experiment sought to remove the effect of dispersion on calculated M_S by empirically estimating a log $[(dU/dT)^{1/2}]$ term at each station for an event. Subtracting these terms from the M_S values did not produce any improvement in the scatter, and it is concluded that other terms predominate in causing the scatter. It was also noted that measured dU/dT was not stable for nearly

NEXT Page

DD FORM 1 JAN 73 1473 EDITION OF 1 NOV 65 IS OBSOLETE

Square root of (dU/dT)

Unclassified

SECURITY CLASSIFICATION OF THIS PAGE (When Data Entered)

408258

identical source-receiver paths and therefore that this quantity cannot be reliably measured in a routine visual manner. The second experiment involved tracing surface-wave rays by laws of geometrical optics over the globe as represented by a grid of phase-velocity values for 20-second Rayleigh waves. The ray-tracing indicated large zones of intense focusing and defocusing, refracted paths, and multipath propagation to stations. The square root of intensity calculated by ray tracing correlated significantly in most cases with observed amplitudes corrected for other effects. However, the full benefit of ray tracing can only be realized with an improved velocity grid, an addition of a Q grid, and corrections for transmission losses at first-order velocity contrasts.

EXPERIMENTS IN REFINING M_S ESTIMATES FOR SEISMIC EVENTS

SEISMIC DATA ANALYSIS CENTER REPORT NO.: SDAC-TR-75-17

AFTAC Project Authorization No.:	VELA T/6709/B/ETR
Project Title:	Seismic Data Analysis Center
ARPA Order No.:	2551
ARPA Program Code No.:	6F10
Name of Contractor:	TELEDYNE GEOTECH
Contract No.:	F08606-76-C-0004
Date of Contract:	01 July 1975
Amount of Contract:	$2,319,926
Contract Expiration Date:	30 June 1976
Project Manager:	Royal A. Hartenberger (703) 836-3882

P. O. Box 334, Alexandria, Virginia 22314

ABSTRACT

Two experiments were conducted to investigate the possibility of reducing the observed scatter in M_s estimates for seismological events. The first experiment sought to remove the effect of dispersion on calculated M_s by empirically estimating a log $[(dU/dT)^{1/2}]$ term at each station for an event. Subtracting these terms from the M_s values did not produce any improvement in the scatter, and it is concluded that other terms predominate in causing the scatter. It was also noted that measured dU/dT was not stable for nearly identical source-receiver paths and therefore that this quantity cannot be reliably measured in a routine visual manner. The second experiment involved tracing surface-wave rays by laws of geometrical optics over the globe as represented by a grid of phase-velocity values for 20-second Rayleigh waves. The ray-tracing indicated large zones of intense focusing and defocusing, refracted paths, and multipath propagation to stations. The square root of intensity calculated by ray tracing correlated significantly in most cases with observed amplitudes corrected for other effects. However, the full benefit of ray tracing can only be realized with an improved velocity grid, an addition of a Q grid, and corrections for transmission losses at first-order velocity contrasts.

TABLE OF CONTENTS

LIST OF FIGURES

LIST OF FIGURES (Continued)

LIST OF FIGURES (Continued)

LIST OF TABLES

INTRODUCTION

The scatter in individual magnitude estimates for seismic events is known to be considerable, standard deviations of 0.3 for m_b and M_s being typical for estimates of event magnitude from a well-distributed network of stations. Scatter of such order is tolerable when a large number of stations record an event since the error in the mean magnitude should be acceptably small; however, for smaller events which only a few stations record, this scatter can result in unacceptably biased estimates of event magnitude (Ringdal, 1975). The problem is especially acute in the context of a limited test-ban treaty for underground nuclear explosions where the yield of presumed explosions must be determined accurately for small events near the threshold of detection.

This report describes two experiments designed to investigate the possibility of reducing scatter in M_s estimates. The first is an empirical method of correcting for the variable dispersion of Rayleigh waves caused by the heterogeneity of the crust and upper mantle of the earth. It requires measurements on the actual recorded signal; results of these measurements are used to correct the M_s value. This method was suggested by von Seggern (1971), and has recently been employed by Filson (1975). We shall call this correction the "dispersion correction". The second experiment involves application of geometrical ray-tracing to predict amplitude variations among particular sites from a given event. Knowledge of these expected variations is then applied to correcting M_s estimates. We shall call this correction the "ray-tracing correction".

Ringdal, F., 1975, Maximum likelihood estimation of seismic event magnitude from network data, Technical Report No. 1, VELA Network Evaluation and Automatic Processing Research, Texas Instruments, Inc., Dallas, Texas.

von Seggern, D. H., 1971, Effects of propagation paths on surface-wave magnitude estimates, SDL Report No. 279, Teledyne Geotech, Alexandria, Virginia.

Filson, J., 1975, Test of the empirical surface wave magnitude path correction, Semiannual Technical Summary - Seismic Discrimination, Lincoln Laboratory, Lexington, Massachusetts.

DISPERSION CORRECTION

Method

The time-domain expression for a Rayleigh-wave signal is given by many authors (e.g. Sato, 1967; Bath, 1969). The form which we will use,

$$w(T,r) \propto \frac{SG\varepsilon_o A_R U}{r^{1/2} C^{1/2} \sin^{1/2}(r/R_o) \exp(\pi r/QUT) T^{3/2} \left|dU/dT\right|^{1/2}}, \qquad (1a)$$

is the envelope of the expression given in von Seggern (1971). Taking logarithms, we have

$$\log[w(T,r)] = \log(SG\varepsilon_o A_R U/C^{1/2}T^{3/2}) - \frac{1}{2}\log r - \frac{1}{2}\log[\sin(r/R_o)] - \frac{1}{2}\log(dU/dT) + \text{constant}. \qquad (1b)$$

The notation is as follows:

- w - vertical displacement
- T - period
- r - epicentral distance (km)
- R_o - earth's radius
- ε_o - ellipticity
- A_R - Harkrider's amplitude factor
- U - group velocity
- C - phase velocity
- Q - quality factor
- S - source amplitude
- G - instrument amplitude response.

The above form does not apply to that part of the signal associated with a minimum or maximum on the group-velocity curve; ordinarily this part of the

---

Sato, R., 1967, Attenuation of seismic waves, J. Physics, Earth, v. 15, p. 32-61.

Bath, M., 1969, Mathematical Aspects of Seismology, Elsevier Publ. Co., New York.

signal is of short duration. In this report we deal only with measurements on signals where (1a) is applicable. All of the above terms that appear in the right-hand side of equation (1a) are dependent on period T. Further, the terms ε_o, A_R, U, C, dU/dT and Q are dependent on structure. Gutenberg (1945) showed that equation (1b) could well be approximated by a straight line when 20-second LR measurements were considered; his empirical relation for Rayleigh-wave magnitude (as modified for use by the ISC) is given by

$$M_s = \log A/T + 1.66 \log \Delta, \qquad (2)$$

where A is peak-to-trough amplitude in nanometers and Δ is epicentral distance in degrees. Small deviations in period from 20 seconds are allowable, the range being 17-23 seconds for M_s measurements in this report. Magnitudes calculated using equation (2) then do not account for variations in the factors ε_o, A_R, U, C, dU/dT, and Q. Variable attenuation of signals due to intrinsic or apparent Q variations in the crust and upper mantle are not within the scope of this report; we merely assume that a uniform Q applies to all recorded Rayleigh-wave signals. For the remaining structure-dependent factors ε_o, A_R, U, C, and dU/dT, we will concentrate on dU/dT and U since these are directly measurable on seismograms while ε_o, A_R, and C are not. The factors ε_o, A_R, and C can be calculated if the structure at the station is known; however, we do not have sufficient knowledge of the structure at the different stations used in this experiment to justify making corrections to M_s based on these factors. The range of ε_o would be only roughly 20% of its average value for 20-second Rayleigh waves, that of A_R roughly 50%, and that of C roughly 15%. Variations in $(dU/dT)^{1/2}$ are much larger as we shall show. Thus the factor $[dU/dT]^{1/2}$ should cause the major portion of amplitude scatter due to non-dissipative structural effects on Rayleigh-wave propagation. Failure to significantly improve M_s estimates by applying this one correction would indicate that more sophisticated corrections including the other structure-dependent factors would be unwarranted.

Gutenberg, B., 1945, Amplitudes of surface waves and magnitudes of shallow earthquakes, Bull. Seism. Soc. Am., v. 35, p. 3-12.

The correction procedure is to measure the group velocity curves, determine dU/dT at the period of the maximum Rayleigh-wave amplitude used to calculate M_s, and then calculate

$$M_s' = M_s + 1/2 \cdot \log(dU/dT) \qquad (3)$$

so as to cancel this one term from equation (1b) and hopefully reduce the scatter in M_s values for events.

Data

Twenty large events, as listed in Table I, were used for this study. Film chips for twenty-five high-quality stations of the WWSSN network were obtained for these events. Initially, amplitude measurements were made on all detected Rayleigh waves and M_s calculated by equation (2). (The overall detection rate was roughly 60%.) The group-velocity curves were determined by the standard means of measuring peak arrival times, differentiating this curve to get periods, and plotting calculated velocity versus period. An example of the procedure is shown in Figure 1. The exact point on the group-velocity curve corresponding to the cycle measured for M_s was marked, and the slope dU/dT calculated for use in equation (3). In plotting the group-velocity curves, we found reason to delete from our analysis those M_s measurements which fell near a minimum in the curve (Airy phase), were associated with a part of the curve which was poorly determined, or were taken from seismograms with only a few detected cycles of LR motion. Only a small fraction of the M_s data was rejected though for these reasons.

Results

Table II summarizes the results of the experiment with the dispersion correction. For each event we have listed M_s, M_s', and dU/dT for all stations which both recorded the event and had M_s measurements on a reasonably well-defined, non-minimum portion of the group-velocity curve. The aim of the experiment was to reduce the standard deviation of individual magnitudes about the mean magnitude for a given event, so Table II lists at the bottom

TABLE I

Focal Parameters for Events used in Dispersion Correction Study
(From USGS Epicenter File)

Date	Time	Latitude	Longitude	Depth	m_b
16 Aug 1966	18:02:36.6	37.400°N	114.200°W	33km	5.60
20 Dec 1966	15:29:38.6	37.300°N	116.400°W	0	6.30
19 Jan 1968	18:15:00.1	38.630°N	116.630°W	0	6.51
26 Apr 1968	15:00:00.0	37.300°N	116.500°W	0	6.30
19 Dec 1968	16:30:00.0	37.232°N	116.477°W	0	6.30
23 Jun 1969	10:45:24.3	51.483°N	179.948°W	36	6.10
4 Aug 1969	10:23:28.9	51.400°N	179.556°W	41	5.30
16 Sep 1969	14:30:00.0	37.314°N	116.460°W	0	6.20
2 Oct 1969	22:06:00.0	51.417°N	179.182°E	1	6.50
26 Mar 1970	19:00:00.2	37.300°N	116.534°W	0	6.50
14 Oct 1970	05:59:37.1	73.315°N	55.146°E	0	6.70
12 Dec 1970	07:00:57.3	43.851°N	54.774°E	0	6.10
27 Sep 1971	05:59:55.2	73.387°N	55.100°E	0	6.40
6 Nov 1971	22:00:00.1	51.472°N	179.107°E	2	6.80
28 Aug 1972	03:59:56.5	73.336°N	55.083°E	0	6.30

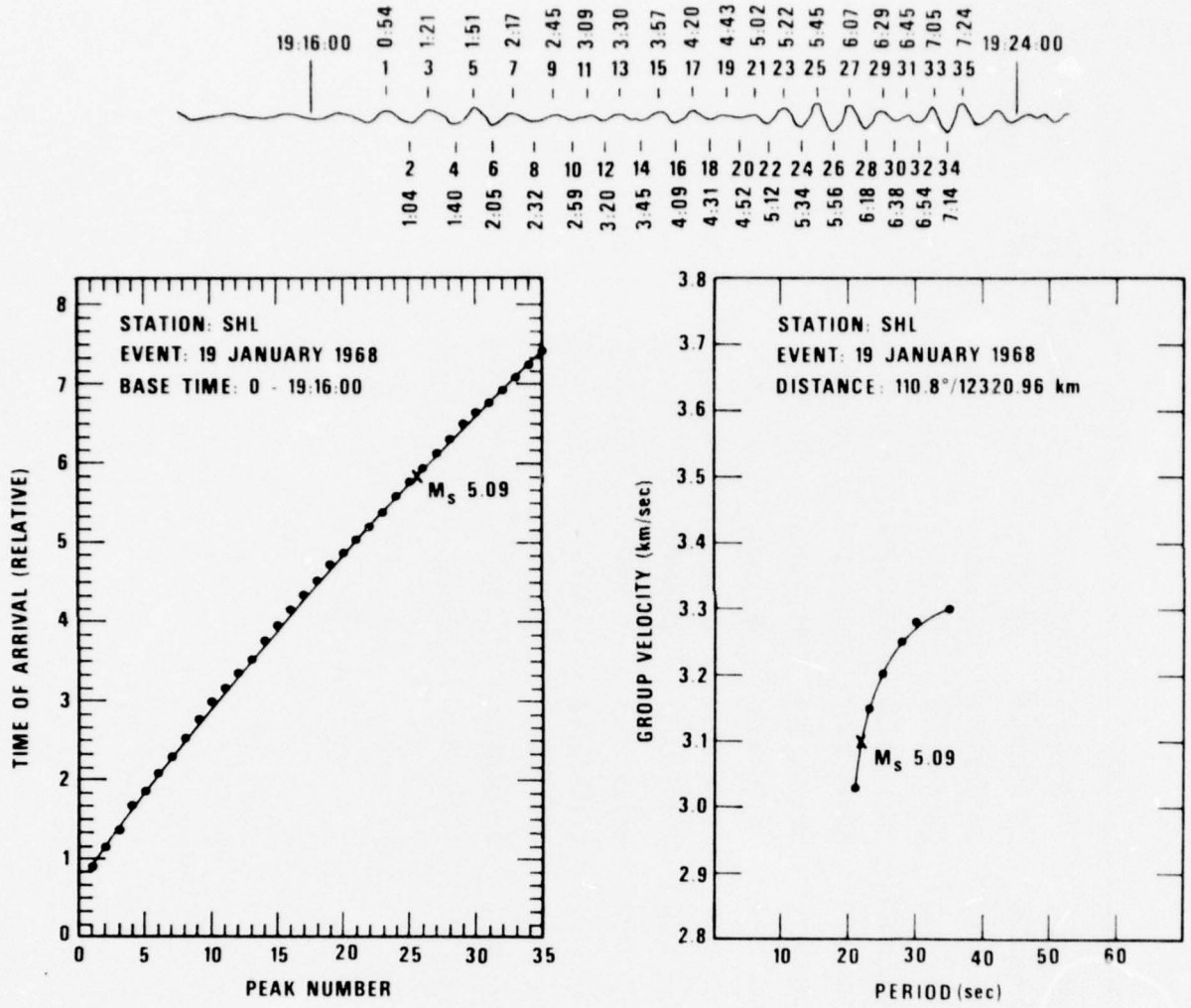

Figure 1. Example of measurements and reduction to obtain dispersion correction for M_S.

TABLE II

M_s Estimates for a Network of Stations Observing Fifteen Events
Using the Dispersion Correction

Station	16 Aug 66			20 Dec 66			19 Jan 68			26 Apr 68		
	M_s	$\frac{dU}{dT}$	M_s'	M_s	$\frac{dU}{dT}$	M_s'	M_s	$\frac{dU}{dT}$	M_s'	M_s	$\frac{dU}{dT}$	M_s'
ALQ												
ANT							4.79	.0461	4.12			
ARE							4.93	.0277	4.15			
BAG	5.60	.0129	4.66	5.21	.0461	4.34	5.02	.0658	4.43	5.33	.0308	4.57
BKS												
BLA												
BUL				5.20	.0258	4.41						
CHG							4.73	.0483	4.07	5.14	.0213	4.31
COL	5.55	.0310	4.80				5.14	.0972	4.63			
COR												
CTA	5.33	.0753	4.77	5.39	.0820	4.84	5.19	.0990	4.69	5.63	.0800	5.08
DUG												
EIL												
ESK	5.62	.0299	4.86							5.62	.0318	4.87
FLO												
HLW												
KBL												
KIP										5.33	.0909	4.81
KON	5.33	.0210	4.49				5.22	.0479	4.56			
LHC												
LPB	5.21	.0364	4.49				5.13	.0365	4.41			
LPS	5.19	.0284	4.42									
MAT				5.24	.0685	4.66				5.36	.1517	4.95
MBC												
MUN	5.67	.0151	4.76									
OGD												
OXF												
QUI	5.28	.0280	4.50	5.20	.0518	4.56	5.13	.0312	4.38	5.23	.0265	4.44
RIV							4.92	.0618	4.31	5.28	.1219	4.82
SHI												
SHL	5.27	.0247	4.47	5.27	.0592	4.66	5.09	.0508	4.44	5.30	.0406	4.60
SPA										5.24	.0400	4.54
TOL	5.23	.0343	4.30									
UMN												
Average	5.39		4.61	5.25		4.61	5.03		4.38	5.35		4.70
Std. Dev.	.18		.16	.07		.15	.16		.20	.16		.24

TABLE II (Continued)

M_s Estimates for a Network of Stations Observing Fifteen Events
Using the Dispersion Correction

Station	19 Dec 68			22 Jun 69			04 Aug 69			16 Sep 69		
	M_s	$\frac{dU}{dT}$	M_s'	M_s	$\frac{dU}{dT}$	M_s'	M_s	$\frac{dU}{dT}$	M_s'	M_s	$\frac{dU}{dT}$	M_s'
ALQ				5.11	.0658	4.52	4.97	.0486	4.31			
ANT												
ARE	4.96	.0459	4.29									
BAG	5.50	.0516	4.36	4.31	.0676	4.22	4.78	.1190	4.32	4.98	.0474	4.32
BKS				5.17	.0550	4.54	5.03	.0706	4.45			
BLA							5.28	.0527	4.64			
BUL												
CHG	5.35	.0490	4.69	5.00	.0893	4.48	4.70	.0474	4.04	4.98	.0352	4.25
COL				5.12	.1000	4.62	4.99	.0283	4.22			
COR												
CTA	5.71	.1190	5.25	5.26	.0700	4.68				5.24	.0322	4.50
DUG				5.13	.0603	4.52	4.82	.0508	4.17			
EIL							5.29	.0254	4.49			
ESK				5.15	.0451	4.48				5.48	.0130	4.34
FLO												
HLW	5.08	.0344	4.35									
KBL	5.44	.0472	4.78	5.43	.0710	4.36	5.25	.0403	4.36	5.07	.0556	4.44
KIP				5.27	.1041	4.78	5.03	.1010	4.53	5.11	.0667	4.52
KON							4.90	.1695	4.60	5.21	.0249	4.41
LHC				4.99	.0407	4.29	4.98	.2175	4.65			
LPB	5.33	.0463	4.66	5.22	.0599	4.61						
LPS												
MAT	5.48	.0788	4.93	4.89	.0654	4.30	5.03	.0622	4.43	5.11	.1040	4.62
MBC				4.85	.1124	4.38	4.63	.1177	4.17			
MUN	5.52	.0764	4.96									
OGD							5.24	.0572	4.62			
OXF				5.06	.0610	4.45	4.89	.1177	4.43			
QUI	5.45	.0219	4.62							4.93	.0310	4.13
RIV	5.28	.0364	4.56	5.15	.0248	4.35						
SHI				5.62	.0625	5.02	5.41	.0663	4.82			
SHL	5.44	.0194	4.58	5.09	.0389	4.38	5.05	.0770	5.49	5.08	.0511	4.43
SPA												
TOL				5.23	.0731	4.66	4.84	.0681	4.26			
UMN				5.23	.0437	4.55						
Average	5.38		4.71	5.14		4.53	5.01		4.43	5.12		4.42
Std. Dev.	.20		.27	.19		.20	.21		.20	.16		.14

TABLE II (Continued)

M_s Estimates for a Network of Stations Observing Fifteen Events
Using the Dispersion Correction

Station	02 Oct 69			26 Mar 70			14 Oct 70			12 Dec 70		
	M_s	$\frac{dU}{dT}$	M_s'	M_s	$\frac{dU}{dT}$	M_s'	M_s	$\frac{dU}{dT}$	M_s'	M_s	$\frac{dU}{dT}$	M_s'
ALQ	4.65	.0420	3.76									
ANT												
ARE				4.98	.0403	4.28						
BAG				3.09	.0322	4.34						
BKS	4.31	.0559	3.88									
BLA	5.03	.0549	4.40									
BUL										4.88	.0476	4.22
CHG										3.41	.0149	2.50
COL	4.74	.0715	4.17				4.69	.0264	3.90			
COR												
CTA	4.95	.0578	4.33	5.41	.0379	4.70						
DUG	4.79	.0629	4.19									
EIL				4.71	.0169	3.82	4.99	.0117	4.02			
ESK							4.47	.0994	3.96	4.36	.0441	3.88
FLO	4.70	.0290	3.93				5.00	.0131	4.06			
HLW												
KBL				5.35	.0695	4.77						
KIP							4.68	.0575	4.06			
KON												
LHC	4.82	.0559	4.19									
LPB												
LPS												
MAT	4.76	.0429	4.08	5.25	.0451	4.58						
MBC	4.61	.0544	3.98				4.37	.0255	3.77			
MUN				5.14	.0300	4.38						
OGD	5.25	.0328	4.51				4.61	.0402	3.91			
OXF	4.94	.0203	4.09				4.79	.0650	4.20			
QUI				5.28	.0218	4.45						
RIV	4.83	.0663	4.24									
SHI				5.24	.0318	4.49						
SHL	4.51	.0233	3.69	5.24	.0645	4.64						
SPA												
TOL												
UMN												
Average	4.79		4.12	5.17		4.45	4.73		3.99	4.28		3.53
Std. Dev.	.20		.22	.20		.27	.19		.13	.77		.91

TABLE II (Continued)

M_s Estimates for a Network of Stations Observing Fifteen Events Using the Dispersion Correction

Station	27 Sep 71			06 Nov 71			28 Aug 72		
	M_s	$\frac{dU}{dT}$	M_s'	M_s	$\frac{dU}{dT}$	M_s'	M_s	$\frac{dU}{dT}$	M_s'
ALQ	5.29	.0103	4.30	5.54	.0515	4.90			
ANT									
ARE									
BAG	5.41	.0136	4.48						
BKS				5.43	.0553	4.80			
BLA	5.16	.0125	4.21	5.71	.0550	5.08	5.24	.0243	4.43
BUL									
CHG				5.01	.0503	4.36			
COL	4.82	.0633	4.22	5.70	.1000	5.20	4.34	.0521	3.90
COR									
CTA				5.40	.1052	4.91			
DUG				5.59	.0963	5.08			
EIL									
ESK	4.72	.0720	4.15	5.43	.0472	4.77	4.33	.0606	3.72
FLO									
HLW									
KBL				5.51	.0313	4.87			
KIP				5.24	.1333	4.80			
KON				5.14	.0770	4.58			
LHC	5.01	.0144	4.09	3.93	.1076	5.45	4.75	.0788	4.20
LPB				5.35	.0758	4.79			
LPS									
MAT				5.55	.0667	4.96			
MBC	4.55	.0212	3.71				4.24	.0474	3.58
MUN				5.41	.0527	4.77			
OGD	4.97	.0618	4.37	5.92	.0700	5.34			
OXF									
QUI									
RIV				5.27	.0532	4.63			
SHI				5.65	.0633	5.05			
SHL				5.17	.0320	4.42			
SPA									
TOL									
UMN									
Average	4.99		4.19	5.47		4.88	4.62		3.97
Std. Dev.	.29		.23	.25		.28	.40		.35

this value for M_s and M_s'. These values reveal that no overall improvement in M_s scatter was achieved though; in fact, no single event showed any truly significant improvement, and for many events the scatter was increased.

The fact that the dispersion correction failed to reduce the magnitude scatter implies that either the correction is being poorly determined or that it is overwhelmed by other effects on recorded amplitudes. We can check the accuracy of the dU/dT measurements by comparing dU/dT measured at a given station among events which have a common location. Seven of our twenty events were underground nuclear explosions detonated at the Nevada Test Site; thus signals from these should be highly correlated at a single station and serve our purpose of comparison. Table III lists the dU/dT values for these seven shots at the various WWSSN stations used in this study. With only a few exceptions the dU/dT values are not stable from one shot to the next. We emphasize that each seismogram was analyzed independently, and so each dU/dT value was obtained in an unbiased manner. The amount of variation among shots at a single station amounts to 0.2 M_s units for the correction $1/2 \cdot \log(dU/dT)$; clearly this is unacceptable when one is attempting to reduce magnitude scatter having roughly a 0.3 M_s standard deviation.

The main reason for widely varying estimates of dU/dT with a given station and several close epicenters is noise on the recordings. The signals at SHL for the seven explosions and the associated group-velocity curves are shown in Figure 2. Undoubtedly more careful construction of the group-velocity curves or use of a more sophisticated technique such as moving-window analysis (Landisman et al., 1969) would insure more repeatability among the dU/dT estimates for common paths; but such larger investments in time are unwarranted since a ready means to remove the dispersion effect lies in computing the spectra of the signal.

Landisman, M., A. Dziewonski, and Y. Sato, 1969, Recent improvements in the analysis of surface wave observations, Geophys. J. R. Astr. Soc., v. 17, p. 369-403.

TABLE III

Values of dU/dT at Maximum Motion for Seven Nevada Events as Recorded at a Common Network

Stations	Δ°	EARTHQUAKE 16 Aug 66		GREELEY 20 Dec 66		FAULTLESS 19 Jan 68		BOXCAR 26 Apr 68		BENHAM 19 Dec 68		JORUM 16 Sep 69		HANDLEY 26 Mar 70	
		$\frac{dU}{dT}$	$\log \frac{dU}{dT}$	$\frac{dU}{dT}$	$\log \frac{dU}{dT}$	$\frac{dU}{dT}$	$\log \frac{dU}{dT}$	$\frac{dU}{dT}$	$\log \frac{dU}{dT}$	$\frac{dU}{dT}$	$\log \frac{dU}{dT}$	$\frac{dU}{dT}$	$\log \frac{dU}{dT}$	$\frac{dU}{dT}$	$\log \frac{dU}{dT}$
ANT	75.4					.0461	- .67								
	68.2-														
ARE	68.9					.0277	- .78			.0459	- .67			.0403	- .70
	103.7-														
BAG	105.5	.0129	- .94	.0461	- .67	.0658	- .59	.0308	- .76	.0516	- .64	.0474	- .66	.0322	- .65
BUL	145.0			.0258	- .79										
	114.0-														
CHG	114.9					.0483	- .66	.0215	- .83	.0490	- .66	.0352	- .73		
	32.3-														
COL	33.8	.0310	- .75			.0972	- .51								
COR	omit														
	107.7-														
CTA	109.4	.0753	- .36	.0820	- .35	.0990	- .50	.0800	- .55	.1190	- .46	.0327	- .74	.0379	- .71
EIL	108.0													.0169	- .89
	70.3-														
ESK	71.4	.0299	- .76					.0318	- .75			.0130	- .94		
HLW	106.5									.0344	- .73				
	108.0-														
KBL	108.1									.0472	- .66	.0556	- .63	.0695	- .58
KIP	39.2							.0909	- .32			.0667	- .39		
	72.3-														
KON	73.4	.0210	- .84			.0479	- .66					.0249	- .80		
	69.2-														
LPB	71.0	.0364	- .71			.0365	- .72			.0463	- .67				
LPS	32.1	.0284	- .77												
MAT	79.1			.0685	- .58			.1517	- .41	.0788	- .55	.1040	- .49	.0451	- .67
	137.0														
MUN	138.7	.0151	- .91							.0764	- .56			.0300	- .76
OGD	omit														
	50.0-														
QUI	51.8	.0280	- .78	.0518	- .64	.0312	- .75	.0265	- .79	.0219	- .83	.0310	- .75	.0218	- .83
	111.4-														
RIV	112.1					.0618	- .61	.1219	- .46	.0364	- .72				
SHI	112.4													.0318	- .75
	110.8-														
SHL	112.4	.0247	- .80	.0592	- .61	.0305	- .65	.0406	- .70	.0194	- .86	.0511	- .65	.0645	- .60
SPA	127.2							.0400	- .70					.0111	
TOL	79.7	.0343	- .73												- .98

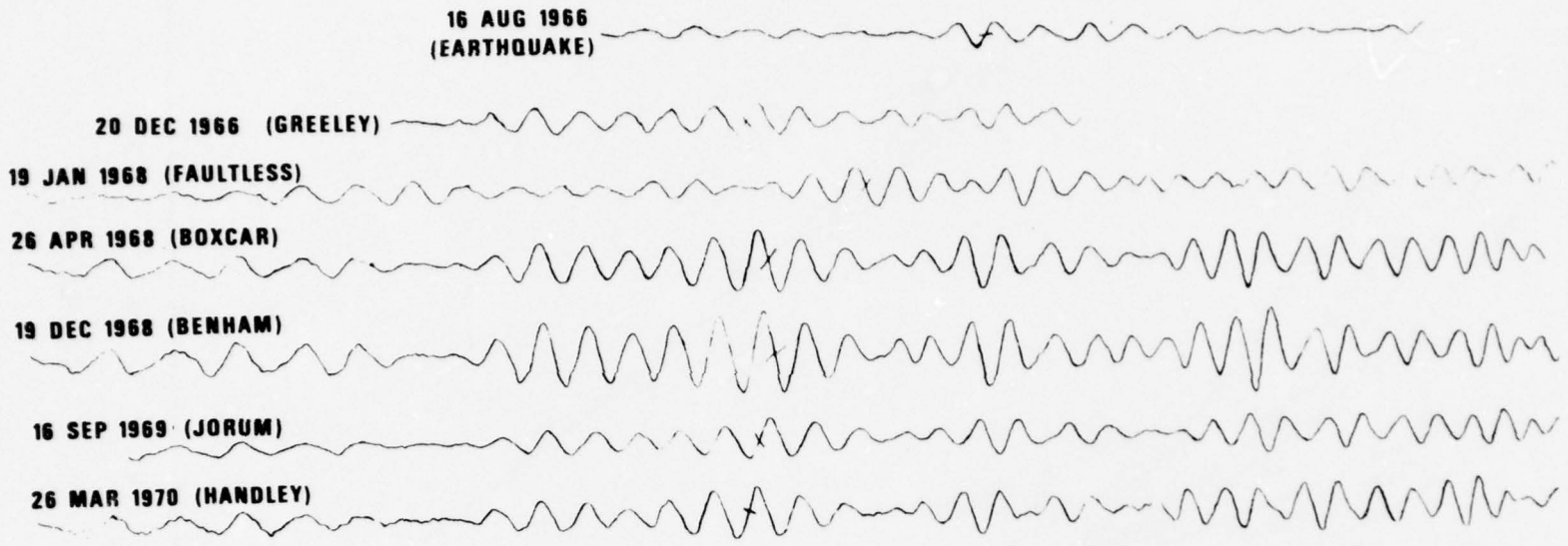

Figure 2. Profile of seven Nevada events at SHL and associated group-velocity curves.

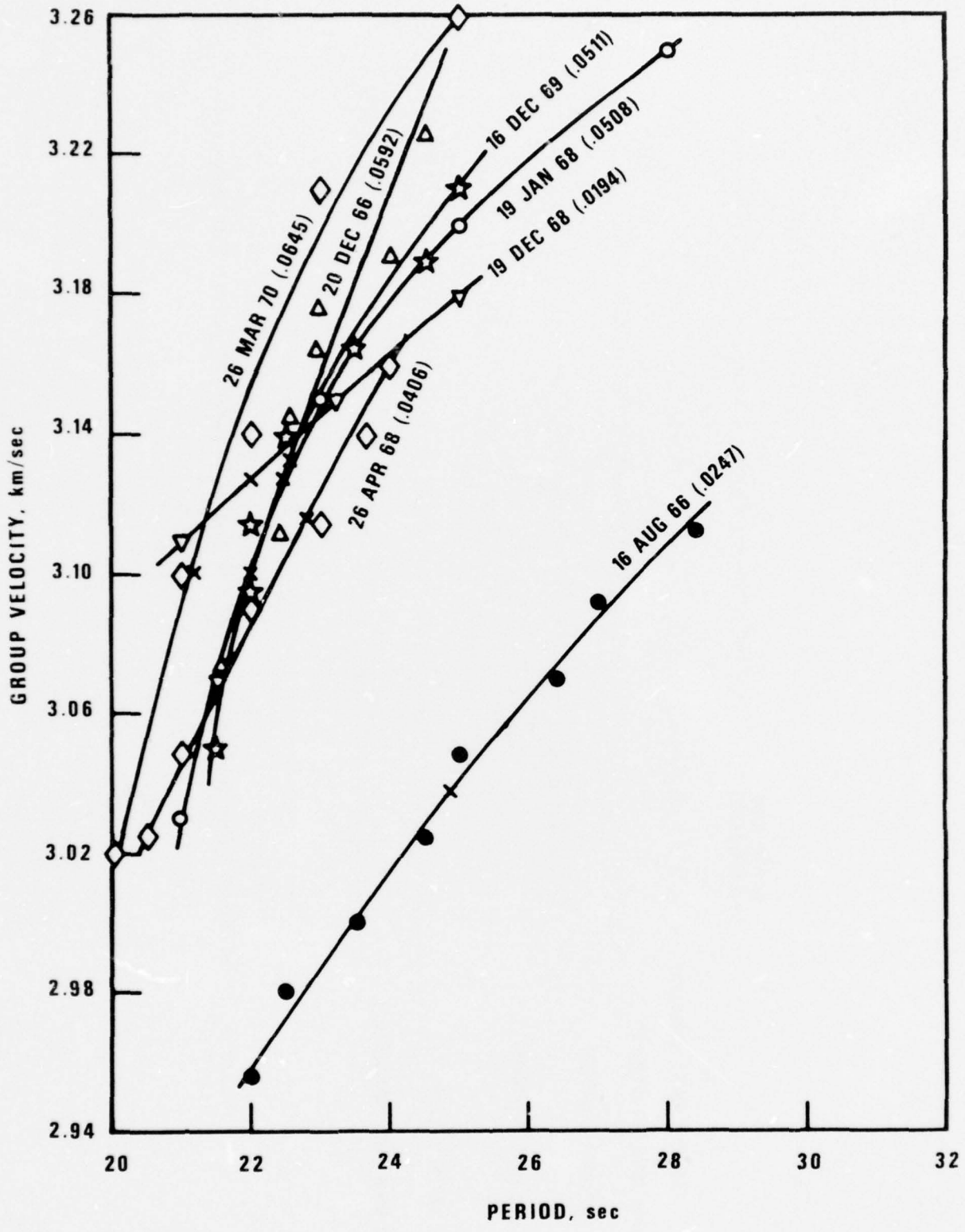

Figure 2 (Continued). Profile of seven Nevada events at SHL and associated group-velocity curves.

SURFACE-WAVE RAY TRACING

Overview

Ray tracing as a means of predicting the direction and intensity of waves has found applications in many fields. Applications to seismology have been most frequent for body waves (Jacobs, 1970; Sorrells et al., 1971; Davies and Julian, 1972; Engdahl, 1973; Engdahl, 1975) where results associated with dipping lithospheric plates have been very useful; but application of the method to surface waves (Woodhouse, 1974; Gjevik, 1974) has not yet produced significant results.

Evidence that Rayleigh waves deviate significantly from the great-circle path in their propagation was given by Evernden (1953, 1954). McGarr (1969) showed that Rayleigh-wave amplitude anomalies could be explained by focusing and defocusing effects of lateral heterogeneities in the earth's crust.

Jacobs, K. H., 1970, Three-dimensional seismic ray tracing in a laterally heterogeneous spherical earth, J. Geophys. Res., v. 75, p. 6675-6689.

Sorrells, G. G., J. B. Crowley and K. F. Veith, 1971, Methods for computing ray paths in complex geological structures, Bull. Seism. Soc. Am., v. 61, p. 27-54.

Davies, D. and B. R. Julian, 1972, A study of short-period P-wave signals from LONGSHOT, Geophys. J. R. Astr. Soc., v. 29, p. 185-202.

Engdahl, E. R., 1973, Relocation of intermediate depth earthquakes in the Central Aleutians by seismic ray tracing, Nature, v. 245, p. 23-25.

Engdahl, E. R., 1975, Effects of plate structure on earthquake focal mechanism determinations, Geophys. J. R. Astr. Soc., in press.

Woodhouse, J. H., 1974, Surface waves in a laterally varying layered structure, Geophys. J. R. Astr. Soc., v. 37, p. 461-490.

Gjevik, B., 1974, Ray tracing for seismic surface waves, Geophys. J. R. Astr. Soc., v. 39, p. 27-39.

Evernden, J. F., 1953, Direction of approach of Rayleigh waves and related problems, Part I, Bull. Seism. Soc. Am., v. 43, p. 225-274.

Evernden, J. F., 1954, Direction of approach of Rayleigh waves and related problems, Part II, Bull. Seism. Soc. Am., v. 44, p. 159-184.

McGarr, A., 1969, Amplitude variations of Rayleigh waves--horizontal refractions, Bull. Seism. Soc. Am., v. 59, p. 1307-1334.

Capon (1970) found evidence which supported several refractions at continental boundaries leading to multiple arrivals of Rayleigh waves at the Montana LASA. All these studies emphasized the importance of considering non-uniform propagation for the wavefront of seismic surface waves. It is the purpose of this part of the report to study these propagation effects with a reasonably well-determined model of the earth's parameters controlling the wavefront propagation.

To this end we will first discuss the method of calculating the raypaths since knowledge of the exact numerical technique is important in evaluating our results. We will next describe in some detail the construction of the global velocity grid which we employed in our calculations. Then several applications of the ray-tracing program will be presented; therein we describe how we compare predictions and observations. Lastly, we will discuss the results in terms of the adequacy of the numerical model we have employed.

Method

In order to calculate the raypath for surface waves, we approximate the wave equation by the eikonal equation; this approximation requires that space changes in the elastic parameters are small. Specifically, Officer (1974) states the requirement as

$$\lambda \frac{\delta c'}{c} << 1$$

where λ is wavelength, c is the velocity (surface-wave phase velocity in our case), and $\delta c'$ is the change in the gradient of c over the distance of a wavelength. This requirement is in fact satisfied by the phase velocities of surface waves over the globe in the period range 17-23 seconds. Solution of the eikonal equation in spherical coordinates leads to three first-order differential equations governing the ray paths (Julian, 1970):

Capon, J., 1970, Analysis of Rayleigh-wave multipath propagation of LASA, Bull. Seism. Soc. Am., v. 60, p. 1701-1731.

Officer, C. B., 1974, Introduction to Theoretical Geophysics, Springer-Verlag, New York, New York.

Julian, B. R., 1970, Ray tracing in arbitrarily heterogeneous media, Technical Note 1970-45, Lincoln Laboratory, Lexington, Massachusetts.

$$d\theta/dt = \frac{C}{R} \cdot \cos\zeta, \tag{4a}$$

$$d\phi/dt = \frac{C}{R\sin\theta} \cdot \sin\zeta, \tag{4b}$$

$$d\zeta/dt = \frac{\sin\zeta}{R} \cdot \frac{dC}{d\theta} - \frac{\cos\zeta}{R\sin\theta} \frac{dC}{d\phi} - \frac{C}{R} \cdot \sin\zeta\cot\theta, \tag{4c}$$

where θ and ϕ are the colatitude and east longitude, R is the earth's radius, ζ is the angle between the ray and the southward meridian and C is Rayleigh-wave phase velocity. Julian also gives the equation for the intensity at any point along the raypath:

$$I = \frac{I_o}{R[(d\theta/d\zeta_o)^2 + \sin^2\theta(d\phi/d\zeta_o)^2]^{1/2}}, \tag{5}$$

where the constant I_o is the intensity at the source. The derivatives $\partial\theta/\partial\zeta_o$ and $\partial\phi/\partial\zeta_o$ at a given point on the raypath are found using the differential equations:

$$\frac{\partial}{\partial t}\frac{\partial\theta}{\partial\zeta_o} = \frac{1}{R}\cos\zeta\left(\frac{\partial C}{\partial\theta}\frac{\partial\theta}{\partial\zeta_o} + \frac{\partial C}{\partial\phi}\frac{\partial\phi}{\partial\zeta_o}\right) - \frac{C}{R}\sin\zeta\frac{\partial\zeta}{\partial\zeta_o}, \tag{6a}$$

$$\frac{\partial}{\partial t}\frac{\partial\phi}{\partial\zeta_o} = \frac{1}{R}\frac{\sin\zeta}{\sin\theta}\left(\frac{\partial C}{\partial\theta}\frac{\partial\theta}{\partial\zeta_o} + \frac{\partial C}{\partial\phi}\frac{\partial\phi}{\partial\zeta_o}\right) + \frac{C}{R}\left(\frac{\cos\zeta}{\sin\theta}\frac{\partial\zeta}{\partial\zeta_o} - \frac{\sin\zeta\cos\theta}{\sin^2\theta}\frac{\partial\theta}{\partial\zeta_o}\right), \tag{6b}$$

$$\begin{aligned}\frac{\partial}{\partial t}\frac{\partial\zeta}{\partial\zeta_o} = {} & \frac{1}{R}\left(\cos\zeta\frac{\partial\zeta}{\partial\zeta_o} - \sin\zeta\cot\theta\frac{\partial\theta}{\partial\zeta_o}\right)\frac{\partial C}{\partial\theta} + \frac{1}{R}\left(\frac{\cos\zeta\cos\theta}{\sin^2\theta}\frac{\partial\theta}{\partial\zeta_o} + \frac{\sin\zeta}{\sin\theta}\frac{\partial\zeta}{\partial\zeta_o}\right. \\ & \left. - \sin\zeta\cot\theta\frac{\partial\phi}{\partial\zeta_o}\right)\frac{\partial C}{\partial\phi} + \frac{\sin\zeta}{R}\left(\frac{\partial^2 C}{\partial\theta^2}\frac{\partial\theta}{\partial\zeta_o} + \frac{\partial^2 C}{\partial\phi\partial\theta}\frac{\partial\phi}{\partial\zeta_o}\right) - \frac{\cos\zeta}{R\sin\theta}\left(\frac{\partial^2 C}{\partial\phi\partial\theta} + \frac{\partial^2 C}{\partial\phi\partial\theta}\frac{\partial\phi}{\partial\zeta_o}\right) \\ & + \frac{C}{R}\left(\frac{\sin\zeta}{\sin^2\theta}\frac{\partial\theta}{\partial\zeta_o} - \cot\theta\cos\zeta\frac{\partial\zeta}{\partial\zeta_o}\right).\end{aligned} \tag{6c}$$

These equations are derived by taking the derivatives of 4a, 4b, and 4c with respect to ζ_o and reversing the order of differentiation. To calculate the

ray paths and intensities, equation sets 4 and 6 are numerically integrated from the epicenter outward along starting azimuths which are incremented by equal steps.

The spatial parameters affecting the raypaths and intensities are C and its derivatives. We are here considering phase velocities of 20-second Rayleigh waves which vary between roughly 3.0 and 4.0 km/sec over the globe. Although it would be convenient to express C as a continuous function (e.g., spherical harmonic series) the computation then of C and its derivatives at points on the earth would be prohibitively costly, even assuming that a high-order continuous function could accurately reflect the true variations in phase velocities. Instead we have specified C discretely, as described in a later section, for each 1° x 1° rectangular area on the earth, and then we computed the derivatives by the method of central differences (Davis and Polonsky, 1964). For computational purposes phase velocity C and its derivatives were taken to be at the center of each 1° x 1° grid rectangle. Interpolation for values at points other than the center was carried out by four-point interpolation (Davis and Polonsky, 1964) using the four defined values nearest the current ray point. Note that C and its derivatives are continuous everywhere using this interpolation scheme. Integration of equations 4 and 6 was performed by the mid-point method wherein the mid-point of a preliminary projected ray was used in obtaining C and its derivatives for the actual ray projection to the next point. The preliminary projected ray is simply a straight-line projection along the great-circle path defined by the head and tail of the previous ray increment. Integration of formulas 4 and 6 proceeds with a time step of 10 seconds (roughly one-half a wavelength or 30 to 40 km) when C is uniform over the space enclosing the preliminary projected ray and with a time step of 5 seconds when C has a non-zero gradient in any direction within this space.

Davis, P. J. and I. Polonsky, 1964, Numerical interpolation, differentiation, and integration, in Handbook of Mathematical Functions, edited by M. Abramowitz and I. A. Stegun, National Bureau of Standards, United States Department of Commerce.

The rays calculated by the above procedure are plotted on suitable map projections for interpretation. The coordinates of stations of interest are entered into the program and calculated intensities (equation 5) are printed out whenever the head of a ray increment falls within 2° of a station. In this way amplitudes at particular stations are predicted and can be compared with observed amplitudes.

It is well-known that the above intensity calculations are invalid where caustics occur (Sato, 1969; Richards, 1973); that is, where

$$\frac{\partial\theta}{\partial\zeta_o} \approx \frac{\partial\phi}{\partial\zeta_o} \approx 0.$$

Although computational schemes have been devised to calculate amplitudes near caustics, we did not feel that use of these is justified since large uncertainties reside in our velocity grid, thereby making the exact position of caustics suspect anyway. We merely note the position of caustics or near-caustics in our plots of the ray paths and avoid quantitative comparisons of observed amplitudes with calculated amplitudes, which become large in the areas with predicted caustics.

The program for tracing rays was checked by computing rays impinging at various angles to an abrupt linear boundary. The refracted angles of the rays agreed very well with predictions according to Snell's law. Intensity calculations were checked by actually measuring visually the quantities $\partial\theta/\partial\zeta_o$ and $\partial\phi/\partial\zeta_o$, inserting them in equation (5), and comparing the result with the program predictions for areas of various ray densities.

Velocity Grid

A period of 20 seconds was chosen in order to apply ray-tracing results to the problem of M_s scatter; that is, we expect that ray-tracing would

---

Sato, R., 1969, Amplitude of body waves in a heterogeneous sphere: comparison of wave theory and ray theory, Geophys. J. R. Astr. Soc. v. 17, p. 527-544.

Richards, P. G., 1973, Calculation of body waves for caustics and tunnelling core phases, Geophys. J. R. Astr. Soc., v. 35, p. 243-264.

produce low and high amplitudes which would correlate to some degree with the amplitudes measured in routine M_s determinations. We obtained phase velocities either directly from published phase-velocity measurements or indirectly by computing the phase-velocity curve for a published or inferred structure. The period of 20 seconds is somewhat fortuitous as regards estimation of phase velocity from structural profiles; for we know that periods less than 20 seconds are influenced heavily by the upper crust which is very heterogeneous over the earth. Sediment thickness, water depth, intrusive bodies, and other elements can cause the elastic parameters to vary rapidly in the upper layers of the earth. Effects of these rapidly-varying elements are somewhat diminished at a period of 20 seconds, however, where the lower crustal layers which are not as rapidly varying have more influence on phase velocity. For much of the earth, geophysical studies over the last two or three decades have defined the gross features of the crust which are needed to estimate phase velocity at 20 seconds while detail on finer features needed to estimate phase velocities at shorter periods is too often lacking. On the other hand, for periods greater than 20 seconds, the Rayleigh waves begin to sample the upper mantle whose detailed structure is again not so well known. We will give evidence to support these statements in a later paragraph.

We assigned a phase velocity to each 1° x 1° rectangle on the basis of published information if it was available and on geophysical intuition if no particular studies or observations covered a given rectangle. This grid is shown in Figure 3. Our preference for information was in this order: 1) two-station phase velocity measurements over homogeneous paths, 2) one-station phase velocity measurements over homogeneous paths, 3) crustal refraction results, 4) crustal reflection results (as primarily done in the U.S.S.R.), 5) crustal density profiles, and 6) group-velocity measurements over homogeneous paths. Many published studies of course combine several of the above and produce superior results. We will in the following paragraphs discuss these sources of data. The number of references consulted for the necessary data was large, and we will not attempt to cite them all; rather we will comment on the general nature of the available data and how

Figure 3. Grid of 20-second Rayleigh-wave phase velocities 1°x1° surfaces defined by the latitudes and longitudes.

(Located at back of report)

it was assimilated into our phase-velocity grid. We have by no means covered all the available data pertinent to this problem; also many areas of the globe are without data at all or have only sketchy data. For these reasons our grid is merely a preliminary version.

An additional type of information was water depth in oceans and seas; our source for this was Grosvenor and Darley (1963). The ocean-continent boundaries are defined by the continental slope. We have consistently used the 1000-fathom isobath (1830 meters) as the boundary between oceanic and continental phase velocities; this demarcation is similar to that used in most pre-drift reconstructions such as by Dietz and Holden (1970), who used the 2000-meter isobath. The ocean-continent boundary in general marks the largest gradient in phase velocity in our global grid. Extreme water depths, such as trenches and deep ocean basins (>3000 fathoms) cause a decrease in the phase velocity of 20-second Rayleigh waves from normal oceanic structure; deep basins will lower it just by roughly .1 km/sec, but trenches may lower it by as much as .7 km/sec depending on their exact depth. These features were noted in preparing our phase-velocity grid.

As stated above, our primary information was phase-velocity measurements over homogeneous paths. Two-station measurements are the most reliable, provided the signals are reasonably close to the great circle path and instrument phase responses are known. Unfortunately, such measurements are extant for only a limited number of paths, almost all of which are continental. However, such measurements have been made in several types of structure and can be extrapolated to areas of similar structure where the phase velocity has not yet been measured; for instance, we have transferred phase velocities measured on parts of the Canadian, Fennoscandian, African, and South American shields to the full extent of these shields and also to other known shield areas. One-station phase-velocity measurements are somewhat less reliable

---

Grosvenor, M. B. and J. M. Darley, 1963, National Geographic Atlas of the World, National Geographic Society, Washington, D. C.

Dietz, R. S. and J. C. Holden, 1970, Reconstruction of Pangaea: Breakup and dispersion of continents, Permian to Present, J. Geophys. Res., v. 75, p. 4939-4956.

due to the problem of 2π indeterminacies in the phase-angle (Brune et al., 1960) which affects all such studies and to lack of correction for initial phase at the source which affects some of these studies. One-station type measurements provided good phase-velocity data over ocean areas: normal oceanic sectors as well as deep basins, spreading ridges, and continental margins. Using these direct phase-velocity measurements, we were able to assign phase velocities to over half of the global grid.

Many regions of the globe were lacking phase-velocity measurements at 20 seconds' period and had structures that could not be arbitrarily associated with known phase velocities for shields or other simple structural regions. For these regions we sought whatever structural information that was available down through at least the crust. Such information was in the form of seismic refraction, gravity, and magnetic data; given or inferred structure from this data was then used to calculate a phase velocity for 20-second Rayleigh waves with a flat-earth dispersion program. In order to calculate the phase velocity, estimates of compressional and shear-wave velocity and density are required. Rarely are all three parameters for the various crustal layers estimated in geophysical studies. Therefore we have assumed a Poisson's ratio of .26 for consolidated sediments, granitic and basaltic layers of the crust (Christensen and Salisbury, 1975) and a higher values, 0.33, for unconsolidated sediments in oceans and seas; this enables us to estimate shear-wave velocities from compressional-wave ones and vice-versa. For the density-velocity relation, we have used the Nafe-Drake (Talwani et al., 1961) curve for crustal rocks.

As stated previously, the period of 20 seconds is a fortuitous choice in regard to estimation of phase velocity since it predominately depends on

---

Brune, J. N., J. E. Nafe, and J. E. Oliver, 1960, A simplified method for the analysis and synthesis of dispersed wave trains, J. Geophys. Res., v. 56, p. 287-304.

Christensen, N. I. and M. H. Salisbury, 1975, Structure and composition of the lower oceanic crust, Rev. Geophys. Space Physics, v. 13, p. 57-86.

Talwani, M., J. L. Worzel, and M. Erving, 1961, Gravity anomalies and crustal section across the Tonga Trench, J. Geophys. Res., v. 66, p. 1265-1278.

layers for which we have the most complete information in a global sense. We shall demonstrate this by illustrating the phase-velocity partial derivatives at a period of 20 seconds for two extreme structures; these partials indicate the relative influence of each layer on the computed phase velocity. The two structures used are the oceanic and shield models given in Harkrider and Anderson (1966); these structures are listed in Table IV. Calculated partials with respect to compressional-wave velocity, shear-wave velocity, and density are shown in Figure 4; they have been normalized by the layer thicknesses which were all kept small so that the values indicate the effect of changes in a parameter at that depth, not just of changes in a parameter for a layer. (For these calculations, the layers given in Table IV have been divided into smaller sublayers.) Note that in general the partial derivatives take their maximum values in the crust of both models although the influence of the upper mantle properties is sizeable. Note also that compressional velocity is a relatively unimportant factor below the crust.

Lateral inhomogeneities in the upper mantle are known to amount to only a few per cent, except for zones which include dipping lithospheric plates where velocity and/or density contrasts may approach 10% (Jacobs, 1970). We desire to establish that changes in upper mantle properties on the scale of these known inhomogeneities will affect calculations of phase velocity for 20-second Rayleigh waves by a tolerable amount, such that use of a uniform upper mantle model for our calculations with various published or inferred crustal structures will not lead to unacceptable error in estimating 20-second phase velocity. The evidence to establish this is given in Table V where for the oceanic model of Table IV we have computed the phase velocity for various permutations of the high-velocity lid (layers 4-6) over the low-velocity zone. In no case has the phase velocity changed by as much as .1 km/sec. Influence of deeper layers becomes minimal; for instance, we removed the low-velocity zone entirely (setting velocities for layers 7-13 equal to that of layer 6)

Harkrider, D. G. and D. L. Anderson, 1966, Surface-wave energy from point sources in plane layered earth models, J. Geophys. Res., v. 71, p. 2967-2980.

TABLE IV

Harkrider-Anderson Earth Models

Layer	Thickness (km)	Compressional Velocity ($\frac{km}{sec}$)	Shear Velocity ($\frac{km}{sec}$)	Density ($\frac{g}{cc}$)
		Oceanic		
1	5.0	1.52	0.00	1.03
2	1.0	2.10	1.00	2.10
3	5.0	6.41	3.70	3.01
4	9.0	8.11	4.61	3.40
5	5.0	8.12	4.61	3.40
6	15.0	8.12	4.61	3.40
7	20.0	8.01	4.56	3.37
8	20.0	7.95	4.56	3.37
9	20.0	7.71	4.40	3.37
10	20.0	7.68	4.34	3.33
11	20.0	7.77	4.34	3.33
12	20.0	7.85	4.34	3.33
13	20.0	8.10	4.45	3.33
14	20.0	8.12	4.45	3.33
		Shield		
1	10.0	6.10	3.54	2.55
2	6.5	6.10	3.54	2.55
3	5.0	6.40	3.70	3.08
4	5.0	6.70	3.92	3.42
5	5.0	6.70	3.92	3.42
6	3.5	6.70	3.92	3.42
7	5.0	8.15	4.75	3.42
8	20.0	8.16	4.75	3.42
9	20.0	8.21	4.75	3.42
10	20.0	8.26	4.75	3.42
11	20.0	8.32	4.75	3.42
12	20.0	8.30	4.70	3.40
13	20.0	8.28	4.54	3.40
14	20.0	8.28	4.54	3.40
15	20.0	8.28	4.54	3.41

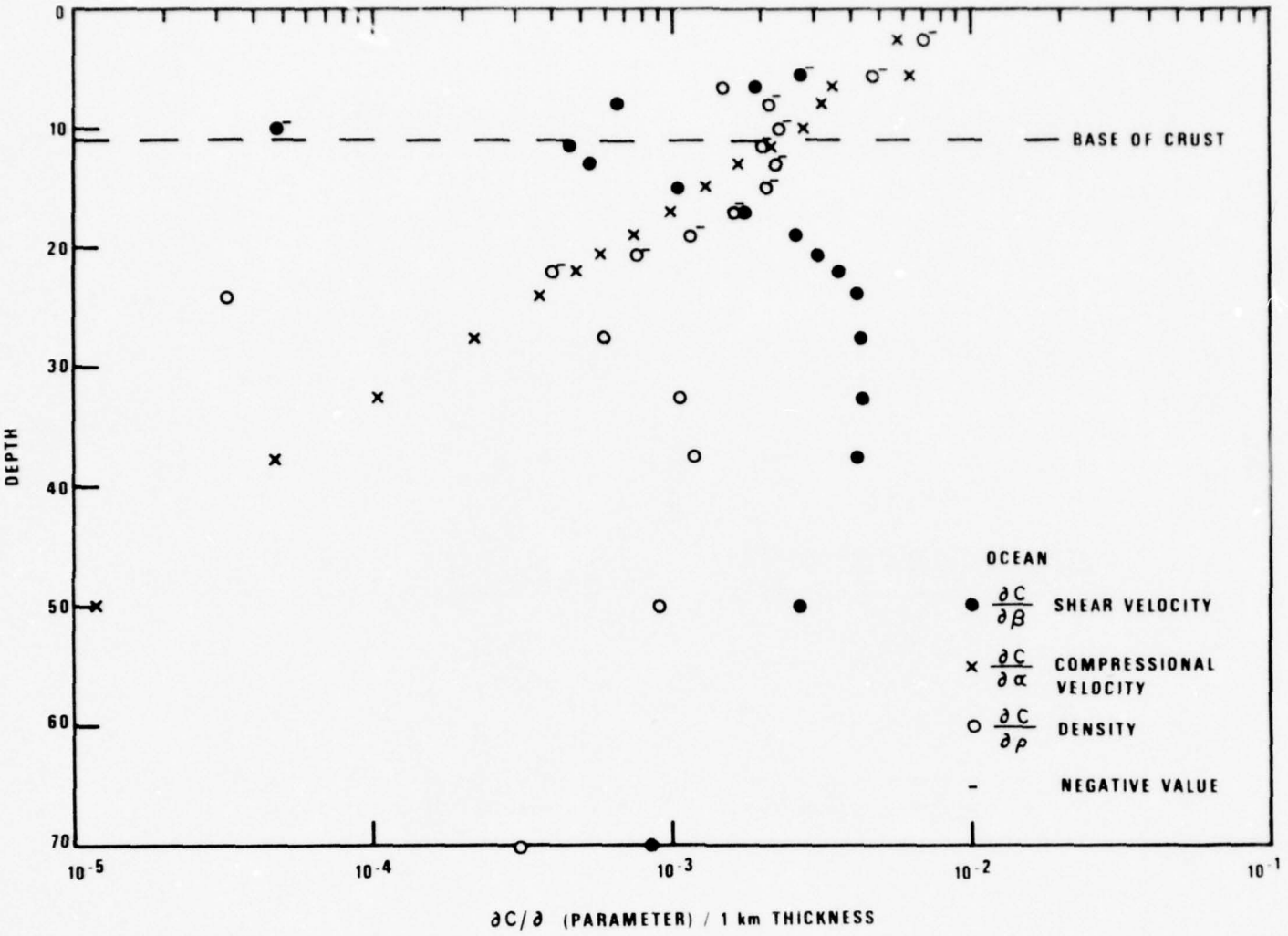

Figure 4a. Partial derivatives of the Harkrider-Anderson oceanic model versus depth.

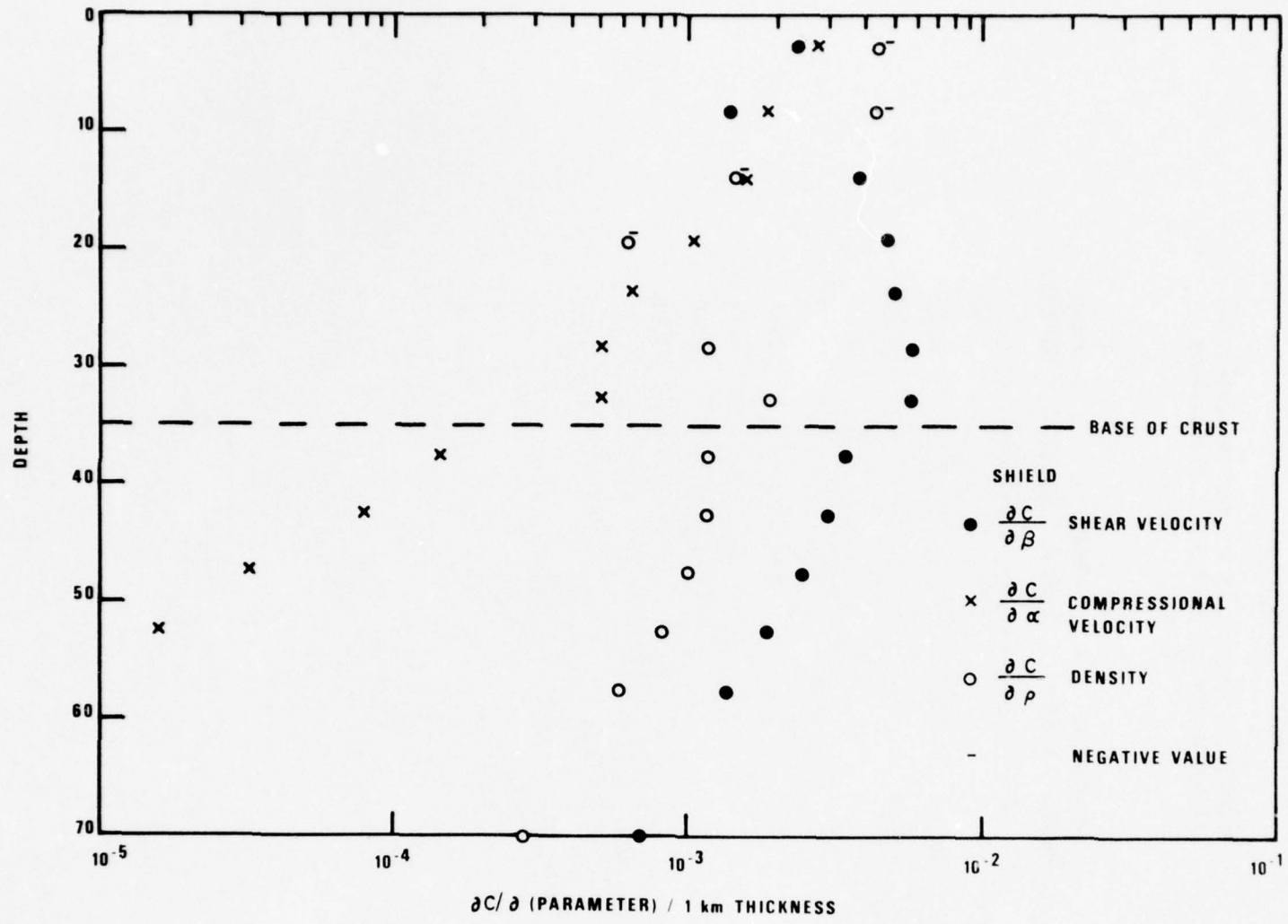

Figure 4b. Partial derivatives of the Harkrider-Anderson shield model versus depth.

TABLE V

Effects of Varying Upper Mantle Properties of Ocean Model 20-Second Rayleigh-Wave Phase Velocity

Velocities Higher		Velocities Lower		Density Higher	Density Lower	Phase Velocity
.1	.2	.1	.2	.1	.1	
						3.96
x						4.00
	x					4.05
		x				3.91
			x			3.87
				x		3.96
					x	3.96
x				x		4.00
		x			x	3.91
x					x	4.01
		x		x		3.91

and found that the phase velocity increased by only .02 km/sec. Similar calculations for the Shield model of Table IV showed that varying the upper mantle properties had even less effect on the phase velocity of 20-second Rayleigh waves. Thus, we feel that unavailability of upper mantle velocities and densities does not preclude calculating the phase velocity, since substitution of a uniform upper mantle model can only lead to errors on the order of .1 km/sec at most. The accuracy of the computed phase velocity at 20 seconds' period depends then on the accuracy of the given or inferred crustal model. The phase velocity calculations, where necessary for the grid of Figure 3, used the upper mantle models of Table IV, whichever was deemed appropriate, or slight modifications thereof.

Roughly a fourth of the globe comprised areas of sufficient crustal information to make phase-velocity calculations as described above. The types of studies used in compiling crustal sections were discussed earlier. Considerable extrapolations from the points of actual geophysical data were often made based on geophysical intuition in order to broaden the coverage of these studies. Areas which were relatively well covered included the United States, Europe, Canada, most oceanic areas, and western U.S.S.R. In most cases calculated phase velocities using crustal structures agreed with observed, published phase velocities where available. Numerous calculations with oceanic crustal structure showed that oceanic phase velocity was remarkably uniform at 3.9-4.0 km/sec except for ridge and trench areas. Thus we can assign phase velocities to much of the globe, which is 70% oceanic, with high confidence.

Areas of the globe with little or no information readily available with which to accurately estimate 20-second phase velocity for Rayleigh waves comprised roughly a quarter of the grid. Here we simply applied geophysical intuition and, not uncommonly, outright conjecture. Larger areas of this type included parts of the polar regions, much of Central America, the upper Andean cordillera, the Mid-East, the Near East, the Far East, and parts of Siberia, Indonesia, and the Philippines. Smaller areas of this type can be critically important if their velocities and configuration are such as to produce strong refraction patterns. Island arcs, trenches, deep sedimentary basins, and

fluvial cones of large rivers are examples of small but important features; and we lacked phase-velocity measurements and structural profiles in many of these cases. The Amazon River cone, Black Sea and Caspian Sea basins, and the Philippine and Mariana trenches are the features which we are most unsure about. Phase velocities in these regions may be significantly lower than we have estimated since shear velocities of the sediments are unknown but may reflect an unusually high Poisson's ratio; for instance, Wiedner (1974) has inferred very low shear velocities in the Amazon cone. The Tibet Plateau is another region of large uncertainty in phase velocity because of its anomalously thick, but largely undertmined, crust. Ray refraction in these areas of strong velocity contrast should be pronounced, and it is unlikely that phase-velocity measurements will soon be accurately made due to this problem; so our best hope for these areas is to accumulate information on the elastic parameters with other geophysical approaches.

Application to LONGSHOT/MILROW/CANNIKAN

The series of three nuclear explosions on Amchitka Island--LONGSHOT, MILROW, and CANNIKAN--provided a world-wide set of amplitude data for which we could ignore radiation patterns typical of earthquakes and thereby hopefully achieve a good prediction of actual observed amplitudes after they were corrected for uniform attenuation and dispersion effects.

Raypaths were calculated for a 20-second LR phase originating at 51.4N, 179.2E. Figure 5 shows the raypaths, which were generated at 1° increments of starting azimuth. The raypaths are seen to deviate significantly from great circle paths. The greatest bending of the raypaths occurs as expected in regions of high velocity gradient, such as continental margins, oceanic trenches, and mountain ranges.

Intensities were found for 151 stations where at least one of the explosions LONGSHOT, MILROW, or CANNIKAN are recorded. These intensities were calculated in the ray-tracing program from equation (5) and were later normalized so that the average of the amplitudes derived from ray tracing

---

Weidner, D. J., 1974, Rayleigh wave phase velocities in the Atlantic Ocean, Geophys. J. R. Astr. Soc., v. 36, p. 105-139.

Figure 5. Raypaths from LONGSHOT/MILROW/CANNIKAN.

(Located at back of report)

were equal to the average of the observed amplitudes. Amplitudes (A_c) were calculated from the intensity values by the equation

$$A_c = [I\sin\Delta/\sin\Delta_c]^{1/2} \tag{7}$$

where I = surface-wave intensity calculation,

Δ = distance in degrees measured along the raypath,

Δ_c = constant epicentral distance.

The calculated amplitudes are thus normalized to the reference distance Δ_c. These calculated amplitudes were compared to the observed amplitudes (A_o) which were normalized to the distance Δ_c by the equation

$$A_o = A_{obs}[\Delta/\Delta_c]^{1/2}[\sin\Delta/\sin\Delta_c]^{1/2}\exp(\pi r/QUT-\pi r_c/QUT) \tag{8}$$

where A_{obs} = measured amplitude,

r = distance in km along the raypath,

r_c = distance Δ_c converted to km,

Q = attenuation factor,

U = group velocity,

T = period.

This correction removes geometrical spreading, the dispersion effect, and attenuation effects from the measured amplitudes for surface waves and follows directly from equation (1). In this study Q was assumed to be 500, U was 3.5 km/sec, T was 20 seconds, and Δ_c was 90 degrees. (In fact the periods of observed amplitudes were allowed to be in the range of 18-22 seconds--this necessarily meant that the trace maximum was not always measured for amplitude.) The attenuation factor of 500 was taken from von Seggern (1975a). Naturally, attenuation varies along the raypath; and using a constant value for Q will introduce errors into any comparison of observed and calculated amplitudes since we make no attempt to regionalize Q. The observed amplitudes were normalized to a yield of 1000kt by multiplying all values by 1000/Y where

---

von Seggern, D. H., 1975a, Q for 20-second Rayleigh waves from complete great-circle paths, Report No. SDAC-TR-75-3, Teledyne Geotech, Alexandria, Virginia.

Y was assumed to be 80 kt for LONGSHOT, 1000 kt for MILROW, and 5000 kt for CANNIKAN. After normalization, all values for a given station were averaged.

Figure 6 shows the observed versus the calculated amplitudes for LONGSHOT/MILROW/CANNIKAN for stations at less than 70 degrees of epicentral distance. (A limit of 70° was imposed due to the ray-tracing errors which accumulate in a random-walk fashion from the errors in the velocity grid.) Points with large calculated amplitudes which were judged to lie near caustics were eliminated prior to making the correlation plot; no amplitudes were removed, added, or adjusted after the plot was made. Since the rays on Figure 5 rarely pass through a station, the calculated intensities were interpolated from closest values on either side of the station. The ray-tracing program prints out the intensity, azimuth, velocity, arrival time, and epicentral distance of the closest point of a ray to each station if that point is less than 2° from the station. Thus it is possible to determine the relative arrival times of rays crossing at a station. Since rays rarely cross exactly at a station, it is difficult to determine whether they interfere constructively or destructively at the station. In certain cases the velocity grid would not permit rays to pass within 2° of a station, as for example at ESK (Scotland) and LOR (France), unless of course we were to increase the density of starting azimuths. In those cases intensities were calculated directly from the ray-tracing plot using equation (5) but were a-priori judged to be too inaccurate to appear in Figure 6.

The correlation coefficient of the data in Figure 6 is .223 which is at about the 95 percent confidence level for non-zero correlation for the 79 stations used in the figure. Figure 7 is a similar plot for only the North American stations. The correlation coefficient for this data is only .116 which is at the 50 percent confidence level. Much of the scatter in the North American data can be attributed to the rays travelling through the Aleutian arc where velocity gradients are crudely depicted by 1° squares. There are no phase-velocity measurements available along this arc, and phase velocities inferred from crustal structure can vary by nearly 1.0 km/sec within a 1° square in such a region. Thus we would expect to see a low correlation coefficient for the North American data until the grid can be

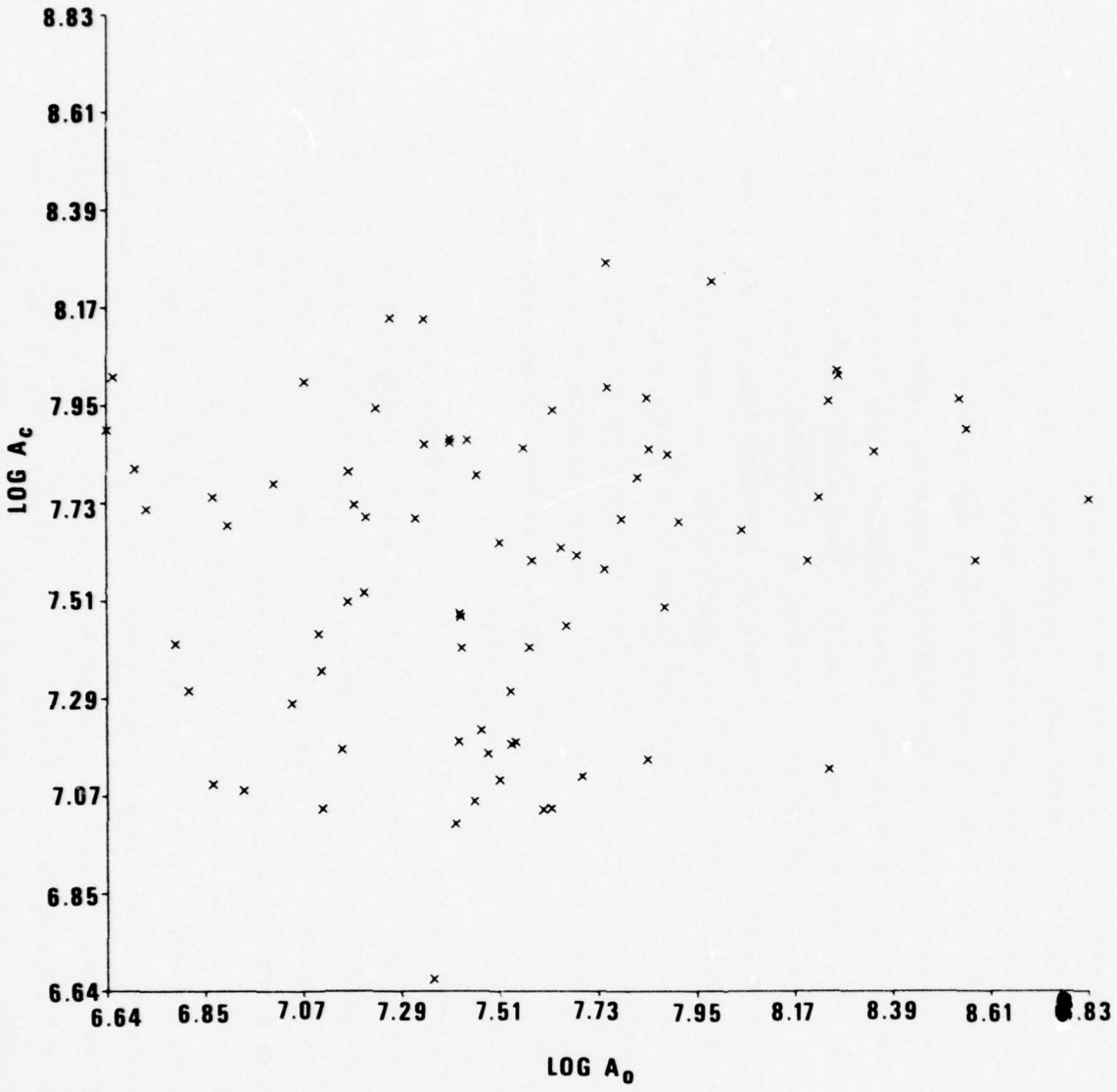

Figure 6. Log A_o versus log A_c for LONGSHOT/MILROW/CANNIKAN - global data.

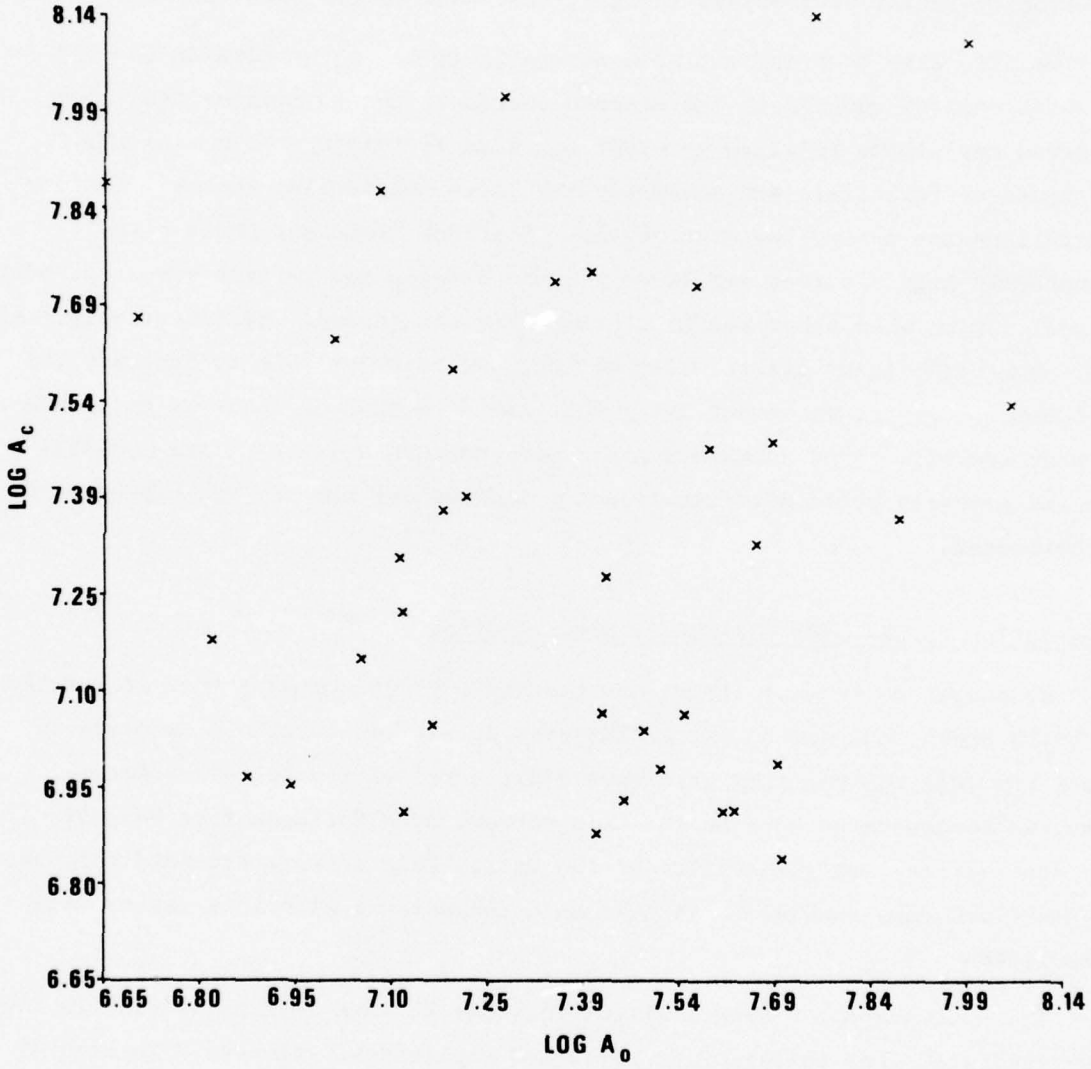

Figure 7. Log A_o versus log A_c for LONGSHOT/MILROW/CANNIKAN - North American data.

further refined. Since the North American data alone had low correlation, the correlation coefficient was recalculated with this part of the data removed, but no improvement was found over the data as a whole. The results for the whole world shown in Figure 6 are somewhat encouraging and indicate that the ray-tracing factor is possibly a significant part of the observed amplitudes.

We also wish to point out some of the large irregularities in the data. The stations TUC and GSC in the western United States have anomalously low observed amplitudes relative to other stations in this area; in fact the amplitude differentials are seemingly too large considering that the station separations are a very few wavelengths. Stations SV-QB and DH-NY have anomalously high observed amplitudes, again showing too large a variation over a small region when other nearby stations are considered. We tentatively feel that some calibration errors exist although we were not able to identify the problems. However, we do not imply that the data base of observed amplitudes is poor overall; these anomalous cases with dubious amplitudes are probably few and probably would not significantly improve our results if they were to be corrected.

Application to the LRSM Network in North America

We sought to essentially repeat the above procedure as performed for the Amchitka shots, but now to use earthquakes in various locations in order to check how well the velocity grid approximates velocities for other paths. Also, we concentrated here on the LRSM network over North America because of the availability and reliability of the data. This network provided a dense coverage and thus enabled us to make more comparisons with less ray-tracing computation.

The epicenters for events listed in Table VI were used as origins in the ray-tracing program to calculate predicted amplitudes. Figures 8 through 21 show the ray paths and plots of calculated amplitudes A_c versus observed amplitudes A_o. The calculated amplitudes were corrected for distance according to equation (7). The observed amplitudes are corrected for distance effects just as the Amchitka shot amplitudes were by equation (8). An additional factor employing average M_s residuals (SC) at each station and source radiation

TABLE VI

Earthquakes Processed
Through Ray Tracing Program

Event No.	Date	Region	Origin Time (GMT)	Lat. (Deg)	Long. (Deg)	Depth	λ (Deg)	δ (Deg)	Reference
1*	--	Nevada Test Site	--	37.0N	116.0W	0	--	1	
2	06 Feb 65	Rat Islands	04:02:53	52.1N	175.7E	35	80	18	Stauder (1968)
3	02 Nov 64	Northern Peru	06:50:58	4.1S	76.9W	91	86	48	Isacks and Molnar (1971)
4	07 May 63	Northern Chile	16:23:12	22.1S	68.7W	95	70	90	Isacks and Molnar (1971)
5	20 Aug 65	South of Fiji Islands	21:21:52	22.8S	176.2W	79	84	85	Isacks and Molnar (1971)
6	01 Mar 65	Mexico-Guatemala Border	21:32:12	15.4N	92.5W	85	71	86	Isacks and Molnar (1971)
7	22 Dec 64	Dominican Republic	08:01:13	18.4N	68.8W	117	70	50	Isacks and Molnar (1971)

*Typical location parameters for an NTS explosion.

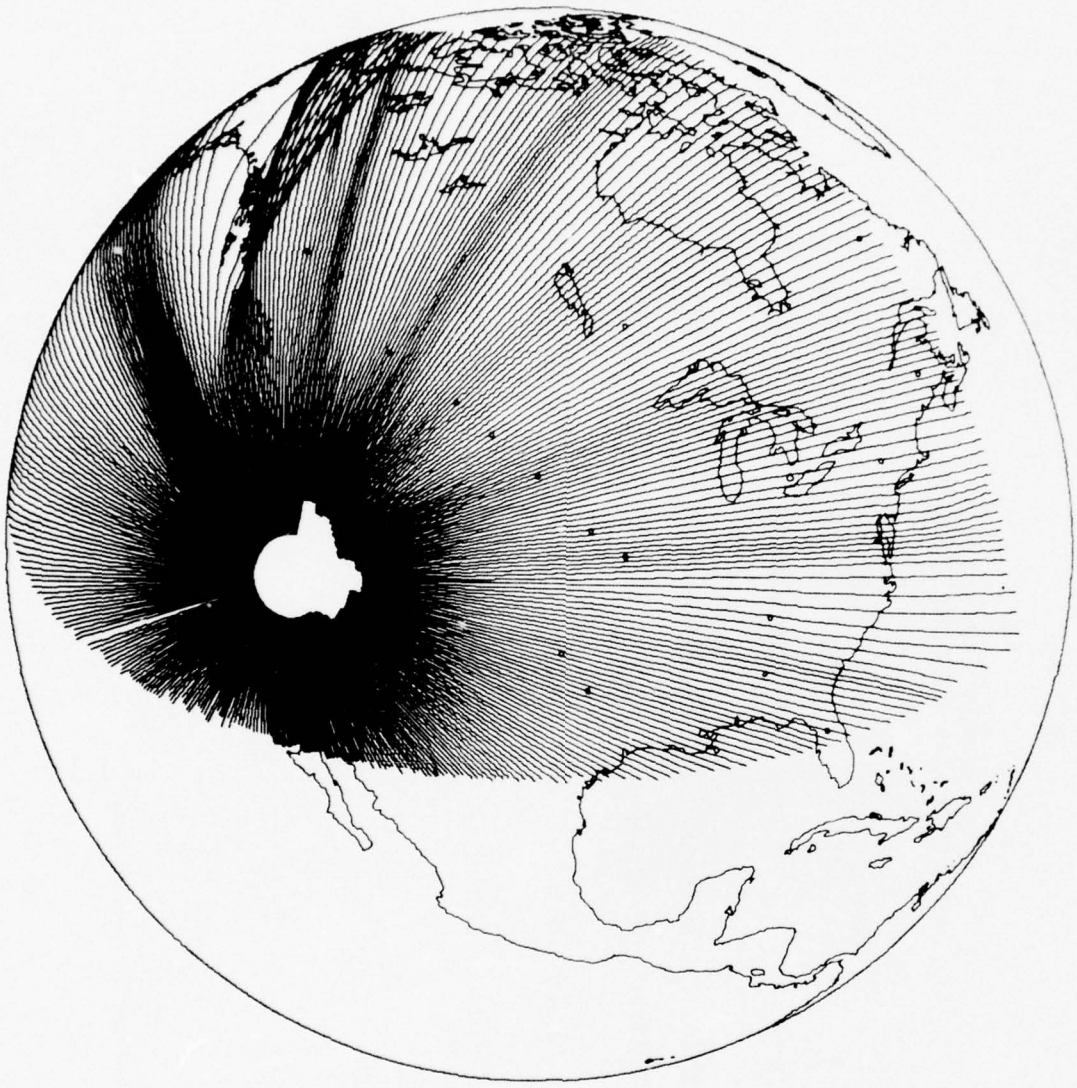

Figure 8. LR 20 raypaths from event 1 - Nevada Test Site.

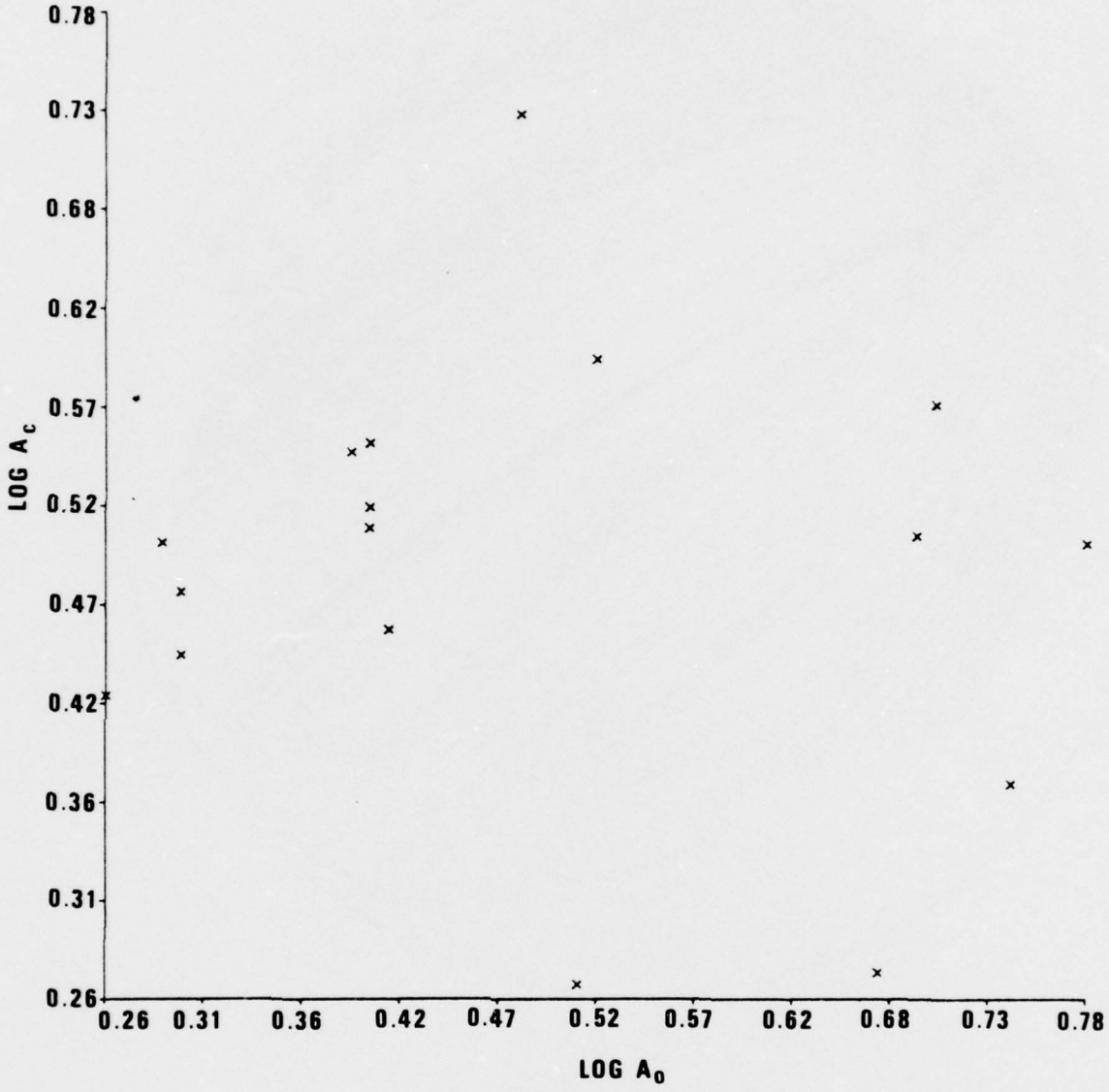

Figure 9. Log A_c versus log A_o for event 1.

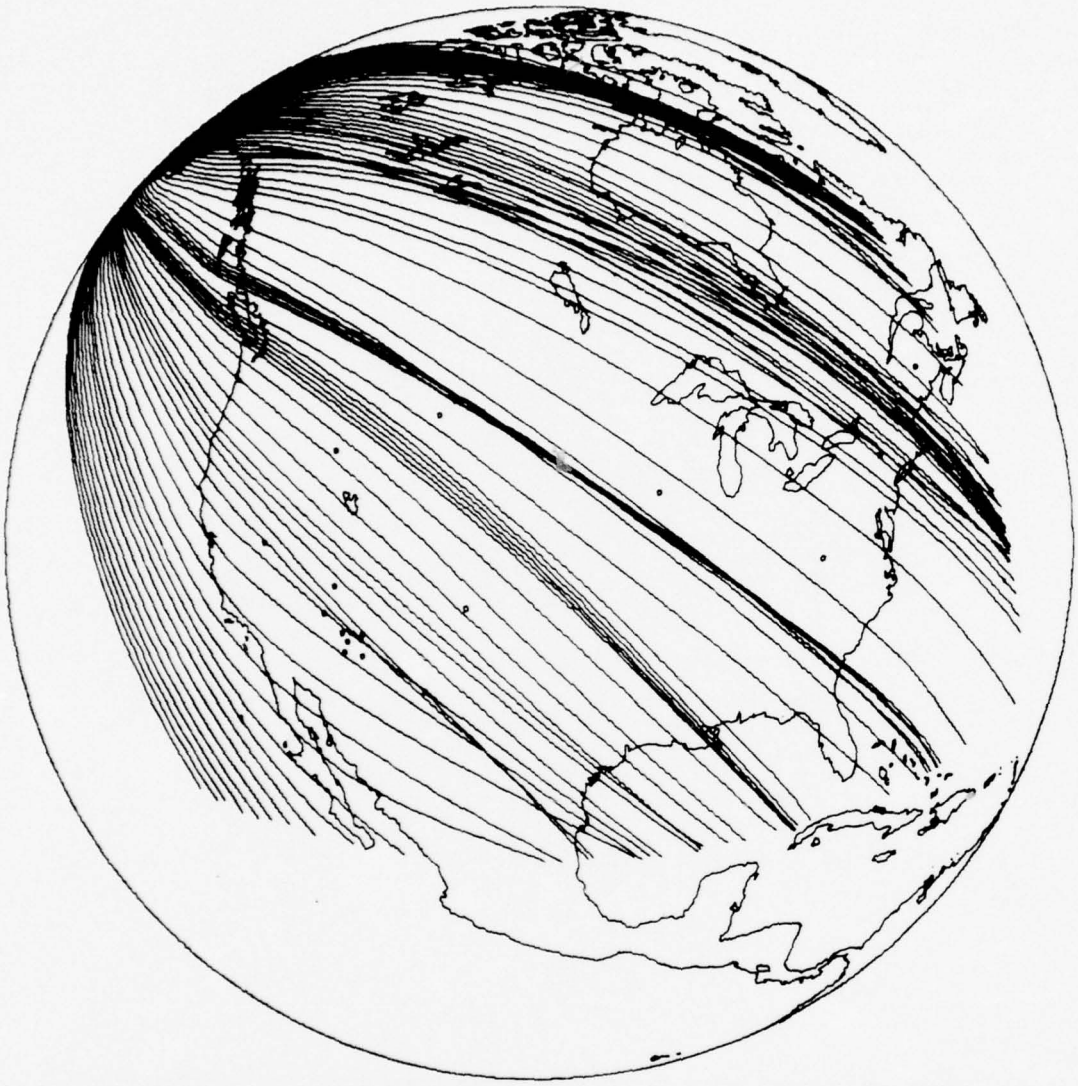

Figure 10. LR20 raypaths from event 2 - Rat Islands.

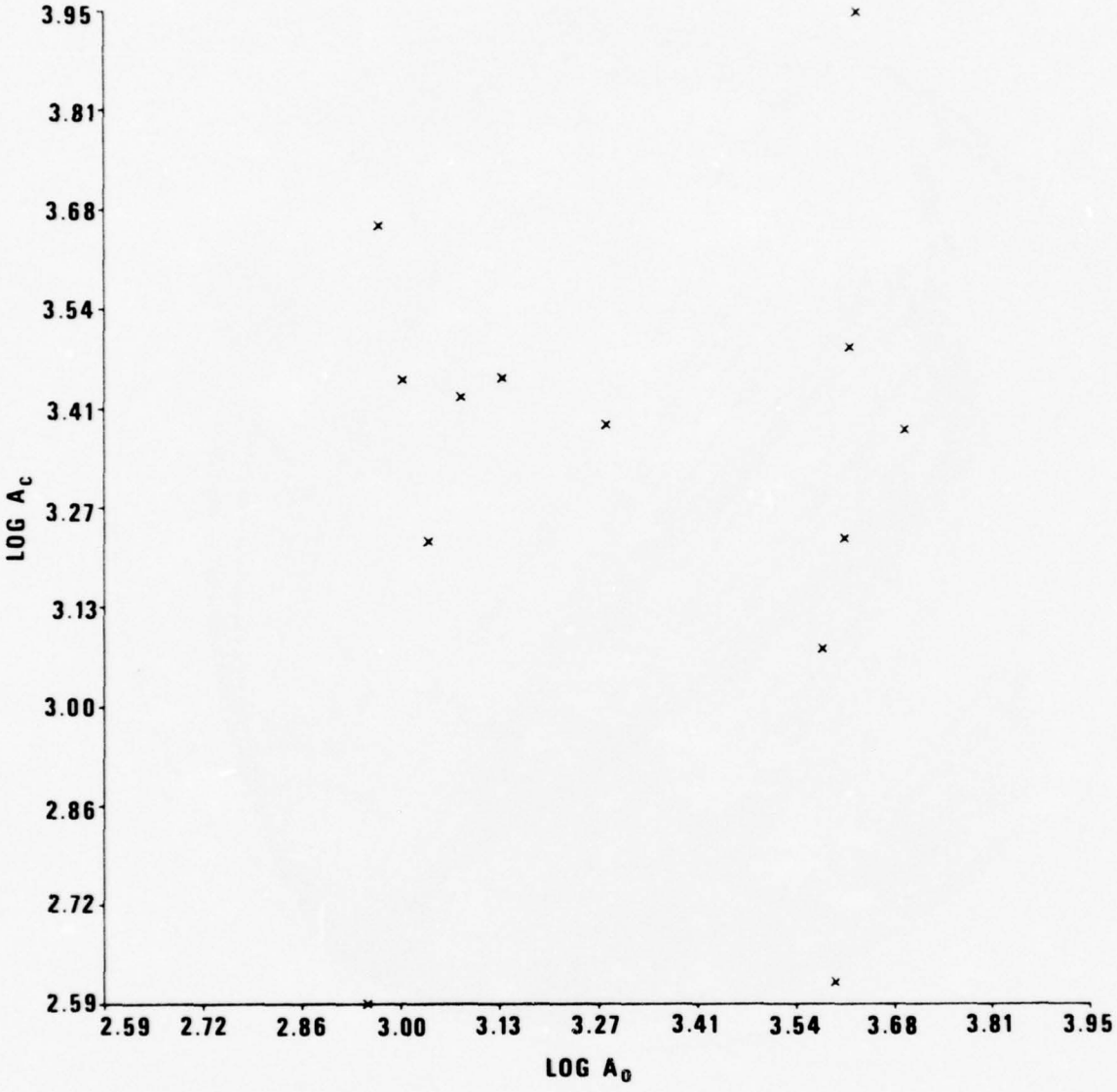

Figure 11. Log A_c versus log A_o for event 2.

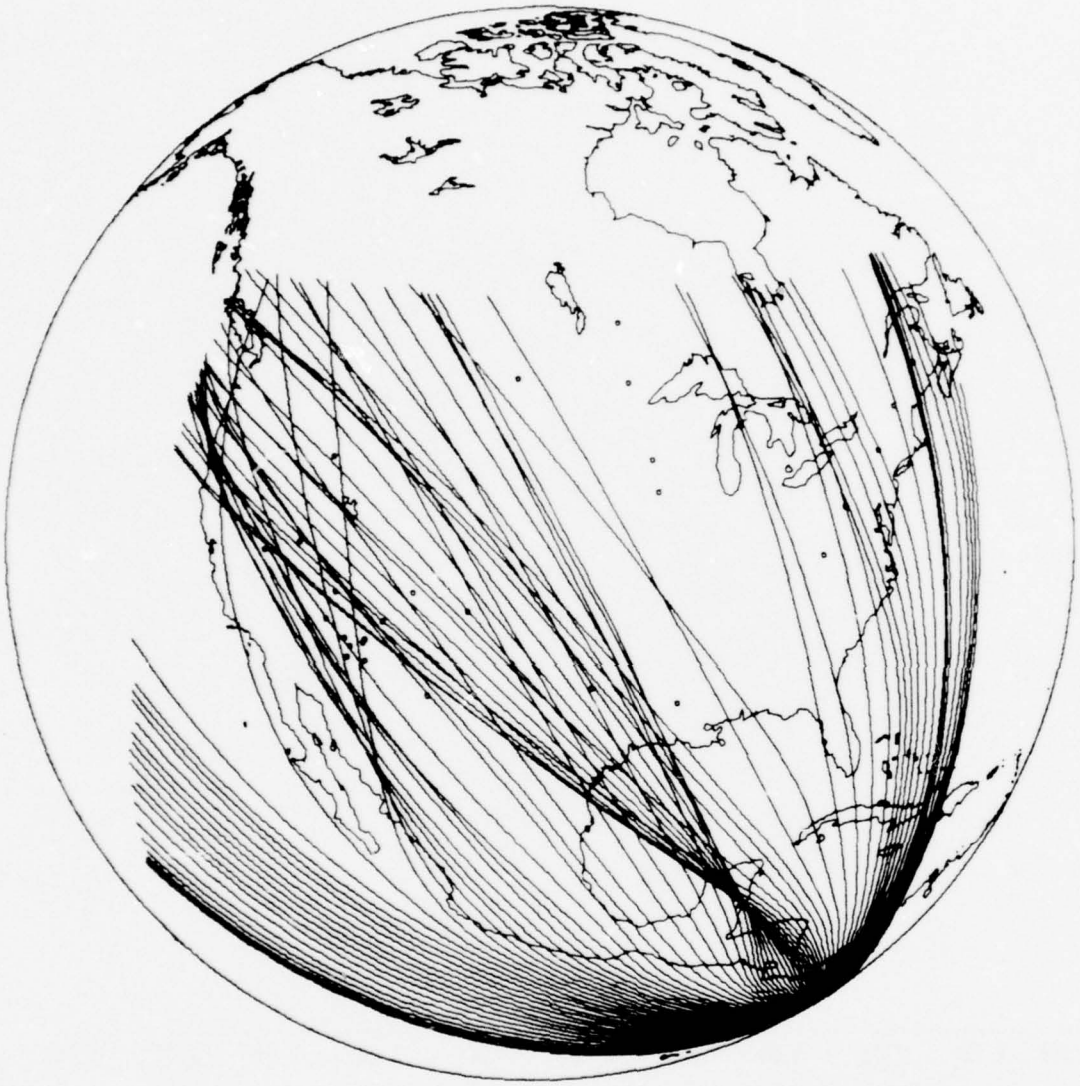

Figure 12. LR20 raypaths from event 3 - Northern Peru.

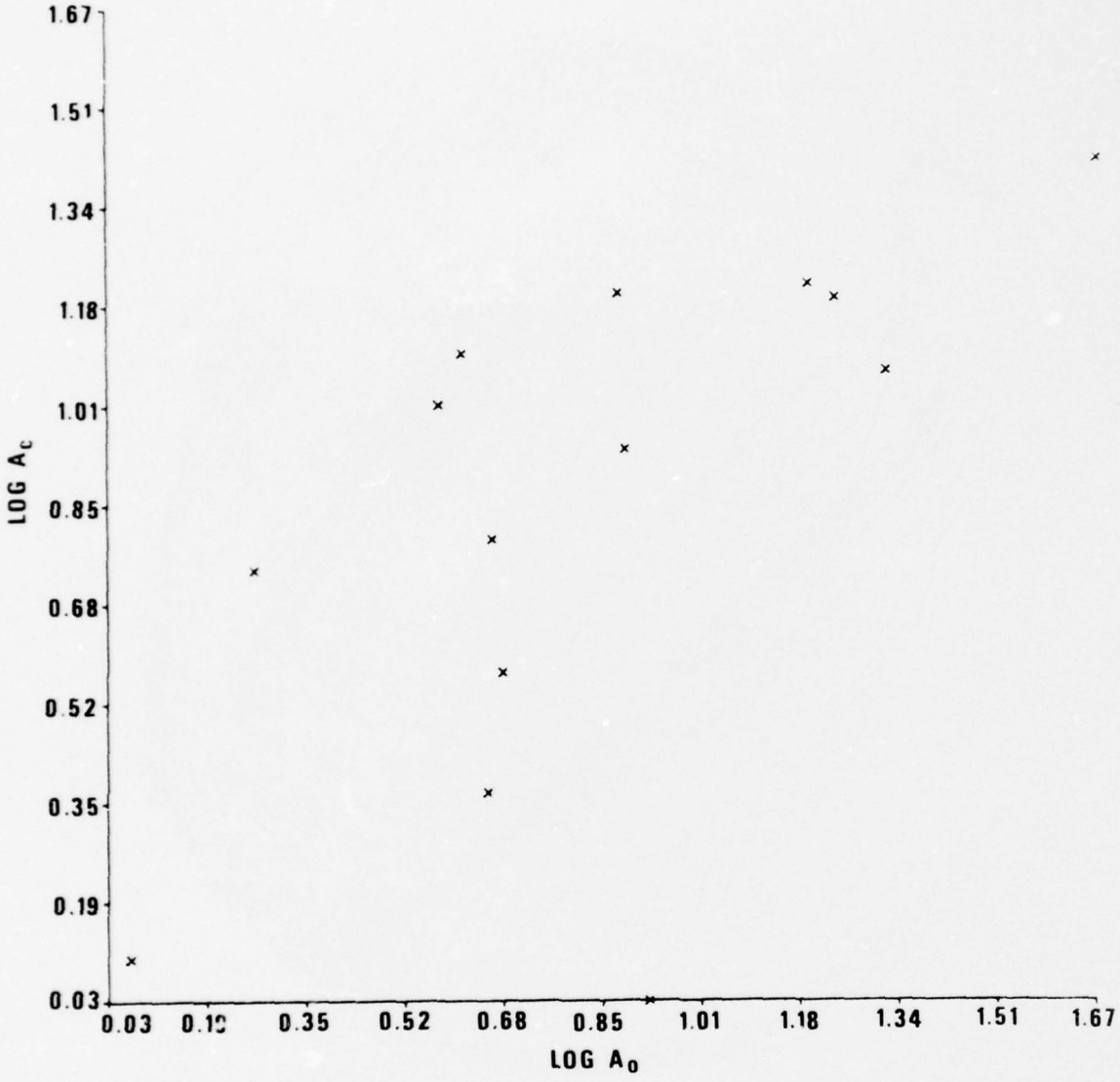

Figure 13. Log A_c versus log A_o for event 3.

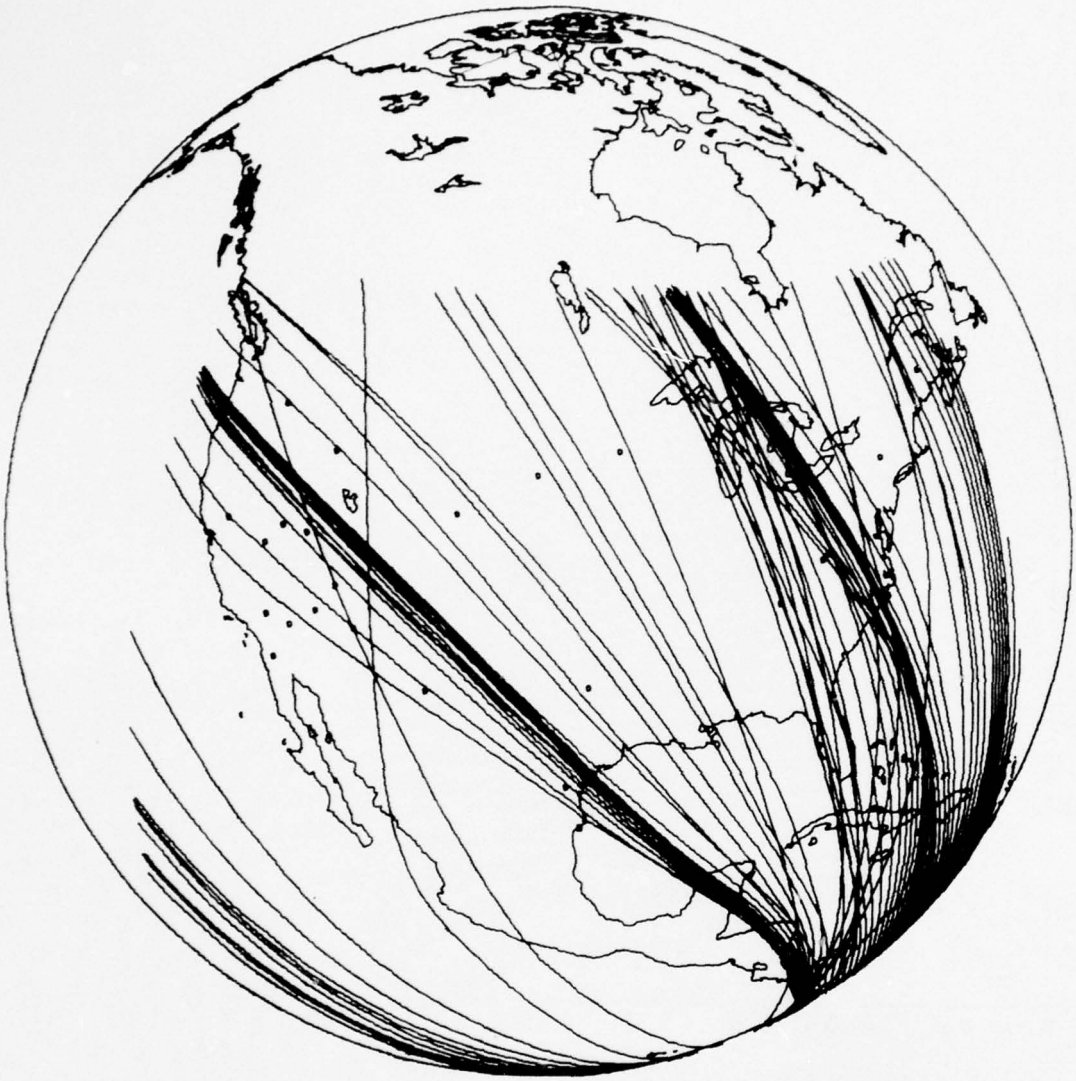

Figure 14. LR20 raypaths from event 4 - Northern Chile.

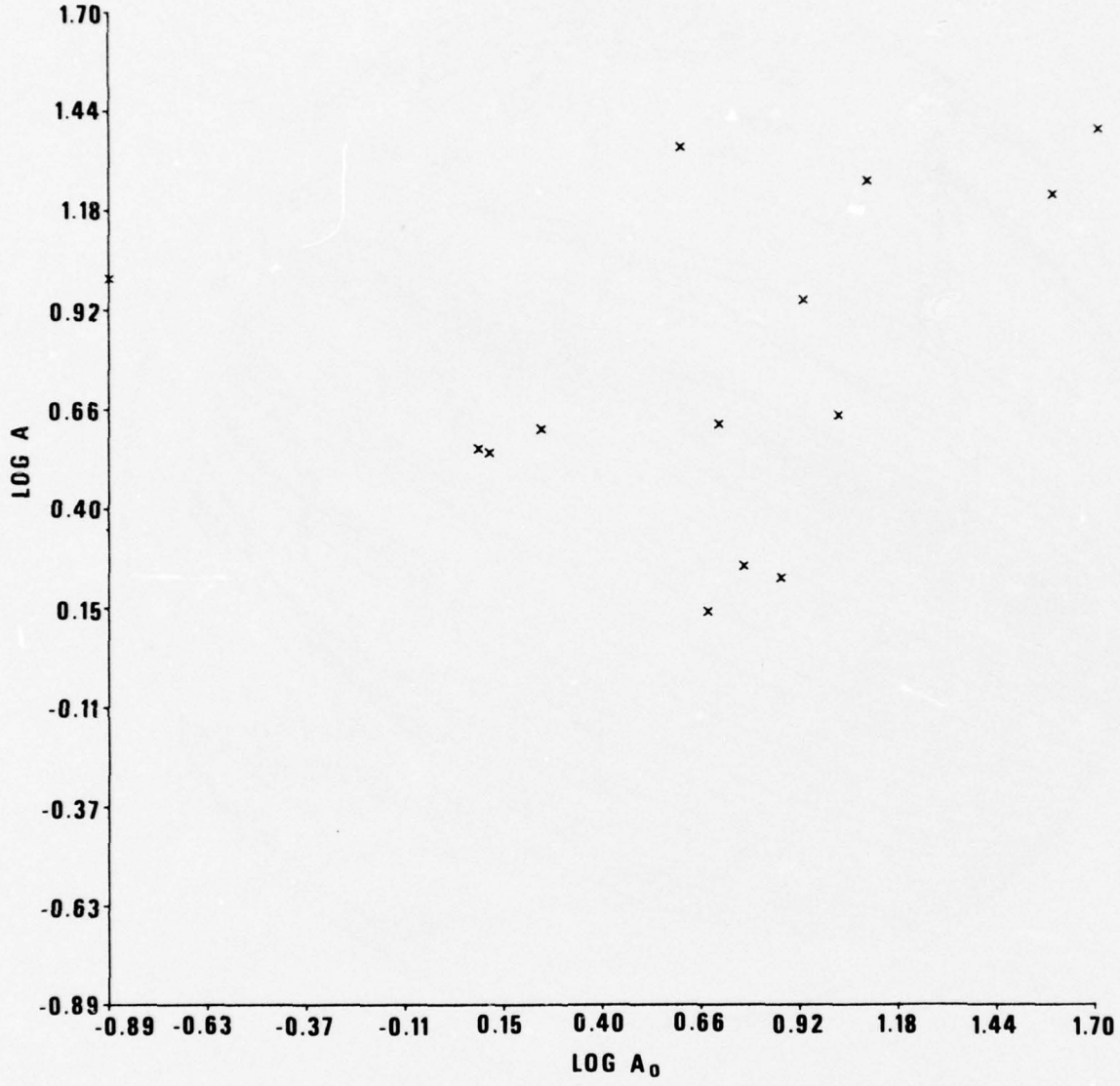

Figure 15. Log A_c versus log A_o for event 4.

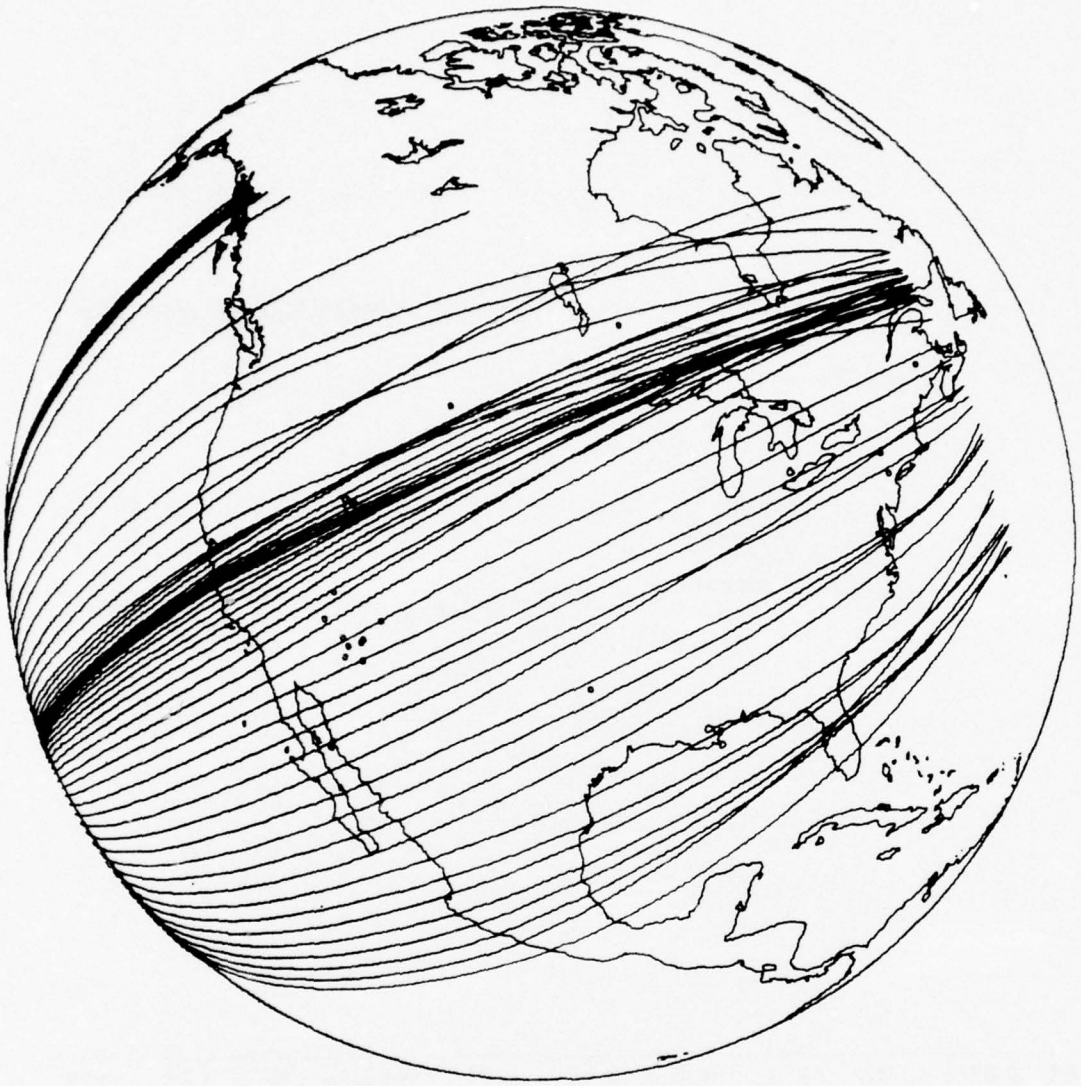

Figure 16. LR20 raypaths from event 5 - South of Fiji Islands.

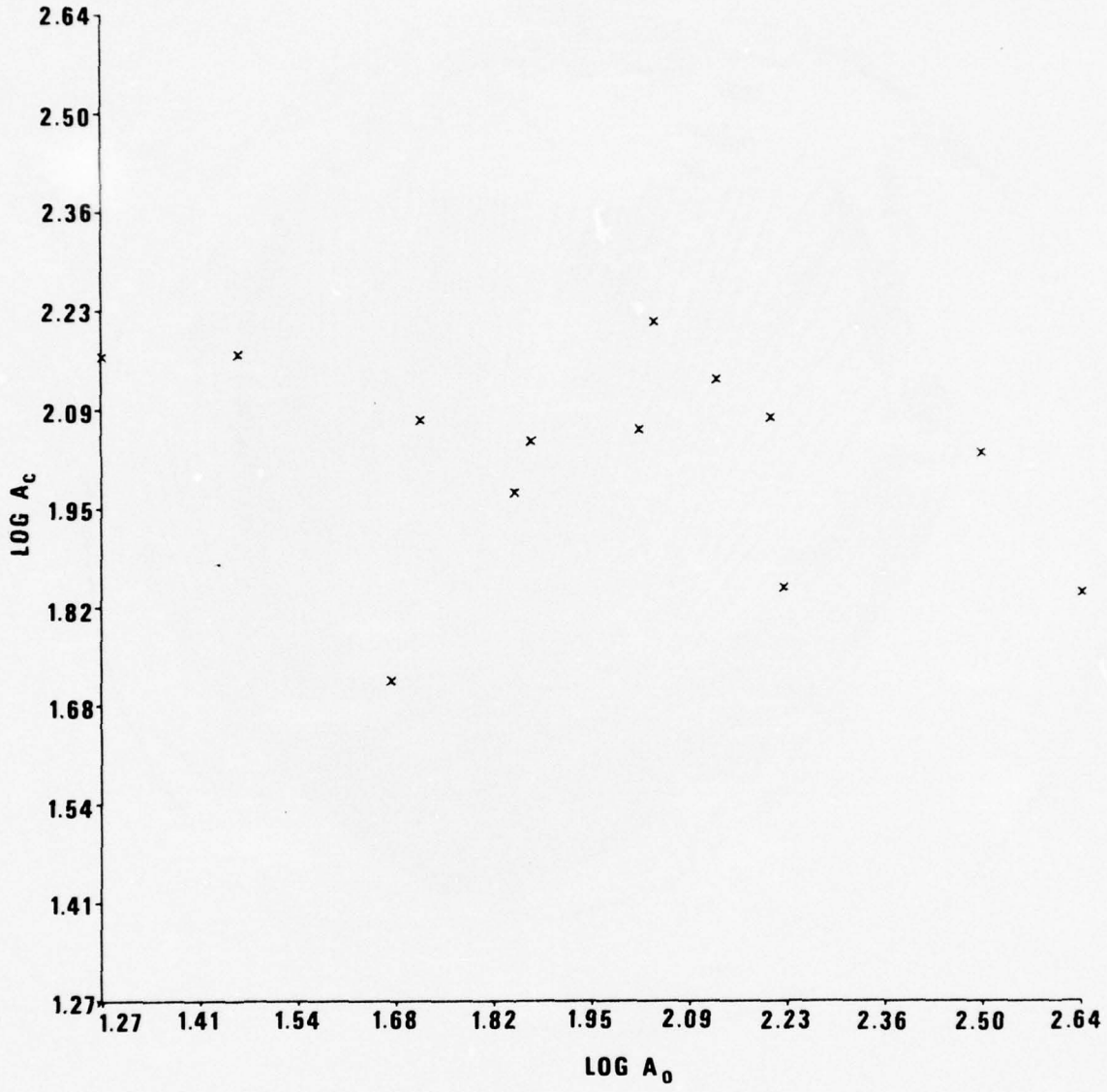

Figure 17. Log A_c versus log A_o for event 5.

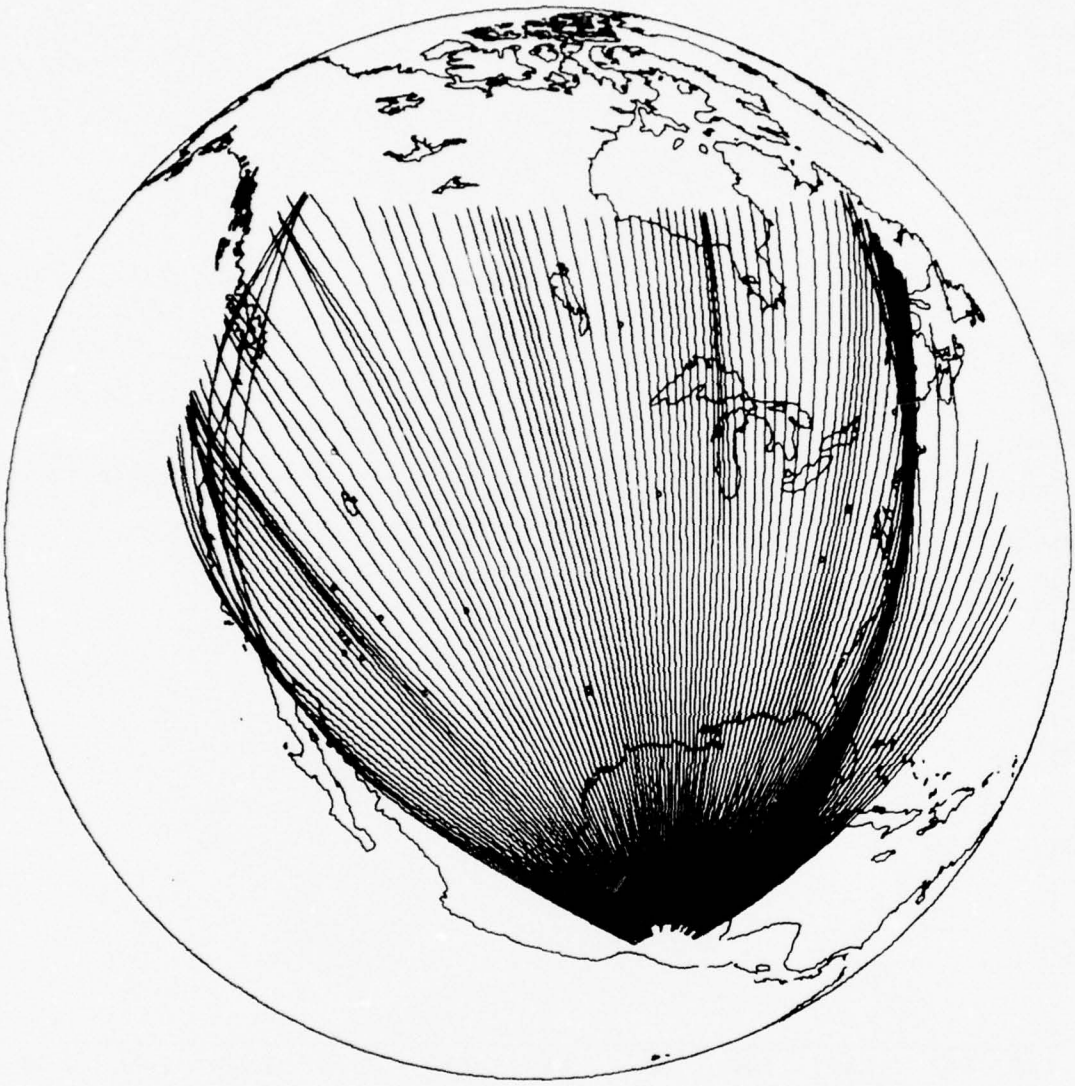

Figure 18. LR20 raypaths from event 6 - Mexico-Guatemala Border.

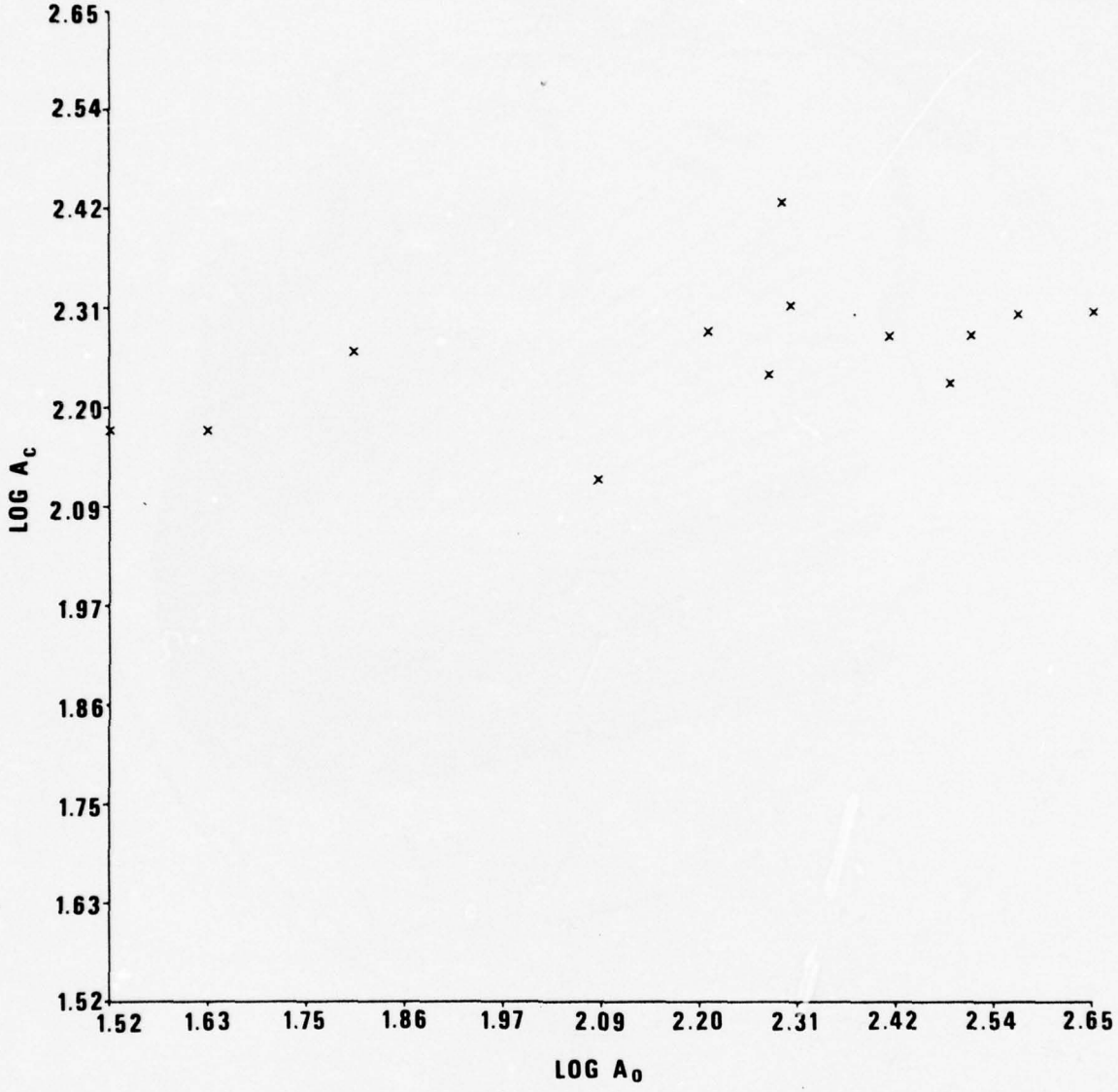

Figure 19. Log A_c versus log A_o for event 6.

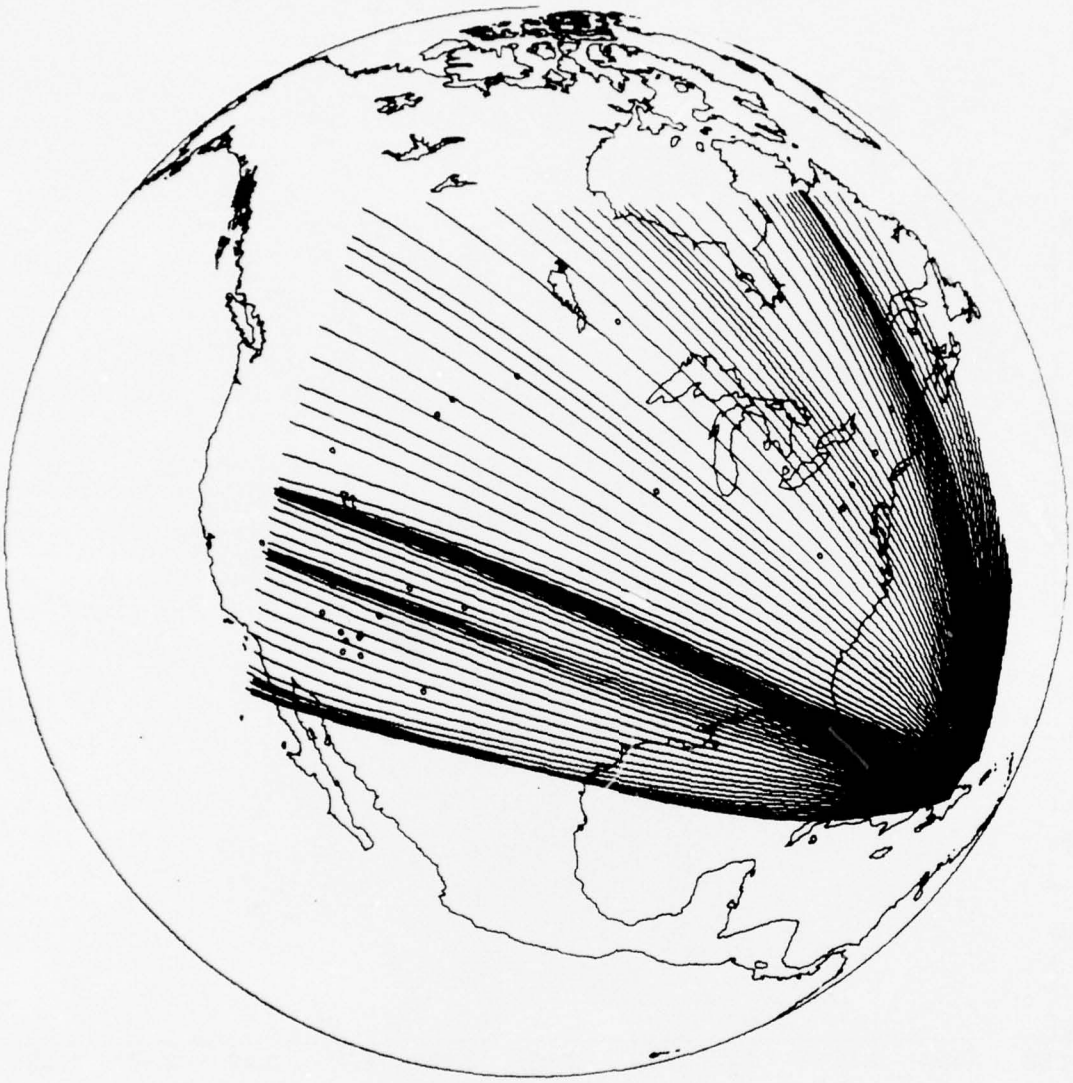

Figure 20. LR20 raypaths from event 7 - Dominican Republic.

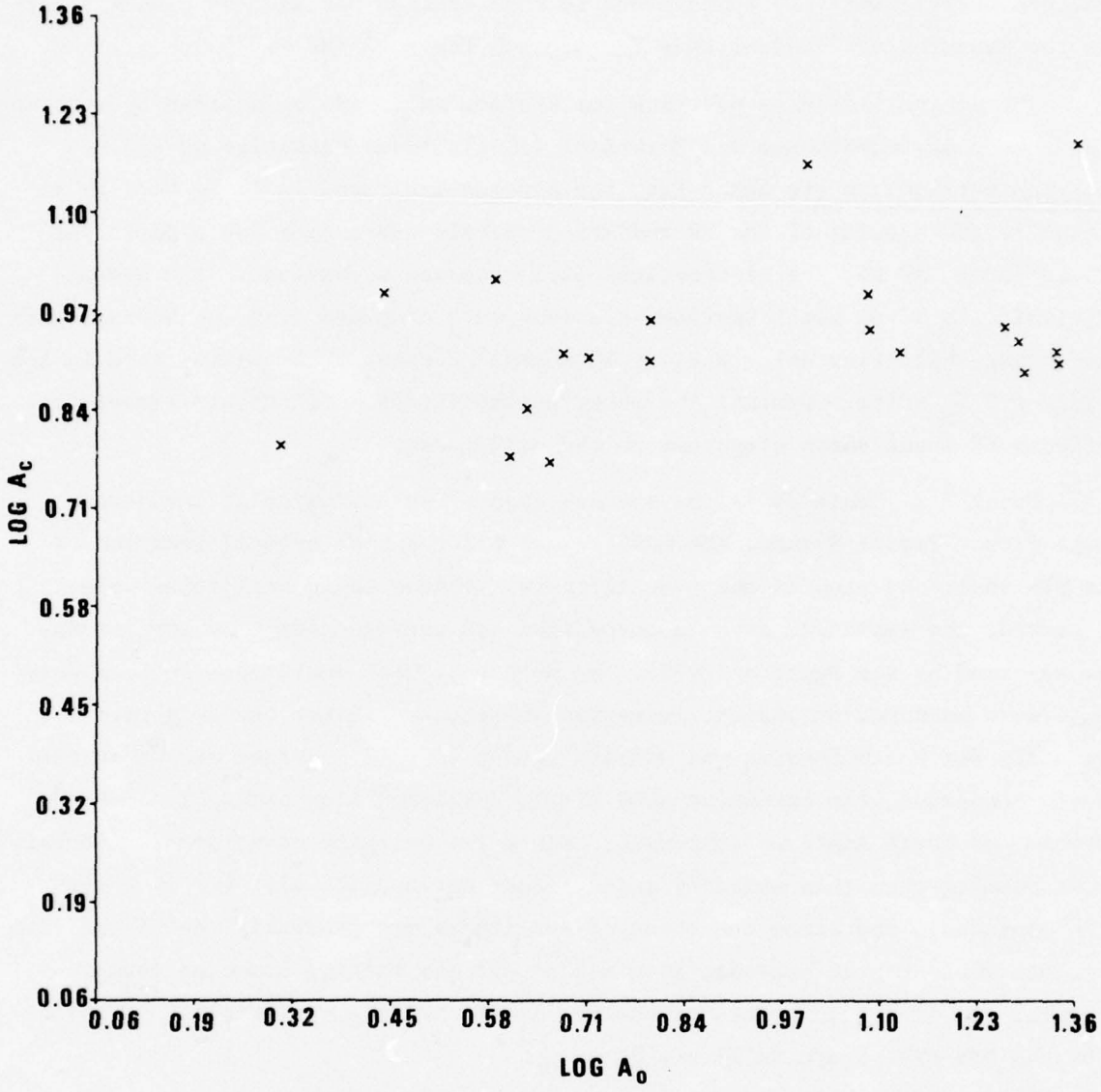

Figure 21. Log A_c versus log A_o for event 7.

pattern coefficient (RP) appropriate to each station was used as a multiplier on the measured amplitudes; this factor took the form $(RP \cdot 10^{SC})^{-1}$.

The source radiation patterns for surface waves are calculated by applying the theory of Ben-Menahem and Harkrider (1964); focal mechanism parameters for the earthquakes are taken from the sources indicated in Table VI. RP is equal to the modulus of the LR radiation pattern expression for a period of 20 seconds. RP for the hypothetical explosion was a constant. The average M_s residuals SC at North American stations were computed from the Geotech LRSM earthquake bulletins using roughly 18 months of data; these values were in the range $\pm .2$ M_s units. Normalizing observed amplitudes by SC should remove the effects of local earth structure on the amplitudes.

Event 1 in Table VI is the special case of an explosion at the Nevada Test Site. Figure 8 shows the LR20 raypaths for a hypothetical location of an NTS shot. Circles on the plot indicate stations where amplitudes were measured; the amplitude data is normalized and averaged for many explosions, as reported by von Seggern (1970). We note that most amplitudes in this data base were measured at periods less than 20 seconds. Since the LR phase velocity for North America was usually chosen to be 3.6 km/sec except in the Rocky Mountains, the ray paths show little deviation from great circle paths within the North American continent. Since the velocity structure is undoubtedly more complex than this velocity model, since attenuation also varies across the continent, and since the observed amplitudes are generally associated with periods less than 20 seconds, thus making our ray tracing somewhat inappropriate, one is not surprised to see the low correlation coefficient of .07 for the NTS data shown in Figure 9.

Figure 10 shows the ray paths for an event in the Rat Islands. The ray paths for this event are largely affected by the Aleutian Islands, as was the

---

Ben-Menahem, A. and D. G. Harkrider, 1964, Radiation patterns of seismic surface waves from buried dipolar point sources in a flat statified earth, J. Geophys. Res., v. 69, p. 2605-2620.

von Seggern, D. H., 1970, Surface-wave amplitude-versus-distance relation in the Western United States, SDL Report No. 249, Teledyne Geotech, Alexandria, Virginia.

case for LONGSHOT/MILROW/CANNIKAN. The correlation coefficient for the data shown in Figure 11 is an insignificant .08.

Figure 12 is a ray-tracing plot for an event in Northern Peru. The event is east of the Andes and raypaths are strongly affected by the coastline of northwestern South America and by the mountain ranges of Middle America. Figure 13 shows that the correlation coefficient of the data for this event is .62, which is above the 98 percent confidence level for non-zero correlation.

Figure 14 shows the raypaths from an event in the Andes of Northern Chile. As in the previous case, the rays are affected strongly by the coastline of northern South America and by the velocity structures in and around the Gulf of Mexico. Figure 15 is a plot of log A_o versus log A_c; and the correlation coefficient for this data is .32, which is significantly different from zero at the 70 percent confidence level.

The raypaths for an event south of the Fiji Islands are shown in Figure 16. The focusing of energy in the northwestern United States originates near the source within the structural features of the Tonga Trench (not shown). The focusing of energy arriving in northern British Columbia is due to the effect of the Hawaiian Islands. Log A_o versus log A_c for this event is plotted in Figure 17. The correlation coefficient for this data is -.28, indicating a poor prediction of observed amplitudes by ray tracing.

Figure 18 shows the raypaths for an event beneath the mountains at the Mexico-Guatemala border. Deviations from great circle raypaths are caused by the Yucatan peninsula and the Rocky Mountains. Observed and calculated amplitudes for this event are shown in Figure 19. The correlation coefficient for this set of data is .39 which is at the 80 percent confidence level. The small range in amplitudes calculated by the ray-tracing program is probably due to the largely uniform velocity grid for North America.

Raypaths for an event in the Dominican Republic are shown in Figure 20. The raypaths are heavily influenced by the velocity structure in the Greater Antilles arc and in the Atlantic Ocean east of the United States. Log A_c versus log A_o for this event is shown in Figure 21. The correlation coefficient for this event is .14 which is significant at only the 50 percent

confidence level. The small variation in predicted amplitudes is probably due to the same reasons mentioned in the previous case.

Application to Multipathing Observed at LASA

Another means of checking the ray-tracing predictions is comparison of calculated directions of approach of Rayleigh waves at a station to actually measured directions such as have been presented by Capon (1970) for LASA in a study on "multipathing" effects. Figure 5 and other previous ones of this report show numerous instances of predicted multipath arrivals at stations. We will here compare ray-tracing predictions to Capon's results for LR20 for six events as listed in Table VII. Using a high-resolution frequency-wavenumber spectra for successive 200-sec intervals, Capon determined power levels, arrival times, and azimuthal deviations of 40-, 33-, 25-, and 20-second energy in each 200-sec window. These results were used to determine the probable propagation paths for each frequency as shown in Figures 22, 24, 26, 28, 30 and 32. LR20 ray-paths generated by the ray-tracing program for these events are shown in Figures 23, 25, 27, 29, 31 and 33. We will briefly discuss each event.

Capon's proposed raypaths for event 1, a Kurile Islands earthquake, and the LR20 ray-tracing results for event 1 are shown in Figures 22 and 23. There are three proposed paths for LR20--one intersects the eastern Aleutian arc and is reflected at the British Columbian coast; the other two are reflected at the northwest Alaskan coastline. The ray-tracing results clearly show the first ray intersecting the eastern Aleutian Trench, refracting at the British Columbian coast north of Vancouver Island and arriving at an azimuth at 298°, which is close to the observed azimuth of 300°. There are, however, no rays that are reflected at the northwest Alaska coastline which pass within 5° of LASA. Since the ray-tracing results are for rays spaced at 1° of starting azimuth, it is possible that a ray starting out at some other azimuth could pass through the northwest Alaska continental margin and arrive at LASA; but, clearly, it would not produce appreciable amplitudes at LASA.

The proposed raypaths and the ray-tracing results for event 2, an earthquake in Mongolia, are shown in Figures 24 and 25. Capon's proposed raypaths arrive at LASA at azimuths of 329° and 336°, with the first ray reflected at

TABLE VII

Events from Capon's (1970)
Multipathing Study at LASA

Event No.	Date	Region	Origin Time (GMT)	Lat. (Deg)	Long. (Deg)	Depth
1	21 Nov 66	Kurile Islands	12:19:27	46.7N	152.5E	40
2	20 Jan 67	Mongolia	01:57:23	48.0N	102.9E	33
8	14 Jun 67	Tonga Islands	05:06:16	15.2S	173.6W	11
12	08 Sep 67	Near Coast of Northern Chile	08:59:59	23.4S	70.7W	33
16	20 Sep 67	Tristan Da Cunha Region	19:46:43	34.1S	14.6W	33
17	22 Sep 67	Central Mid-Atlantic Ridge	08:08:04	0.7S	20.1W	33

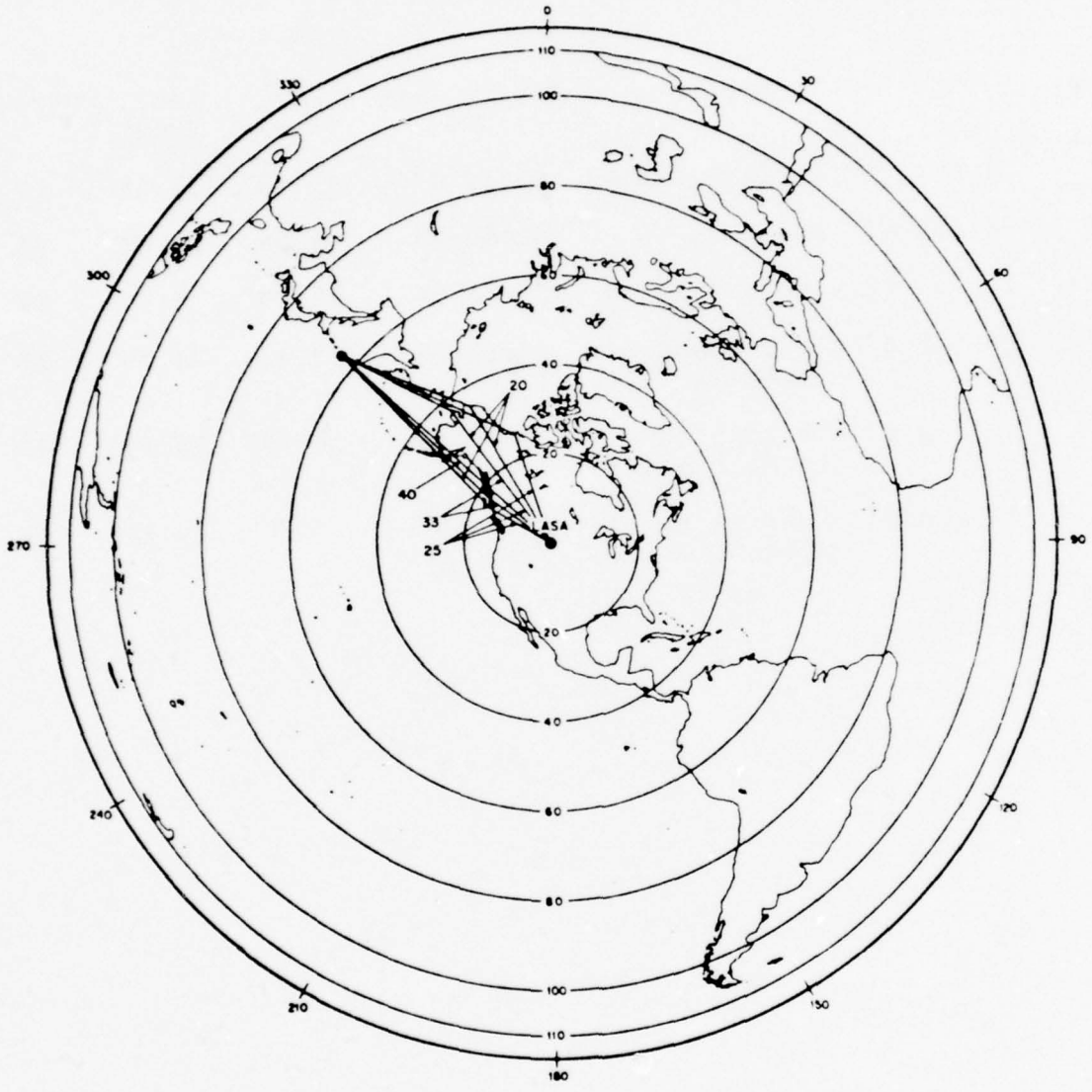

Figure 22. Capon's proposed propagation paths for event 1 - Kurile Islands.

Figure 23. LR20 raypaths for Capon's event 1 - Kurile Islands.

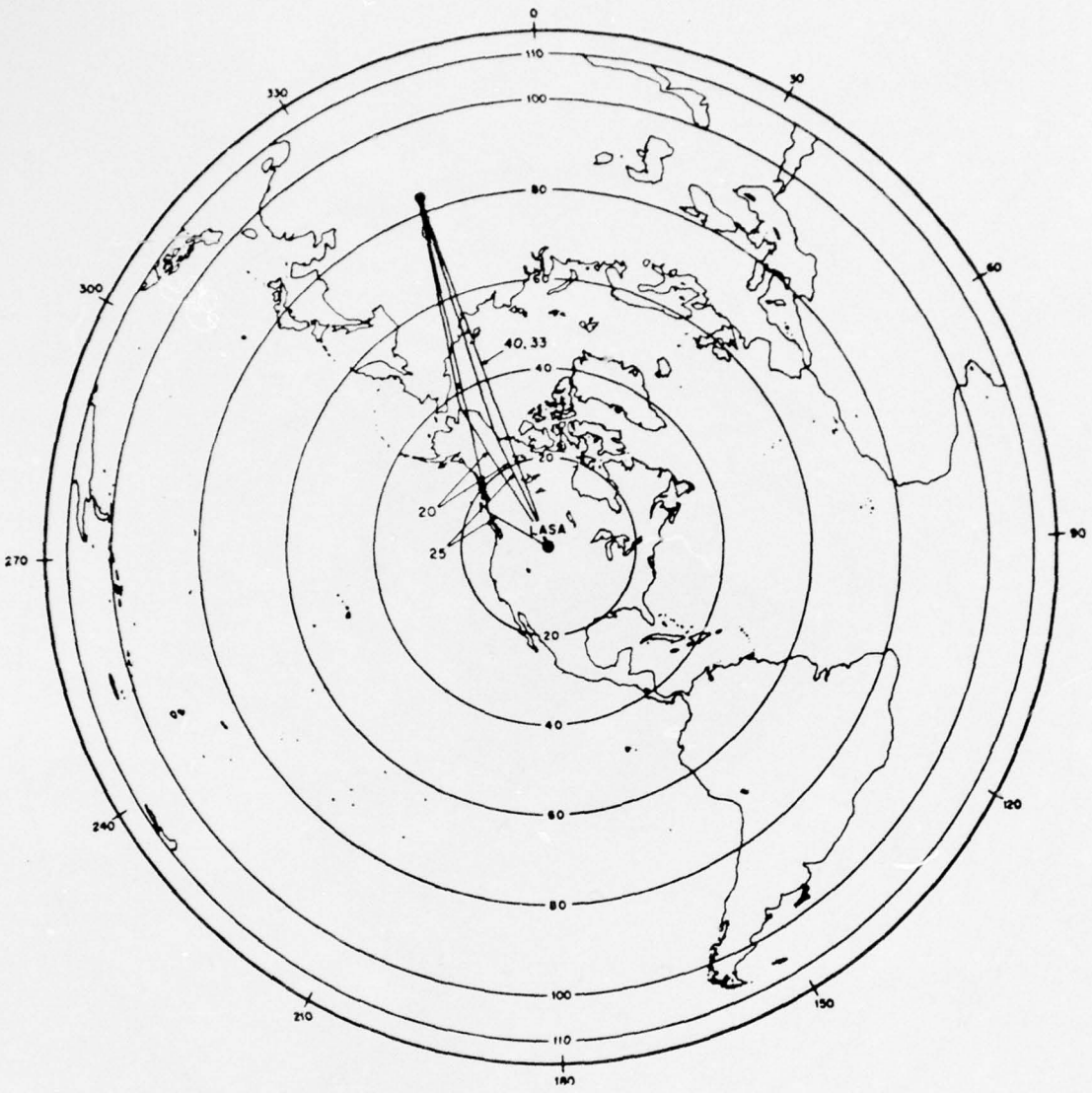

Figure 24. Proposed Propagation paths for Capon's event 2 - Mongolia.

Figure 25. LR20 raypaths for Capon's event 2 - Mongolia.

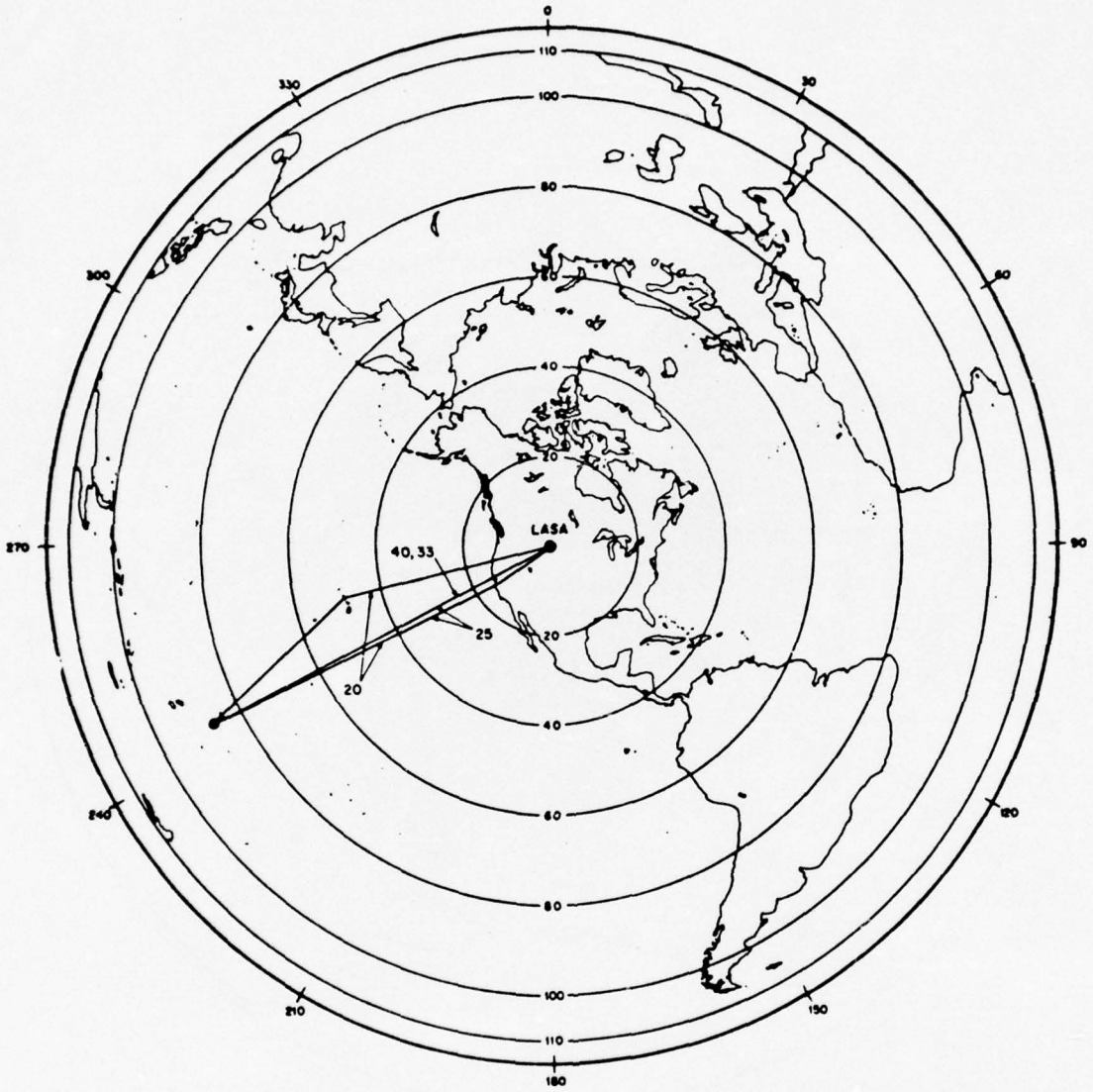

Figure 26. Proposed propagation paths for Capon's event 8 - Tonga Islands.

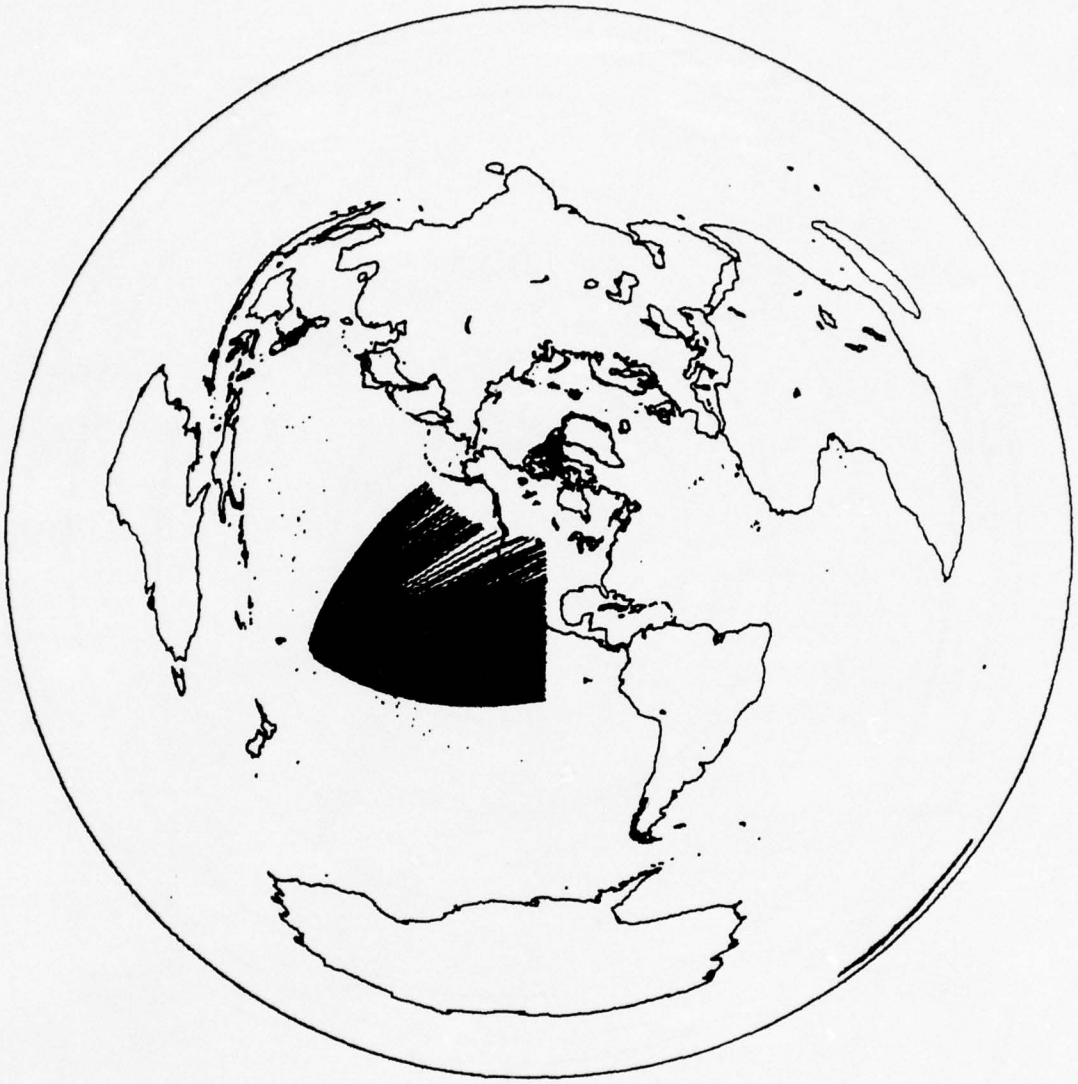

Figure 27. LR20 raypaths for Capon's event 8 - Tonga Islands.

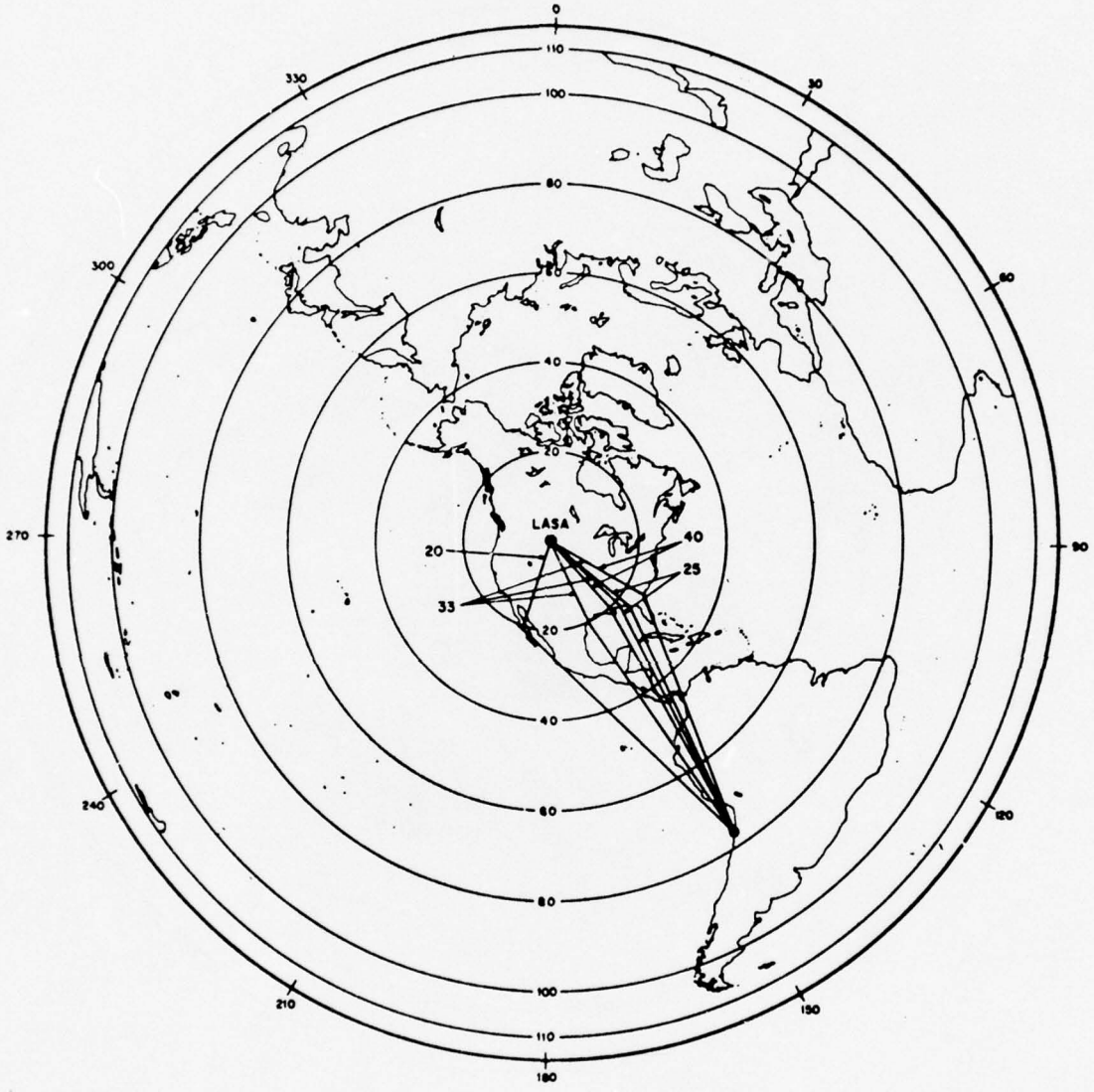

Figure 28. Proposed propagation paths for Capon's event 12 - near coast of Northern Chile.

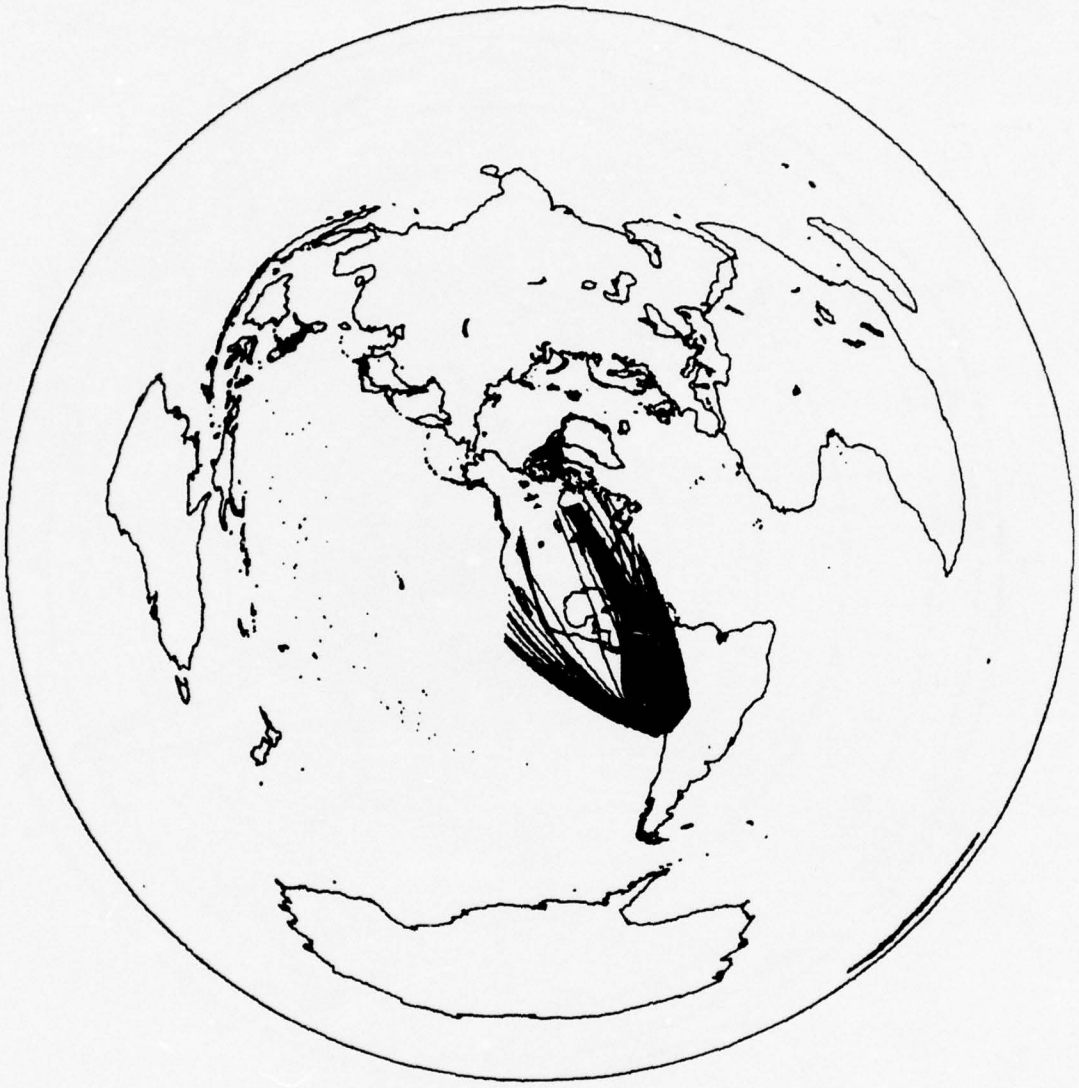

Figure 29. LR20 raypaths for Capon's event 12 - near coast of Northern Chile.

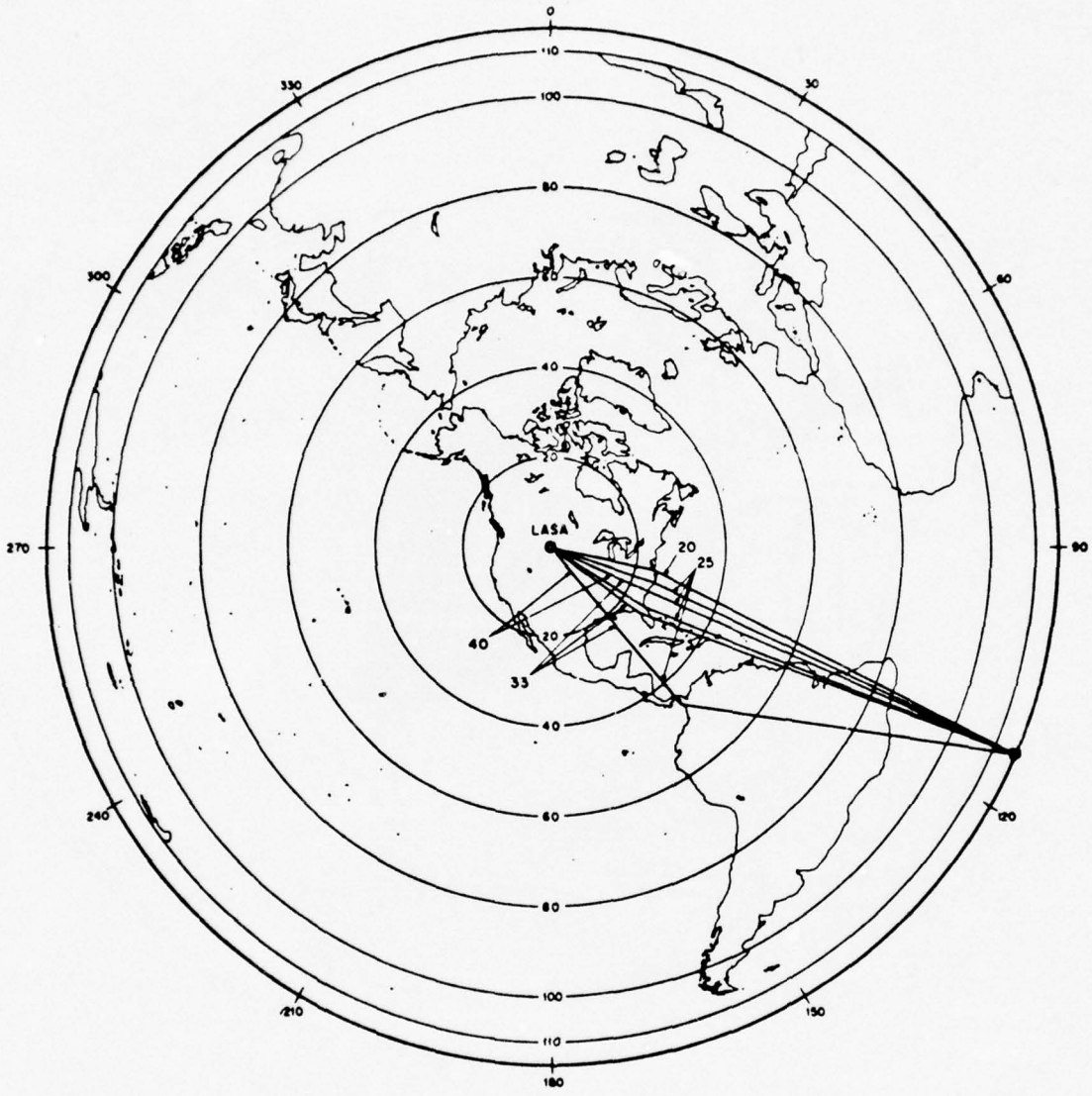

Figure 30. Proposed propagation paths for Capon's event 16 - Tristan Da Cunha Region.

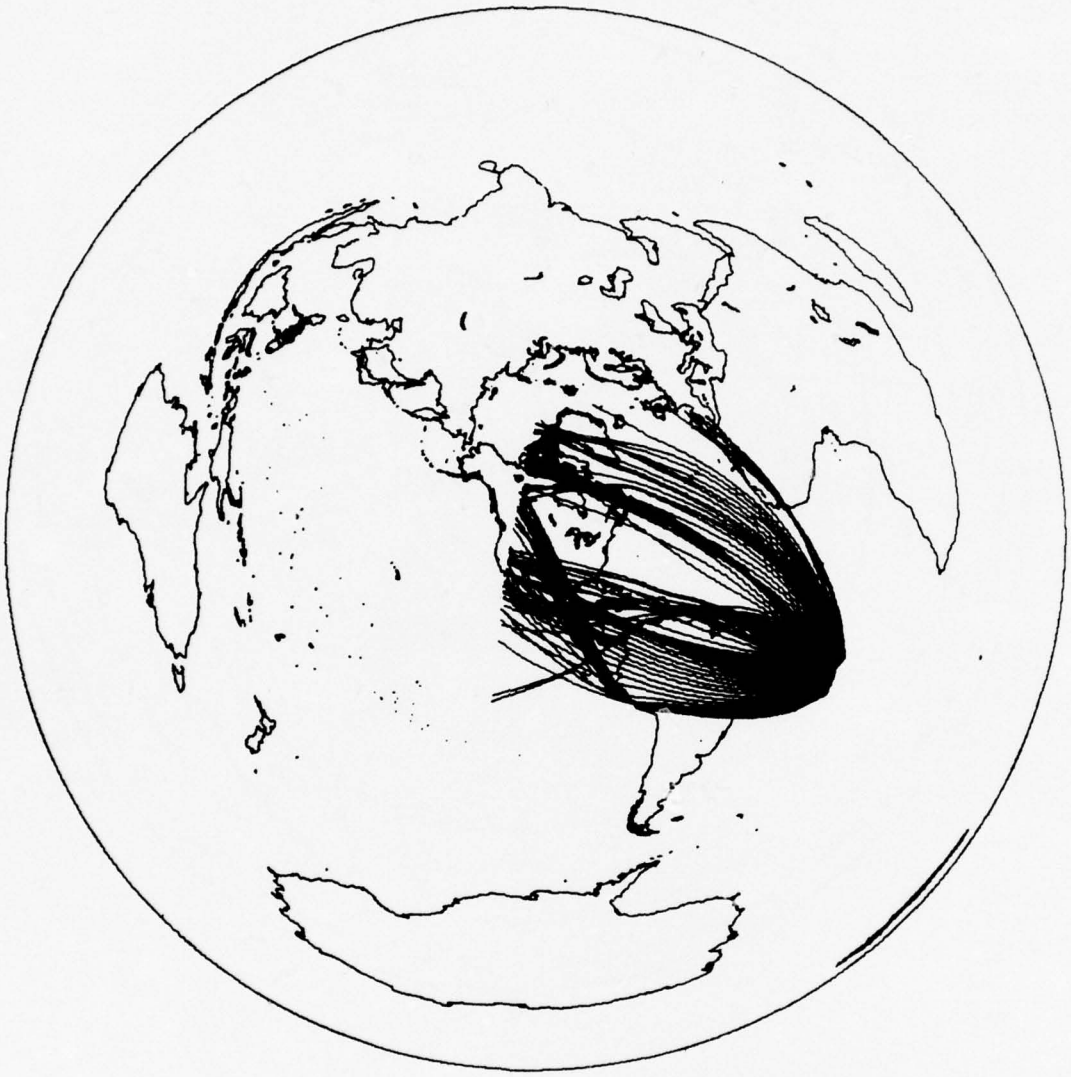

Figure 31. LR20 raypaths for Capon's event 16 - Tristan Da Cunha Region.

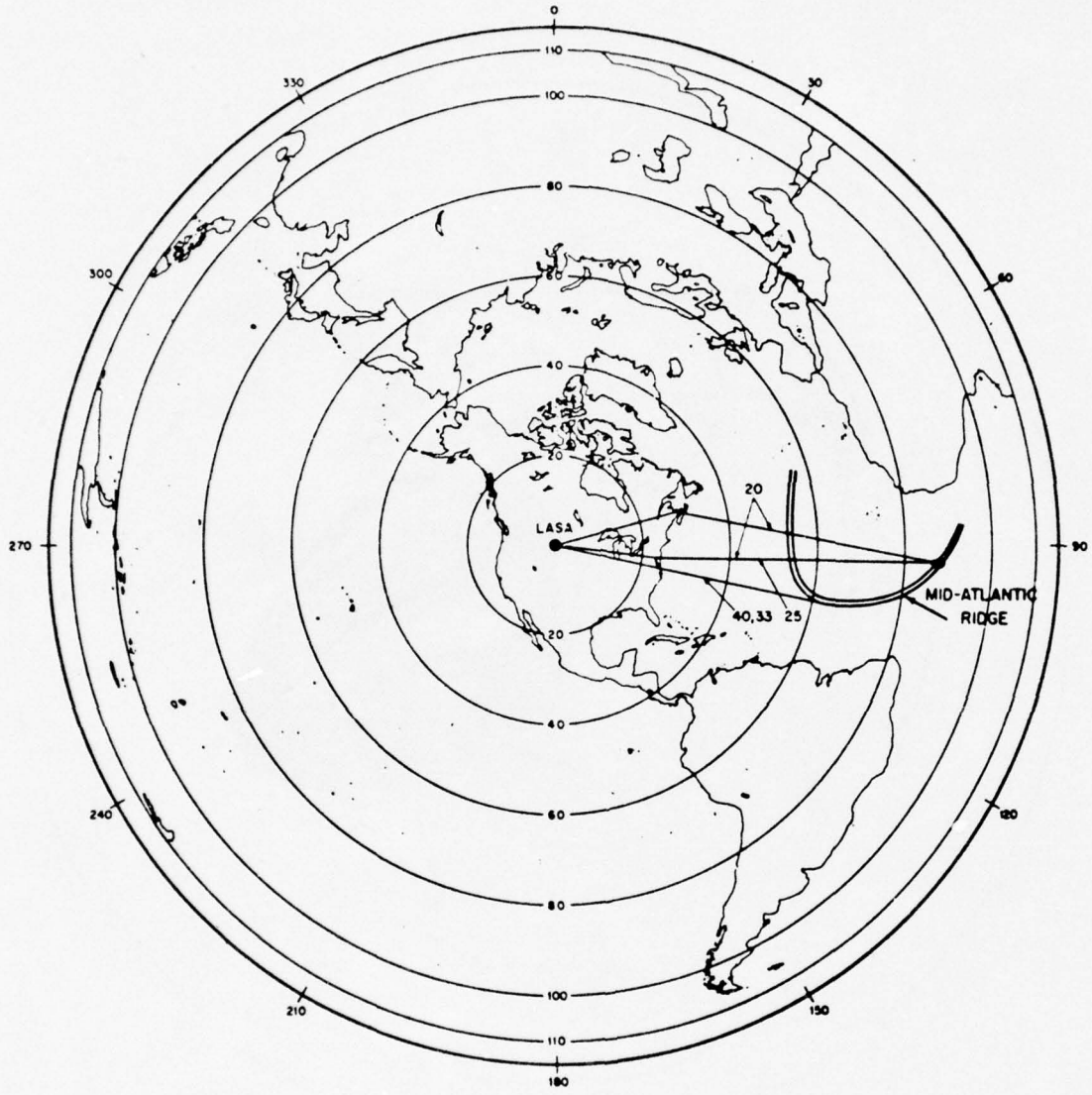

Figure 32. Proposed Propagation paths for Capon's event 17 - Central Mid-Atlantic Ridge.

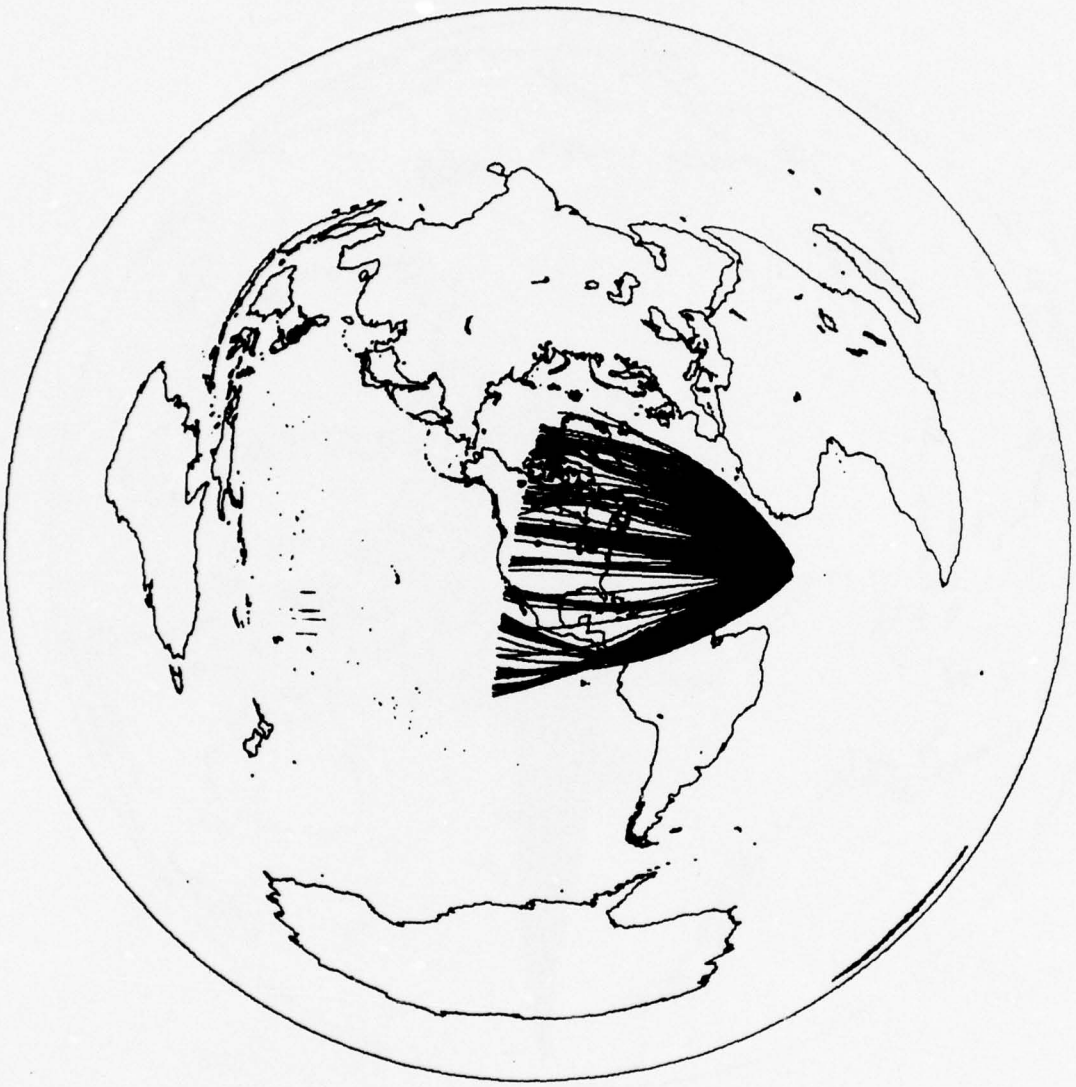

Figure 33. LR20 raypaths for event 17 - Central Mid-Atlantic Ridge.

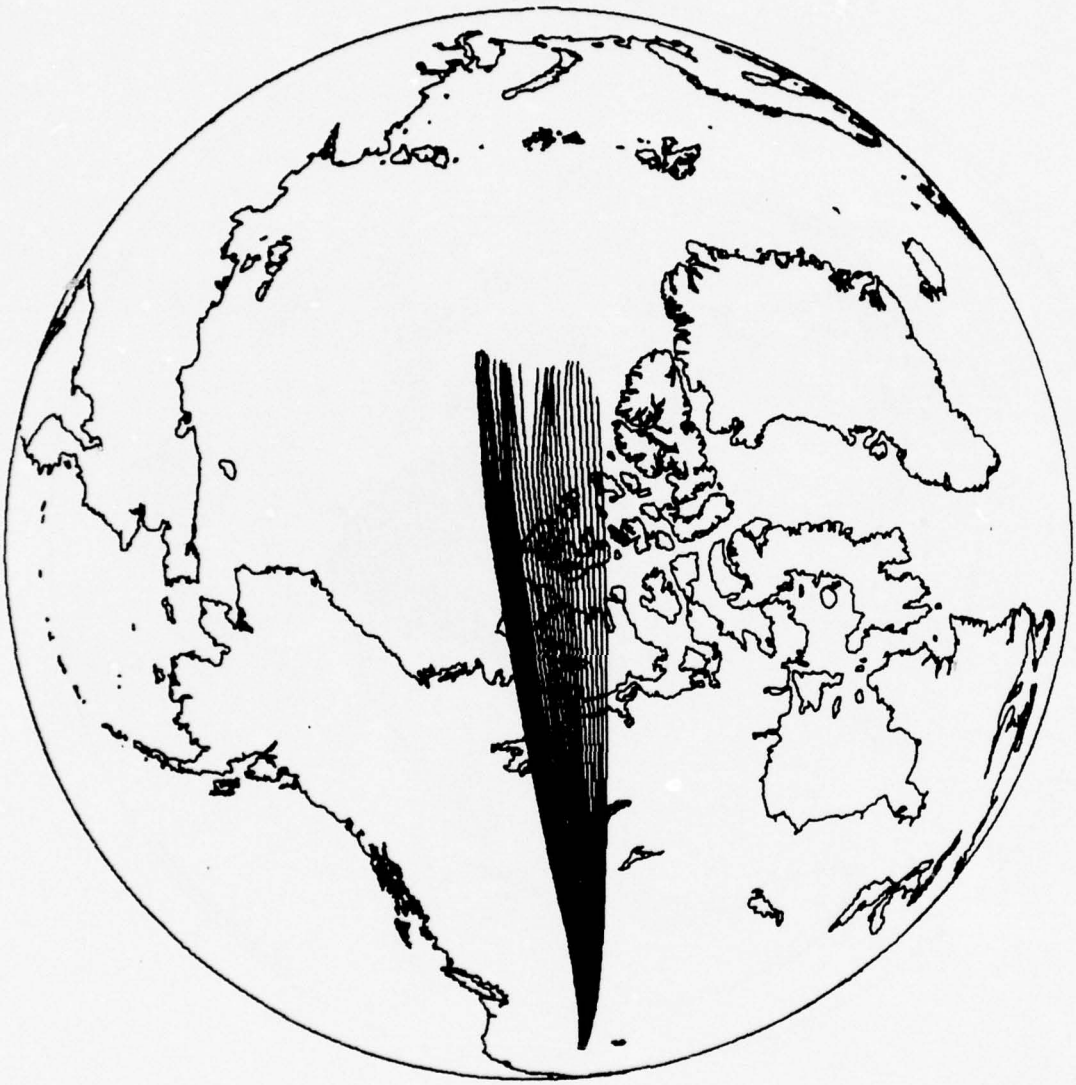

Figure 34. LR20 raypaths from the Nevada Test Site to NPNT.

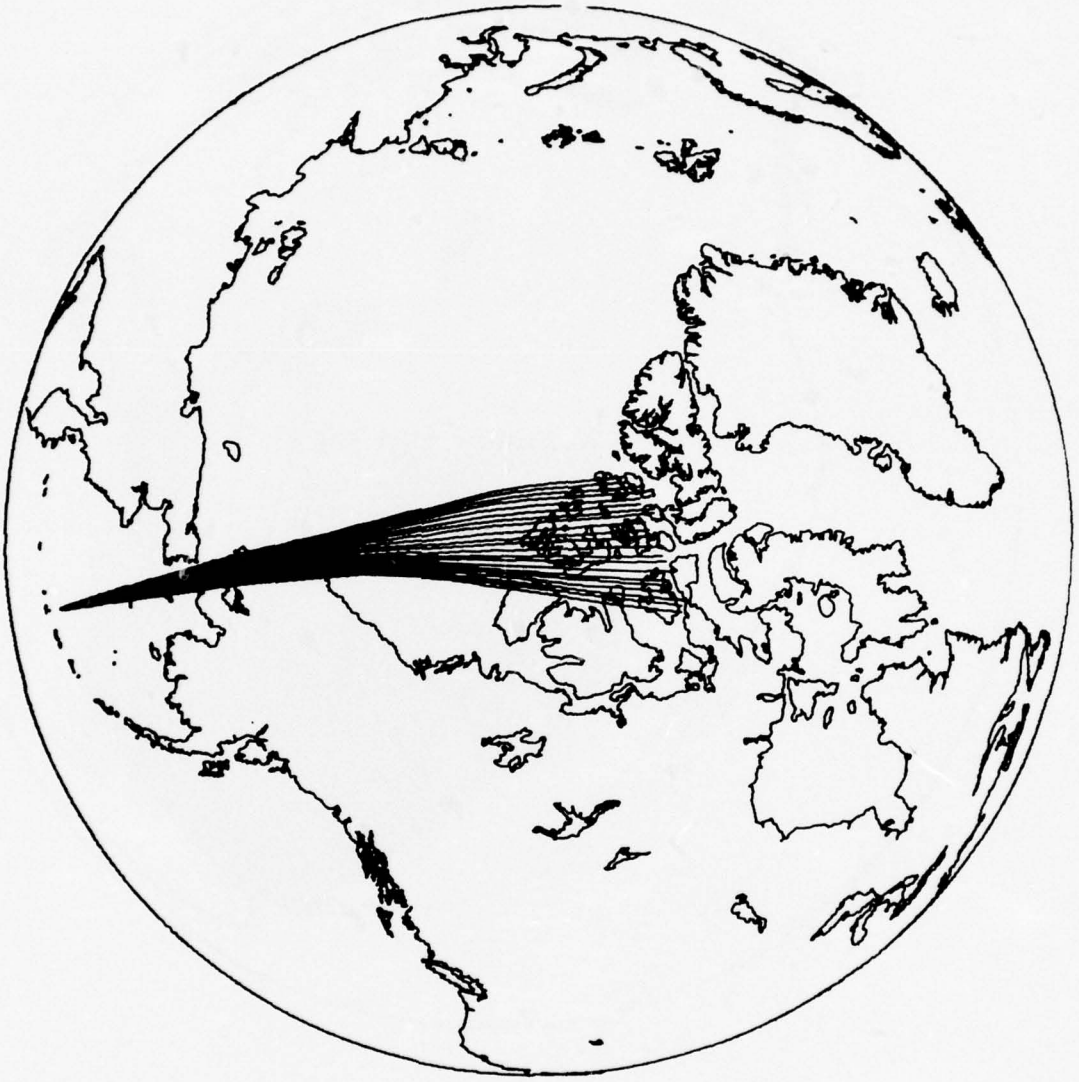

Figure 35. LR20 raypaths from the Amchitka Test Site to NPNT.

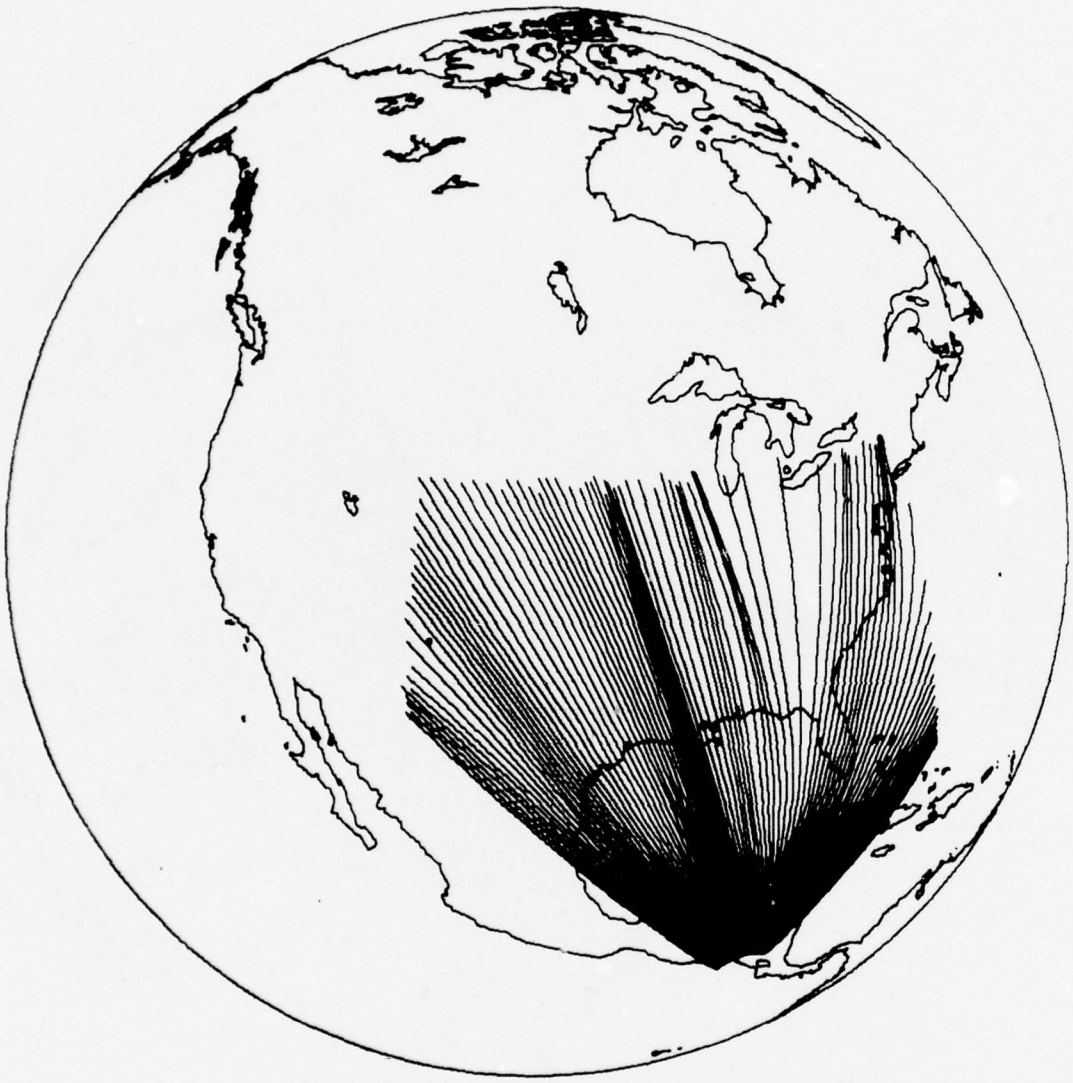

Figure 36. LR20 raypaths from an event in Middle America at 11.0N, 87.0W to ALQ and OGD.

Figure 37a. LR20 raypaths from Amchitka Island using original velocity grids.

Figure 37b. LR20 raypaths from Amchitka Island using randomized velocity grids.

the northwest Alaska coastline and the second and larger amplitude ray reflected at the Yukon coast. The ray-tracing results show two rays passing close to LASA. The larger amplitude ray crosses into North America at the northwest Alaska coastline and arrives at LASA with an azimuth of 316°. The smaller-amplitude second ray crosses into North America in the western Northwest Territories and arrives at LASA with an azimuth of 345°. The ray-tracing predictions for arrival azimuth are off by -13° for the first ray and +9° for the second ray, and the relative amplitudes of the ray-tracing predictions are the reverse of the measured amplitudes. Refinements in the velocity grid, especially in the Arctic Ocean and in northern Russia, could improve these results. Although the azimuth measurements were off by about 10° and the relative intensities were reversed, the ray-tracing program did predict the two different observed raypaths approaching LASA, one from Alaska and the other from north of LASA.

Capon's event 8 is an earthquake in the Tonga Islands. Figure 26 shows the two proposed raypaths: the larger amplitude arrival is refracted near the Hawaiian Islands and arrives at an azimuth of 257° and the smaller amplitude arrival approximately follows a great circle path and arrives at an azimuth of 238°. The LR20 ray-tracing results in Figure 27 show only one raypath arriving at 250°, or close to Capon's azimuth for a raypath reflected by the Hawaiian Islands. The large deviation in the ray-tracing results from a ray expected along a great circle path is probably due to refraction of the raypath as it passes through the western mountain ranges of North America. Mountain ranges such as the Sierra Nevada show more areal extent and larger velocity variations than the Hawaiian Islands region and would be a better possibility as a site of Rayleigh-wave refraction.

Figures 28 and 29 show Capon's proposed raypaths and LR20 ray-tracing results for an event near the coast of Northern Chile. There is only one raypath proposed by Capon for this event--it is refracted by Baja California and arrives at LASA at an azimuth of 197°, 50° off of the expected great circle arrival. Figure 29 shows no LR20 raypaths within 5 degrees of LASA, but some rays are refracted by the western continental margin of Mexico and it is possible that a ray starting out at some other azimuth than the ones

used in the computations could be refracted by the coastlines of western Mexico or Baja California and arrive at LASA.

Capon's proposed raypaths for an event near the Tristan Da Cunha Region on the South Mid-Atlantic ridge are shown in Figure 30. There is one LR20 raypath which is refracted at the North American continental margin near Virginia and arrives at LASA with an azimuth of 104°. The LR20 ray-tracing results in Figure 31 show that the possibility of such a raypath with the present velocity grid would be small because the ray would be refracted by the continental margin off northeast Brazil. Instead the ray-tracing program predicted an arrival refracted off the coastline of Peru, arriving at LASA with an azimuth of 149°, which is close to the expected azimuth for 25- and 33-second waves shown in Capon's plot as refracted by the western continental margin of Columbia. There is the possibility that at some azimuth not shown in Figure 31, or with a refined velocity grid, a ray could pass through Brazil or north of Brazil and arrive at the expected azimuth at LASA.

Figure 32 shows Capon's proposed raypaths for an event on the Central Mid-Atlantic Ridge. There are two LR20 raypaths--one approximately along a great circle path arriving at LASA with an azimuth of 98° and another one of the same amplitude refracted off Nova Scotia and arriving at LASA with an azimuth of 76°. The LR20 ray tracing results illustrated in Figure 33 show only the raypath along the great circle arriving at LASA with an azimuth of 96 degrees. The velocity structure around the Grand Banks region off Newfoundland could produce a large refraction but none was seen in Figure 33. There is some refraction in the area of the Labrador Basin southwest of Greenland and this is an alternative raypath to the one shown by Capon to be refracted off Nova Scotia.

The ray-tracing results for Capon's six events show some agreement with observed azimuths for arrival at LASA but do not duplicate all the observed arrivals. We feel that the arrival directions seen by Capon are mostly correct; such data could serve to make improvements in our velocity grid. A greater density of rays starting at the source could perhaps produce more of the rays observed at LASA. Rayleigh-wave ray-tracing could be used to confirm arrivals observed on a high-resolution frequency-wavenumber plots and also to indicate possibly spurious signals on such plots.

Special Cases

One special case to be considered is that of amplitudes at station NPNT from the Nevada Test Site (NTS) and from the Amchitka Test Site (ATS). Von Seggern (1971) has shown that for equivalent-yield explosions the spectral amplitude at 20-sec period from NTS is larger than that from ATS by a factor of roughly two. Figures 34 and 35 show that LR20 raypaths from NTS and from ATS to NPNT. The station NPNT is marked by a circle at the center of the plot. From the ray-tracing results in these figures, the amplitude at NPNT from an explosion at NTS is predicted to be larger than the amplitude from an explosion at ATS by roughly 20%. This result is in the right sense but still does not fully explain the observed amplitudes.

A second special case to be considered is that of amplitudes at the LPE sites ALQ and OGD from an event in Middle America. Calculation of M_s residuals for 8 months of data recorded at high-gain long-period stations (von Seggern, 1975b) revealed an unusually high relative residual between these two stations for events in this area: M_s residuals at OGD average +.20 and those at ALQ average -.17. This means that amplitudes at OGD should be about 2.3 times the amplitudes at ALQ when distance effects are removed. Figure 36 shows raypaths from an imaginary event in Middle America at 11.0N, 87.0W. The only correction applied to the ray-tracing intensity calculation was for distance. The amplitude at OGD was found to be 1.8 times that at ALQ, which is a good approximation to the observed amplitudes. Note that we have made no corrections for radiation pattern since we are considering average empirical results from many events or for attenuation which is largely unknown for these paths.

Discussion of Calculated and Observed Amplitudes

Although some of the results with the ray-tracing program are good and demonstrate that the ray-tracing program can be used to predict amplitudes, a majority of the calculated amplitudes showed a poor correlation with observed amplitudes. One major cause of error is the velocity grid. The grid used in this study was our initial attempt at defining an LR20 grid for the world; and further ray-tracing work would lead to improvements in the velocity grid.

---

von Seggern, D. H., 1975b, Distance-amplitude relationships for long period P, S, and LR from measurements on recordings of the long-period Experimental stations, SDAC-TR-75-14, Teledyne Geotech, Alexandria, Virginia.

Errors in the velocity grid overwhelm any numerical errors in ray tracing in regard to the intensity calculations, especially when one considers the cumulative effect of changes in the velocity grid along the raypath. Moreover, since each 1° square represents an average velocity for that square, in cases where velocities vary by a few tenth km/sec over a distance of one or two wavelengths, as for example at continental and plate boundaries, velocity gradients calculated by the ray-tracing program would be in error. One method of solving this problem would be to reduce the grid spacing in regions of large velocity gradients, although one is limited in this approach by computer storage space.

Another problem with the ray-tracing program is that it assumes uniform attenuation. As is evidenced in those cases where the rays travel through large regions of homogeneous velocity and there are still large amplitude deviations observed from real events, attenuation variations are surely a large contributor to the scatter in observed amplitudes. The ray-tracing algorithm could easily accommodate an attenuation grid along with the velocity grid, but our knowledge of attenuation is much less detailed than of velocity.

The radiation-pattern correction, which was divided into the observed amplitude, varied from 0.2 to 1.0. A slight change in the orientation of the fault plane could thus have a large effect on A_o. Therefore the radiation-pattern correction should also be considered a source of error in the comparisons of A_o and A_c.

A critical test of the ray-tracing program concerns those amplitudes near caustics. Remember that, for the events in Table VI studied earlier, we had avoided comparing predicted amplitudes of rays near caustics with observed rays. This amounted to 13% of the data available, or 31 points. However, if the ray-tracing is meaningful, we should expect observed amplitudes at these points to be high, on the average, relative to observed amplitudes for points not predicted to lie near caustics. A simple check on this hypothesis can be made by noting how many of the observed data points not used for this reason actually had positive M_s residual for the event with which they were associated. Of the 31 data points, only 15 in fact had the desired positive

M_S residual. This result is the basis of a conclusion that the positions of caustics is predicted very inaccurately and that even small errors in the velocity grid can show caustics to occur where none do in reality. Thus, perhaps only gross features of the observed amplitude pattern can be predicted with ray tracing unless a highly accurate velocity grid is achieved.

A method of simulating errors in the velocity grid is to randomize the velocity values at each grid point by adding a normally distributed variable to each velocity, rerun the ray-tracing program, and compare the results with that from the original grid. We chose to add randomly $\pm$.1 km/sec to each velocity value in that part of the grid needed for computing rays over North America from Amchitka Island. We earlier stated that we felt that our velocity grid was accurate in most places to within .1 km/sec. Of course the magnitude of actual errors in the velocity grid is not uniform over the grid but varies with region according to how well the phase velocities could be estimated. Thus we are not exactly simulating possible errors in the grid by randomizing it everywhere by the same amount; but to do so exactly would require for each grid value a measure of confidence which we have not attempted to compile.

The ray-tracing diagrams over North America for the orginal grid and the randomized grid are shown in Figures 37a and 37b. Note that the gross features of the two patterns agree; but if particular stations, as marked by circles in these diagrams, are considered, the predicted amplitude might differ greatly between the two runs. This result affirms that only the general pattern of the ray-tracing results is meaningful and that comparisons of predicted amplitudes with observed ones are tenuous, especially near caustics.

CONCLUSIONS

Application of a dispersion correction to M_s measured visually from seismic Rayleigh waves failed in general to reduce the scatter in M_s over a network observing an event. This result indicated that the dispersion factor in the theoretical prediction of amplitude in actuality has small variance relative to the combined effect of variance in other factors, such as attenuation, crustal structure, transmission losses at boundaries or focussing and defocussing. Also a review of our measurements indicated that the dispersion factor cannot be accurately estimated from recordings, especially when intefering noise is present. We therefore conclude that the dispersion correction is not useful in routine seismological estimates of magnitude. It does not seem that one could justify the additional amount of work required in estimating M_s with this correction. This conclusion essentially echoes that of Filson (1975). We would prefer to establish station corrections empirically for events in given areas; such corrections would include the elusive dispersion correction as well as all the other corrections which together seem to dominate the dispersion one. Calculating spectra is certainly the preferred method for removing the dispersion effect.

Results from the ray-tracing model were somewhat encouraging. Although we did not cast the predicted ray-tracing intensities into the form of an M_s correction, the positive correlation found for most of the cases studied between predicted and observed amplitudes indicates that reductions in M_s scatter would be achieved and would be significant in some cases.

The ray-tracing program predicted some, but not all, of the paths for 20-second LR observed at LASA. It may therefore be a good tool for predicting or verifying propagation off the back azimuth or multipath propagation in surface-wave studies where solely great-circle propagation is required for accurate group-velocity or phase-velocity measurements or for attenuation measurements. Ray-tracing for the entire globe shows that deviations from great circle paths and multipath problems should increase with distance from the epicenter, such that at 20-seconds' period for large epicentral distances should be used with caution in any study. Ray tracing may be useful in

explaining peculiar signal properties which do not apparently arise from the structure along the great circle path when it confirms that the signals do not truly follow this path. Better match filters and better beamforming could be achieved by study of ray-tracing paths. One use of the present program would be to find stations where pertubations in the phase velocities along the raypath lead to small pertubations in M_s. These stations would then be used preferentially for yield estimation.

Surface-wave ray tracing will have a number of important applications besides for M_s correction; however, a formidable task will be the completion of global velocity grids for periods other than 20 seconds. As discussed in this report, extension to other periods will involve structure which we, at present, know generally less about than that required for creating the 20-second velocity grid.

Except for the analysis of spectral data from NTS and ATS shots as seen at NP-NT, we have not in this report combined the dispersion and ray-tracing corrections on a common data set. Since results in both cases were poor, we do not expect that combination of the two corrections would be dramatically better. In order to provide good amplitude predictions for Rayleigh waves, we believe that variations in Q must be mapped and incorporated into the ray-tracing scheme, that the velocity grid be refined, and that transmission losses at high velocity gradients be calculated. At present, there is insufficient detailed knowledge of Q for Rayleigh waves; and, given the sparse coverage of seismic stations over the globe, it is unfeasible to acquire this knowledge. Concerning transmission losses at boundaries, for any angle of incidence other than normal, the calculations can only be done with three-dimensional numerical models which are just now being developed.

REFERENCES

Bath, M., 1969, Mathematical Aspects of Seismology, Elsevier Publ. Co., New York.

Ben-Menahem, A. and D. G. Harkrider, 1964, Radiation patterns of seismic surface waves from buried dipolar point sources in a flat statified earth, J. Geophys. Res., v. 69, p. 2605-2620.

Brune, J. N., J. E. Nafe, and J. E. Oliver, 1960, A simplified method for the analysis and synthesis of dispersed wave trains, J. Geophys. Res., v. 56, p. 287-304.

Capon, J., 1970, Analysis of Rayleigh-wave multipath propagation of LASA, Bull. Seism. Soc. Am., v. 60, p. 1701-1731.

Christensen, N. I. and M. H. Salisbury, 1975, Structure and composition of the lower oceanic crust, Rev. Geophys. Space Physics, v. 13, p. 57-86.

Davies, D. and B. R. Julian, 1972, A study of short-period P-wave signals from LONGSHOT, Geophys. J. R. Astr. Soc., v. 29, p. 185-202.

Davis, P. J. and I. Polonsky, 1964, Numerical interpolation, differentiation, and integration, in Handbook of Mathematical Functions, edited by M. Abramowitz and I. A. Stegun, National Bureau of Standards, United States Department of Commerce.

Dietz, R. S. and J. C. Holden, 1970, Reconstruction of Pangaea: Breakup and dispersion of continents, Permian to Present, J. Geophys. Res., v. 75, p. 4939-4956.

Engdahl, E. R., 1973, Relocation of intermediate depth earthquakes in the Central Aleutians by seismic ray tracing, Nature, v. 245, p. 23-25.

Engdhal, E. R., 1975, Effects of plate structure on earthquake focal mechanism determinations, Geophys. J. R. Astr. Soc., in press.

Evernden, J. F., 1953, Direction of approach of Rayleigh waves and related problems, Part I, Bull. Seism. Soc. Am., v. 43, p. 225-274.

Evernden, J. F., 1954, Direction of approach of Rayleigh waves and related problems, Part II, Bull. Seism. Soc. Am., v. 44, p. 159-184.

Filson, J., 1975, Test of the empirical surface wave magnitude path correction, Semiannual Technical Summary-Seismic Discrimination, Lincoln Laboratory, Lexington, Massachusetts.

Gjevik, B., 1974, Ray tracing for seismic surface waves, Geophys. J. R. Astr. Soc., v. 39, p. 27-39.

Grosvenor, M. B. and J. M. Darley, 1963, National Geographic Atlas of the World, National Geographic Society, Washington, D. C.

Gutenberg, B., 1945, Amplitudes of surface waves and magnitudes of shallow earthquakes, Bull. Seism. Soc. Am., v. 35, p. 3-12.

Harkrider, D. G. and D. L. Anderson, 1966, Surface-wave energy from point sources in plane layered earth models, J. Geophys. Res., v. 71, p. 2967-2980.

Isacks, B. and P. Molnar, 1971, Distribution of stresses in the descending lithosphere from a global survey of focal-mechanism solutions of mantle earthquakes, Reviews of Geophysics and Space Physics, v. 9, p. 103-174.

Jacobs, K. H., 1970, Three-dimensional seismic ray tracing in a laterally heterogeneous spherical earth, J. Geophys. Res., v. 75, p. 6675-6689.

Julian, B. R., 1970, Ray tracing in arbitrarily heterogeneous media, Technical Note 1970-45, Lincoln Laboratory, Lexington, Massachusetts.

Landisman, M., A. Dziewonski, and Y. Sato, 1969, Recent improvements in the analysis of surface wave observations, Geophys. J. R. Astr. Soc., v. 17, p. 369-403.

McGarr, A., 1969, Amplitude variations of Rayleigh waves--horizontal refractions, Bull. Seism. Soc. Am., v. 59, p. 1307-1334.

Officer, C. B., 1974, Introduction to Theoretical Geophysics, Springer-Verlag, New York, New York.

Richards, P. G., 1973, Calculation of body waves for caustics and tunnelling core phases, Geophys. J. R. Astr. Soc., v. 35, p. 243-264.

Ringdal, F., 1975, Maximum likelihood estimation at seismic event magnitude from network data, Technical Report No. 1, VELA Network Evaluation and Automatic Processing Research, Texas Instruments, Inc., Dallas, Texas.

Sata, R., 1967. Attenuation of seismic waves, J. Physics Earth, v. 15, p. 32-61.

Sato, R., 1969, Amplitude of body waves in a heterogeneous sphere: comparison of wave theory and ray theory, Geophys. J. R. Astr. Soc. v. 17, p. 527-544.

Sorrells, G. G., J. B. Crowley, and K. F. Veith, 1971, Methods for computing ray paths in complex geological structures, Bull. Seism. Soc. Am., v. 61, p. 27-54.

Stauder, W., 1968, Mechanism of the Rat Island earthquake sequence of February 4, 1965, with relation to island arcs and sea-floor spreading, J. Geophys. Res., v. 73, p. 3847-3858.

Talwani, M., T. L. Worzel, and M. Ewing, 1961, Gravity anomalies and crustal section across the Tonga Trench, J. Geophys. Res., v. 66, p. 1265-1278.

von Seggern, D. H., 1970, Surface-wave amplitude-versus-distance relation in the Western United States, SDL Report No. 249, Teledyne Geotech, Alexandria, Virginia.

von Seggern, D. H., 1971, Effects of propagation paths on surface-wave magnitude estimates, SDL Report No. 279, Teledyne Geotech, Alexandria, Virginia.

von Seggern, D. H., 1975a, Q for 20-second Rayleigh waves from complete great-circle paths, Report No. SDAC-TR-75-3, Teledyne Geotech, Alexandria, Virginia.

von Seggern, D. H., 1975b, Distance-amplitude relationships for long-period P, S, and LR from measurements on recordings of the long-period experimental stations, SDCS-TR-75-14, Teledyne Geotech, Alexandria, Virginia.

Weidner, D. H., 1974, Rayleigh wave phase velocities in the Atlantic Ocean, Geophys. J. R. Astr. Soc., v. 36, p. 105-139.

Woodhouse, J. H., 1974, Surface waves in a laterally varying layered structure, Geophys. J. R. Astr. Soc., v. 37, p. 461-490.

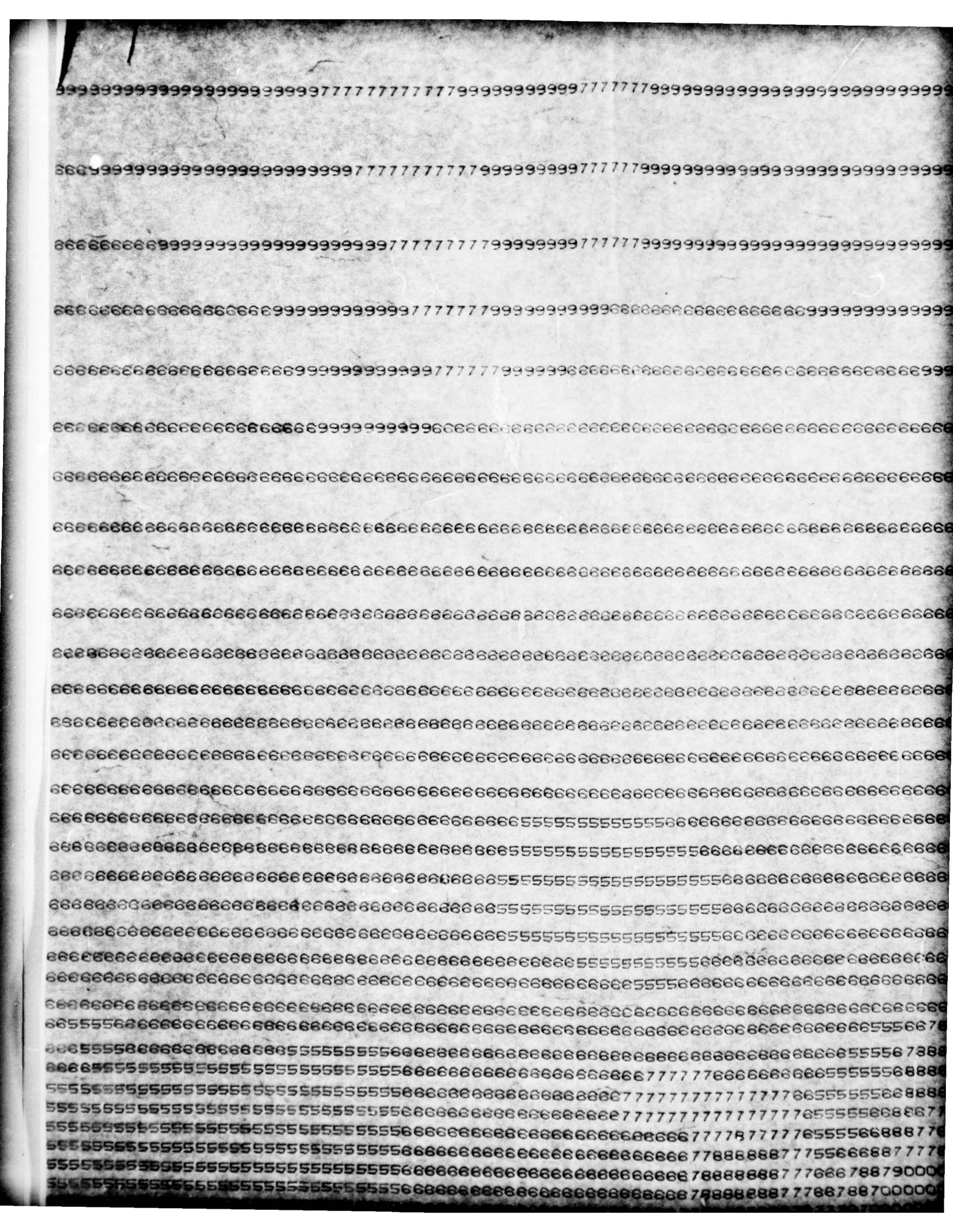

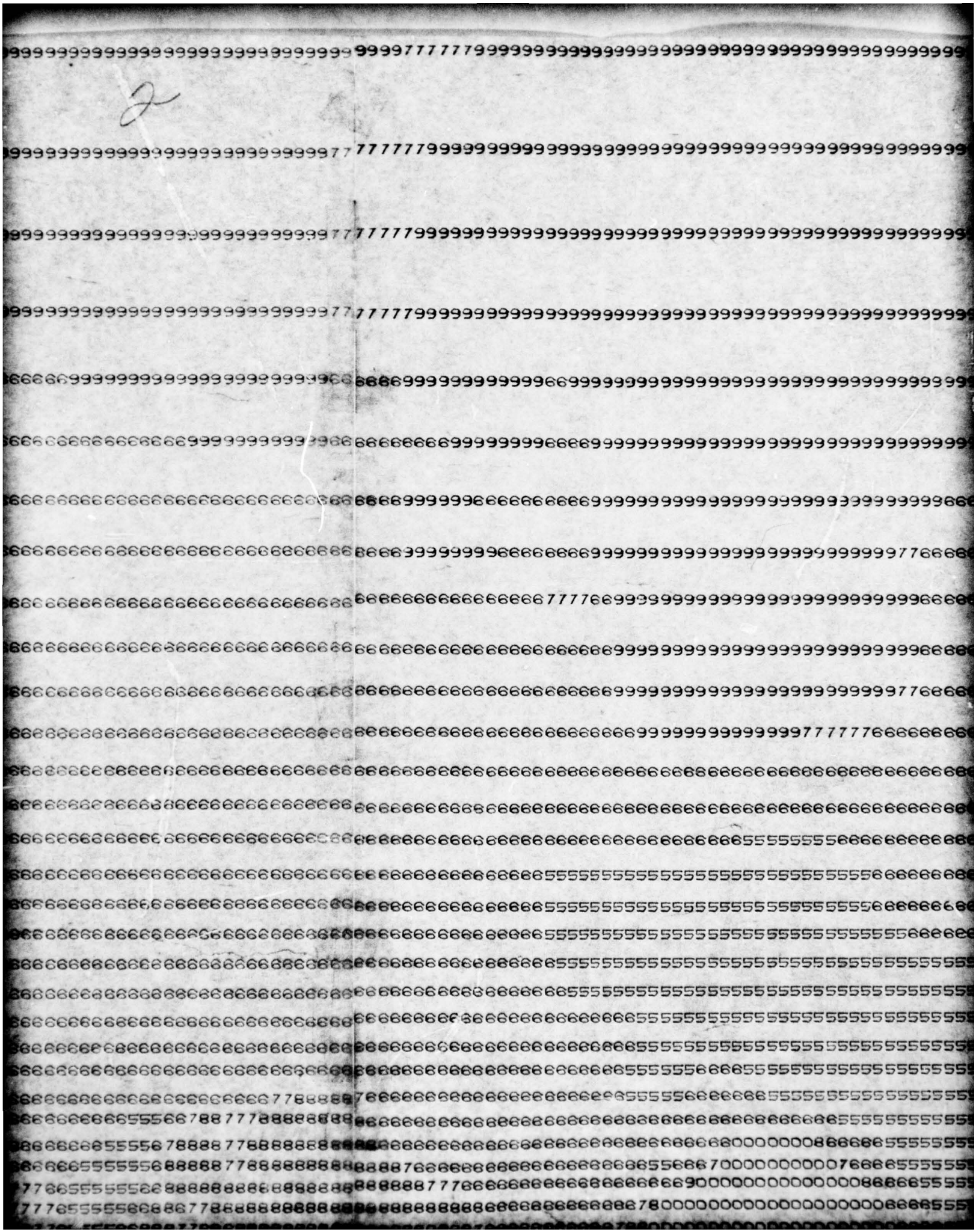

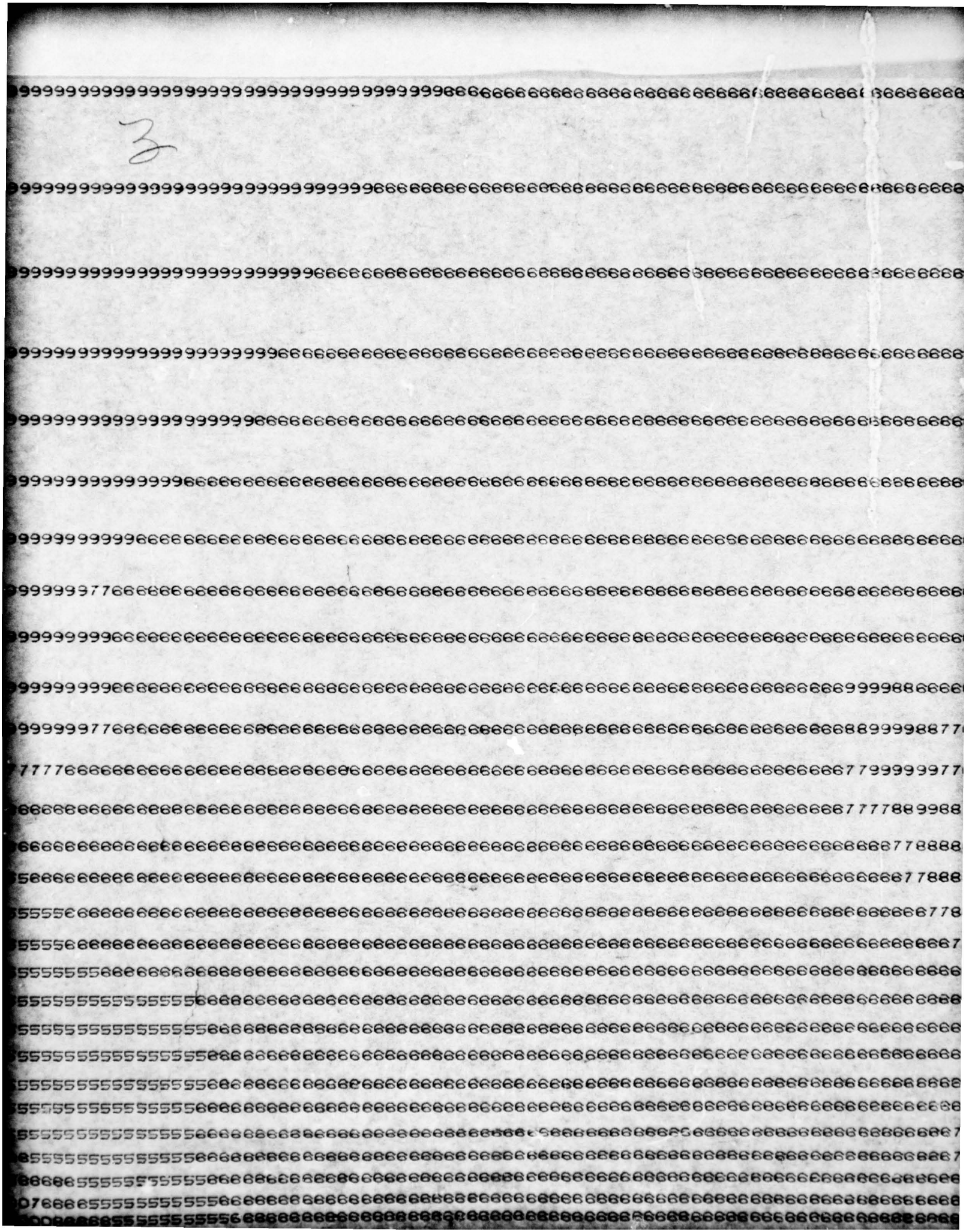

AD-A032 074 TELEDYNE GEOTECH ALEXANDRIA VA SEISMIC DATA ANALYSIS--ETC F/G 8/11
EXPERIMENTS IN REFINING SEISMIC MAGNITUDE ESTIMATES FOR SEISMIC--ETC(U)
NOV 75 D H VON SEGGERN, P A SOBEL, D W RIVERS F08606-76-C-0004

UNCLASSIFIED SDAC-TR-75-17 NL

2 OF 2
ADA032074

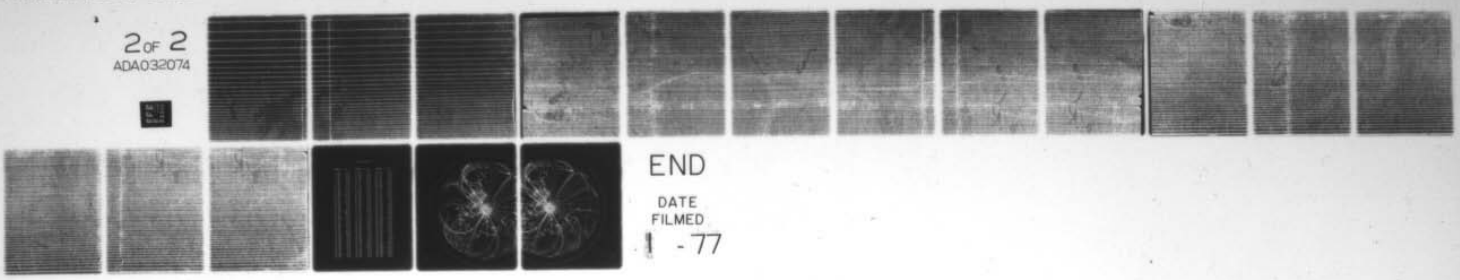

END

DATE
FILMED
1 -77

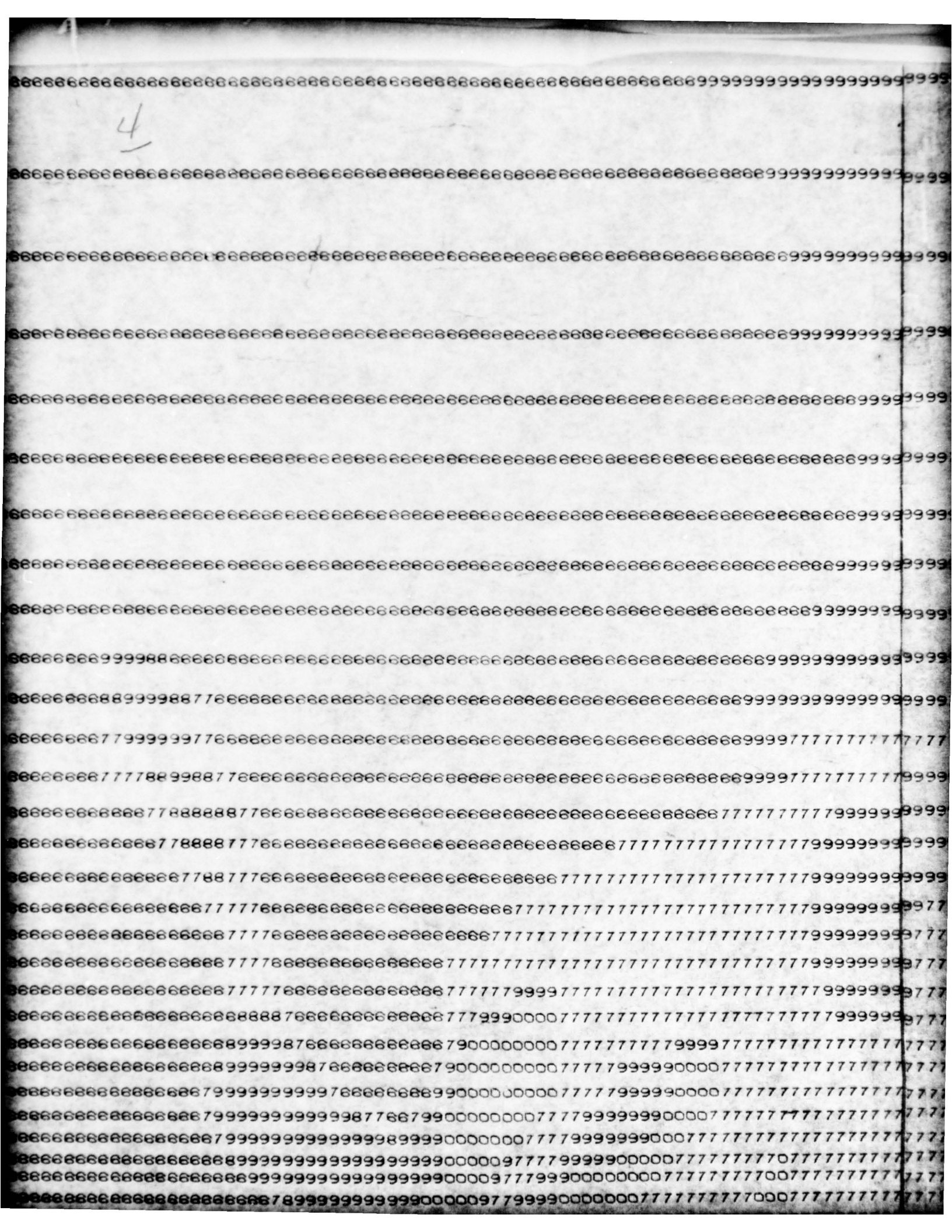

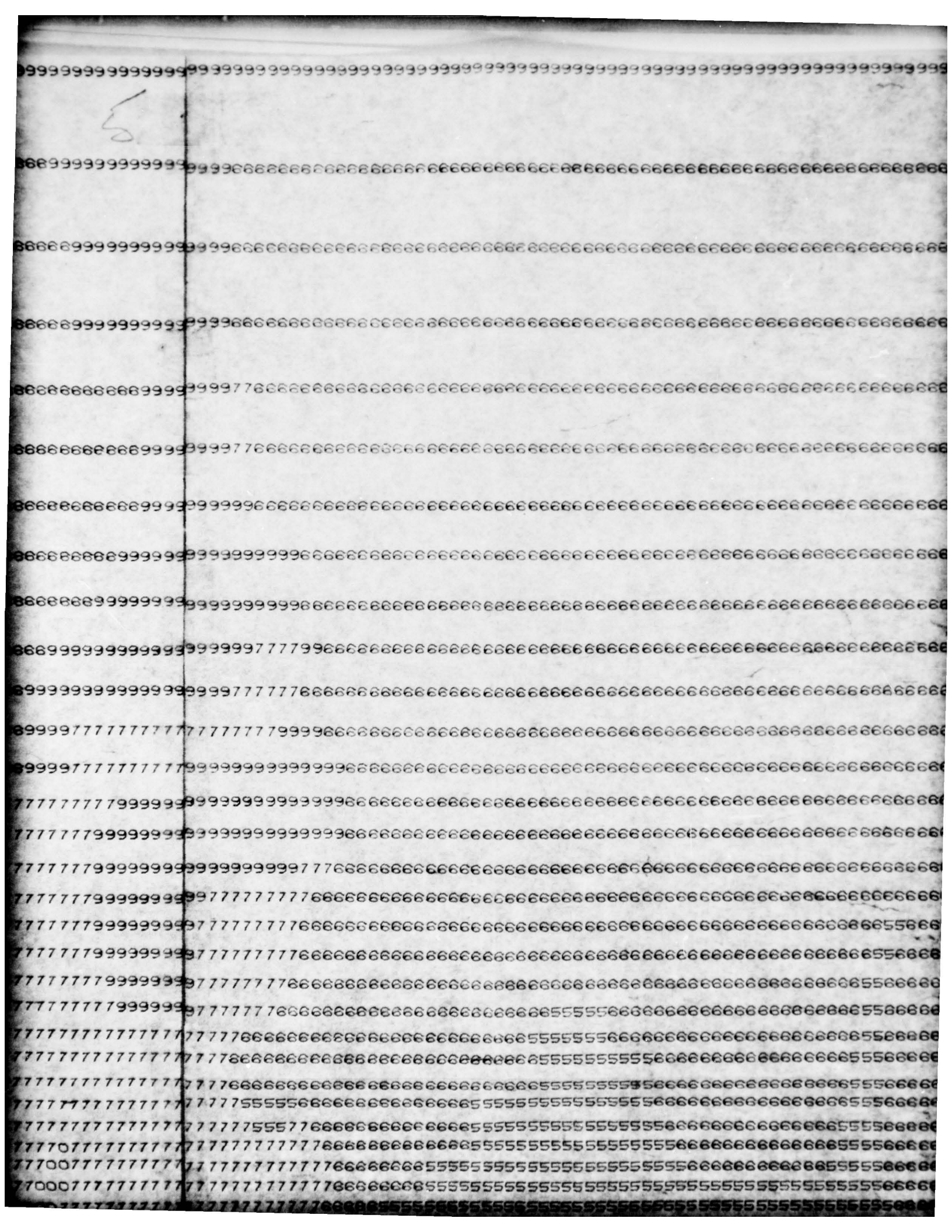

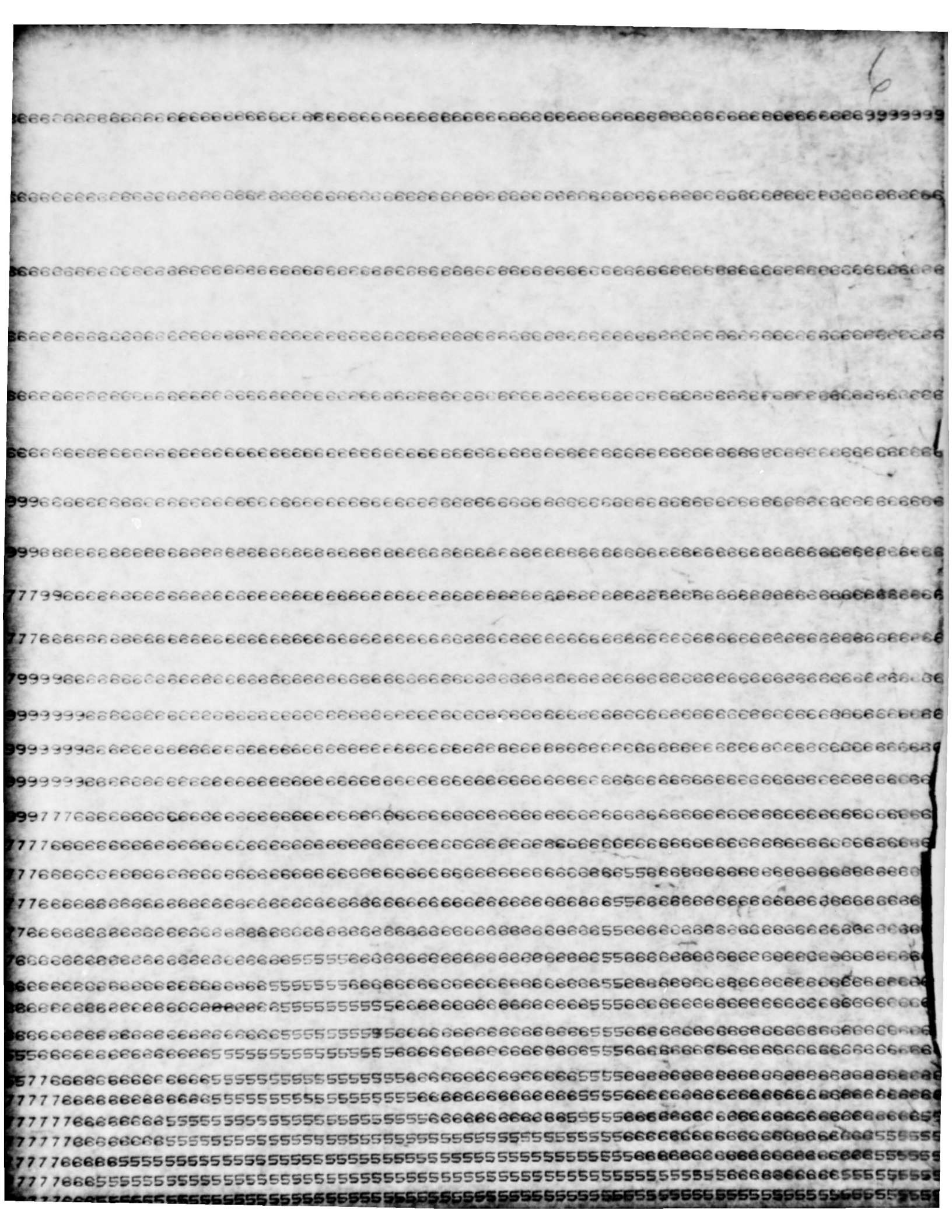

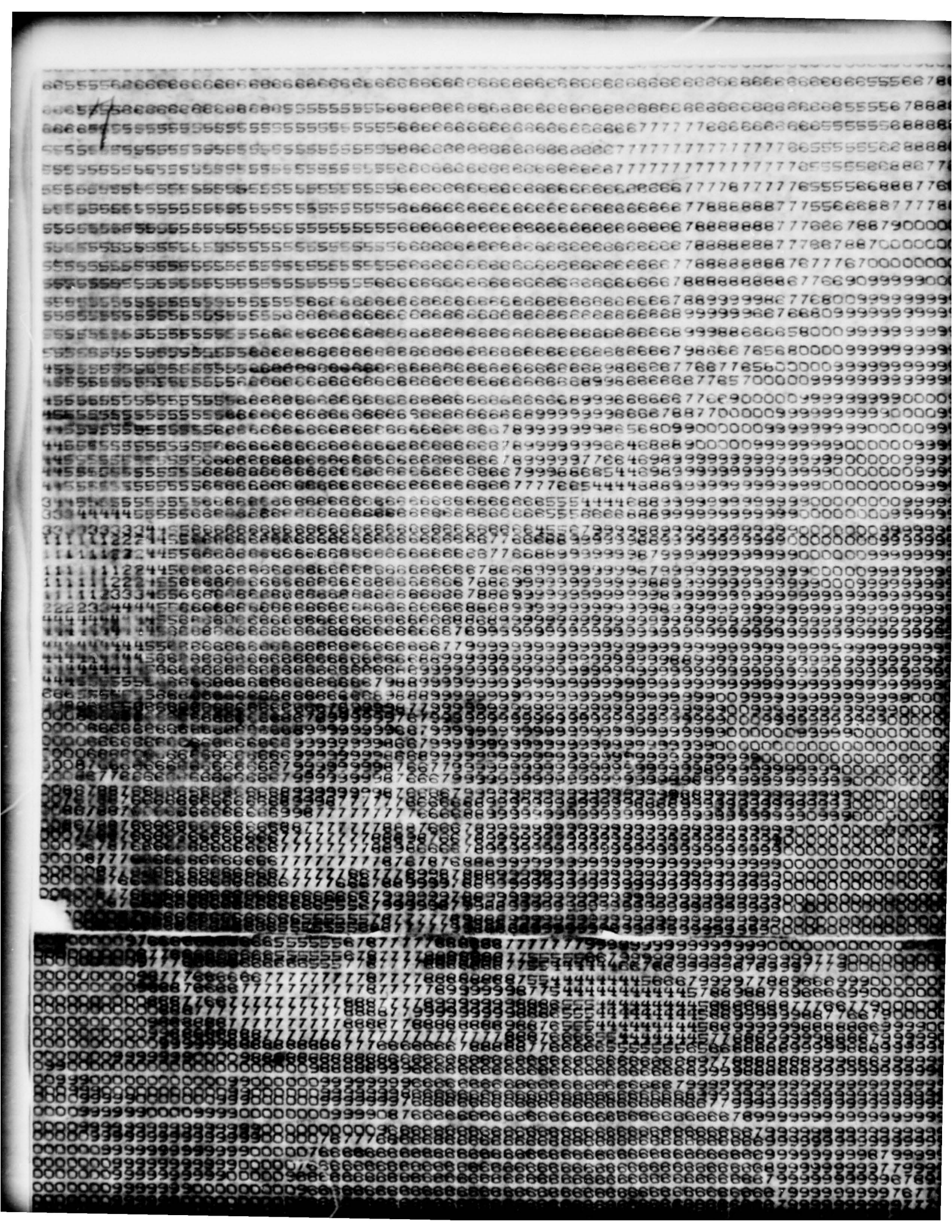

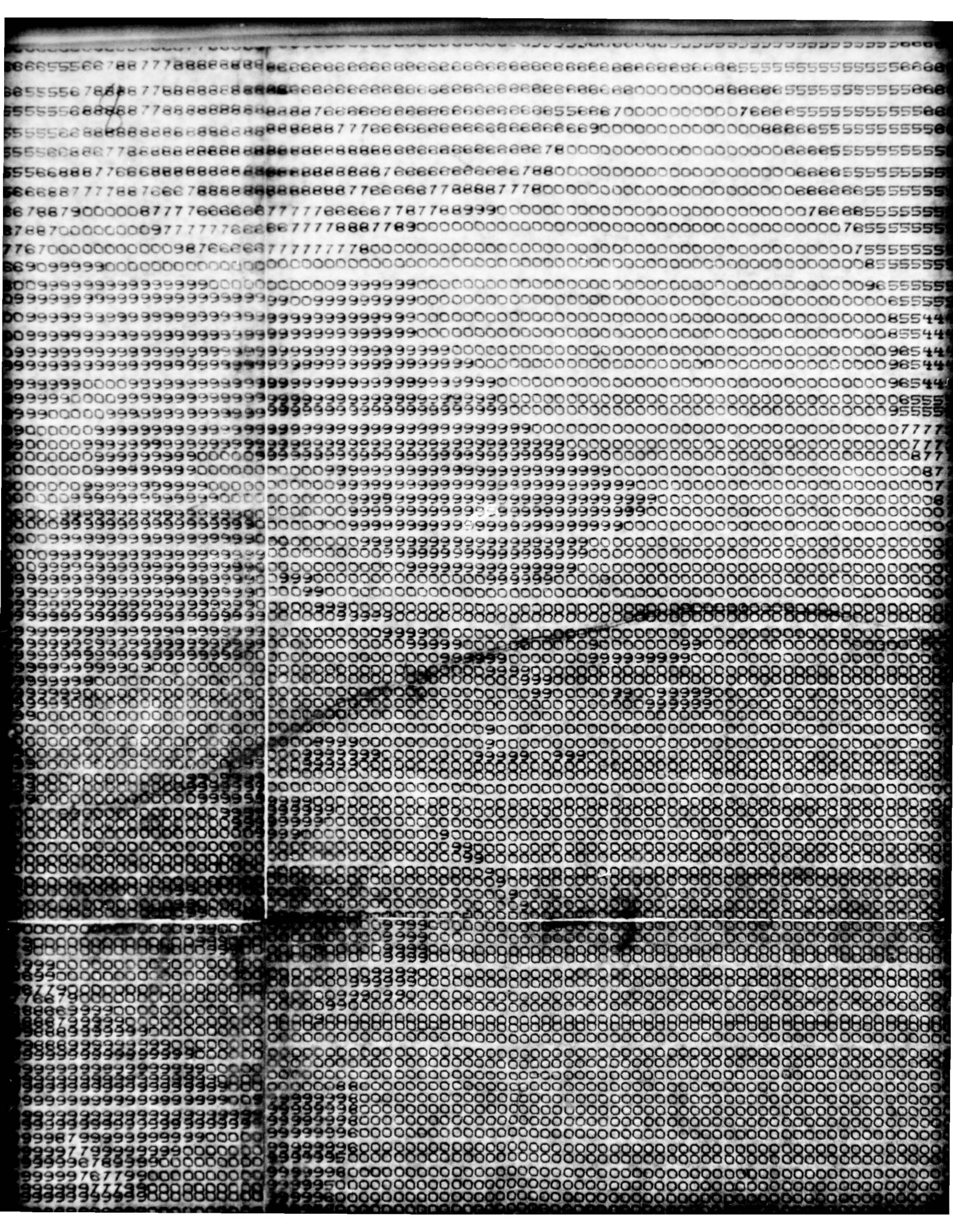

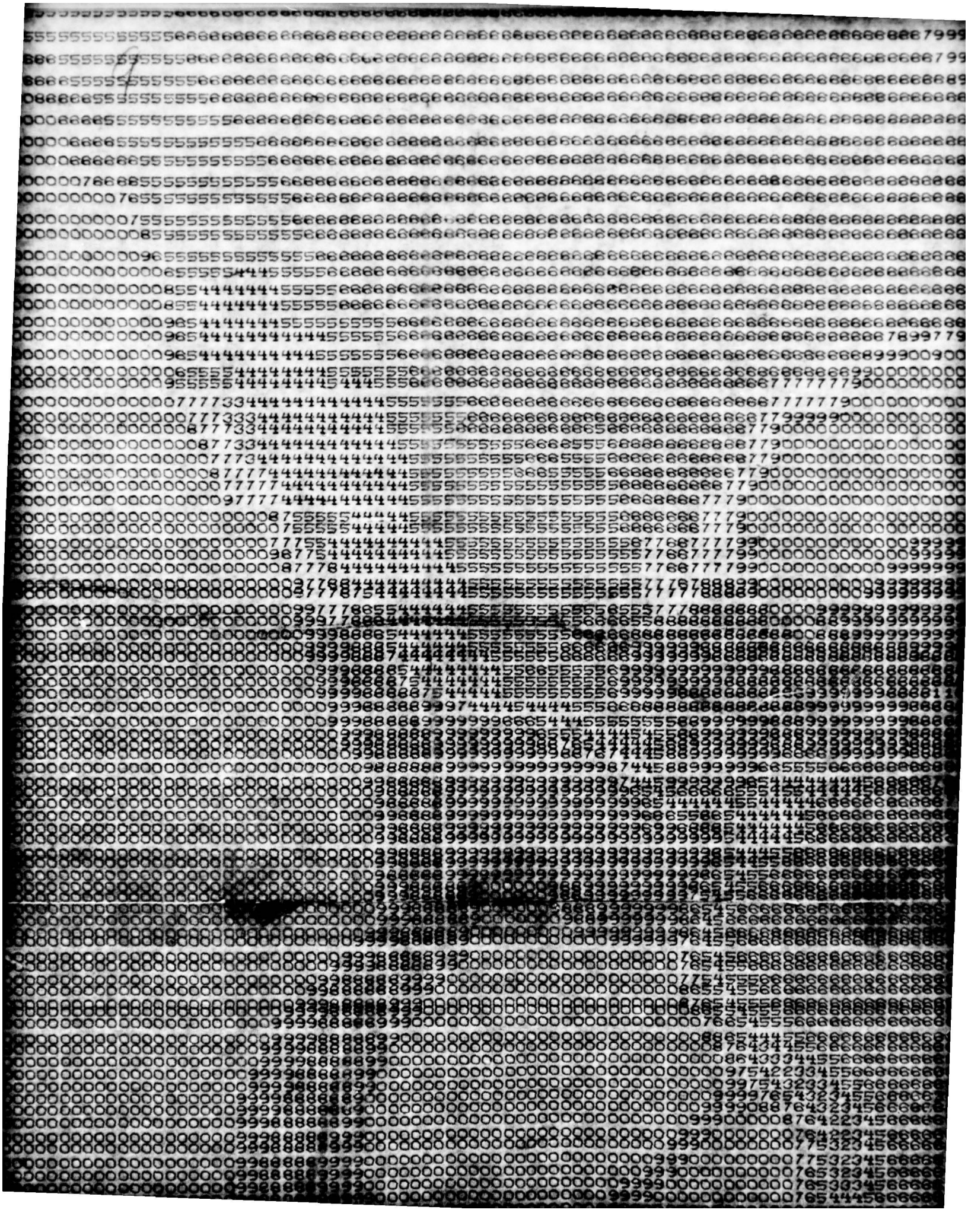

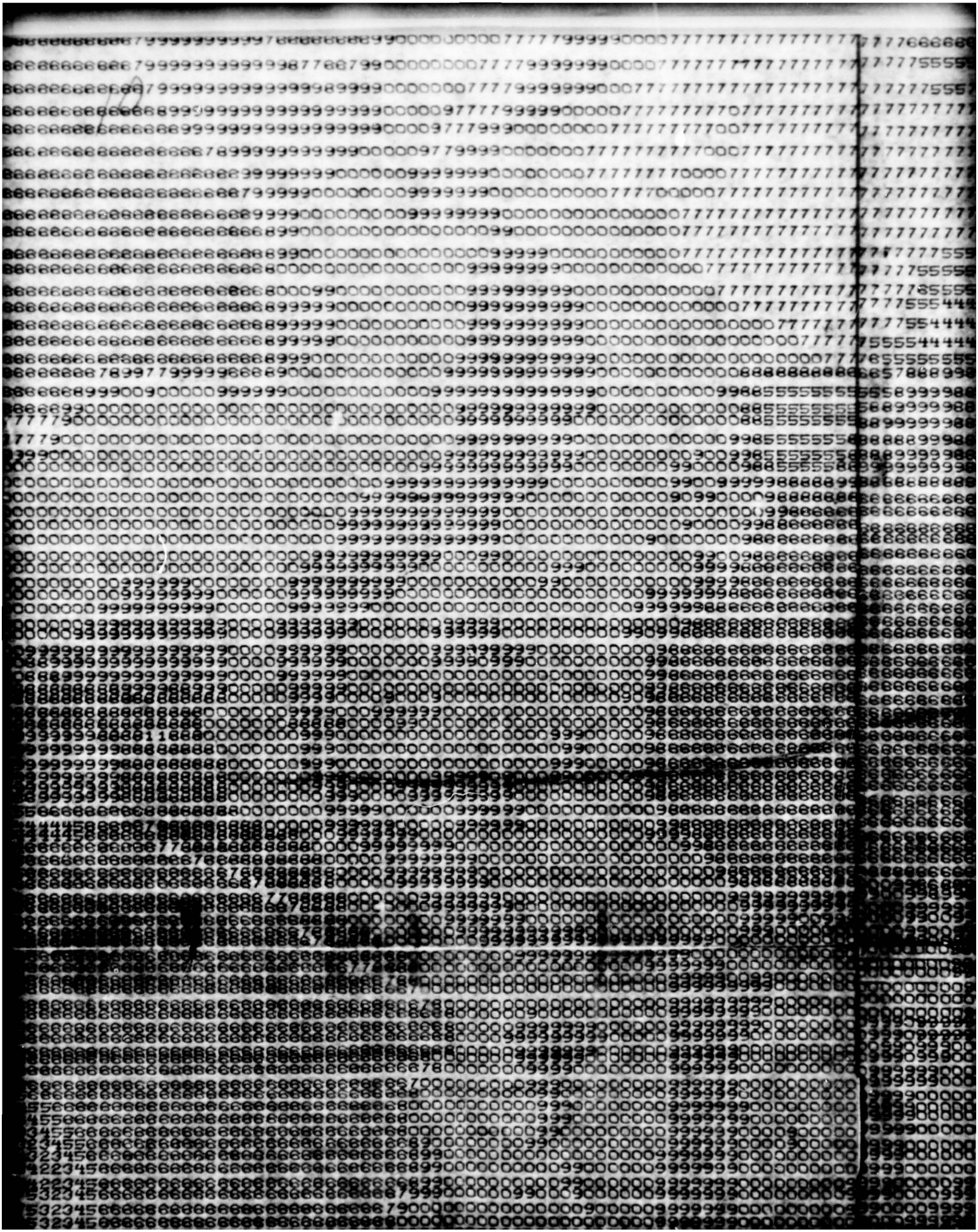

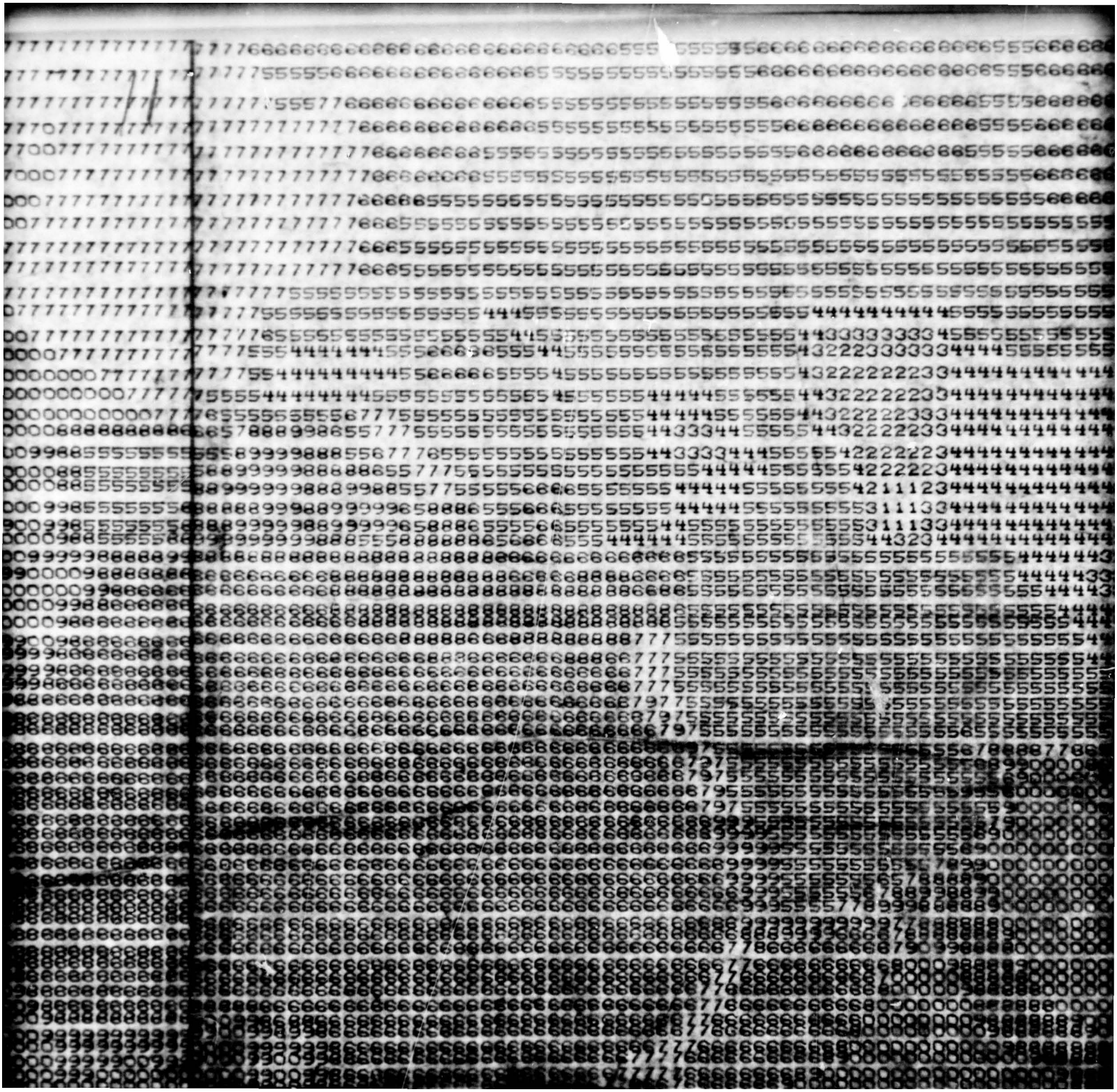

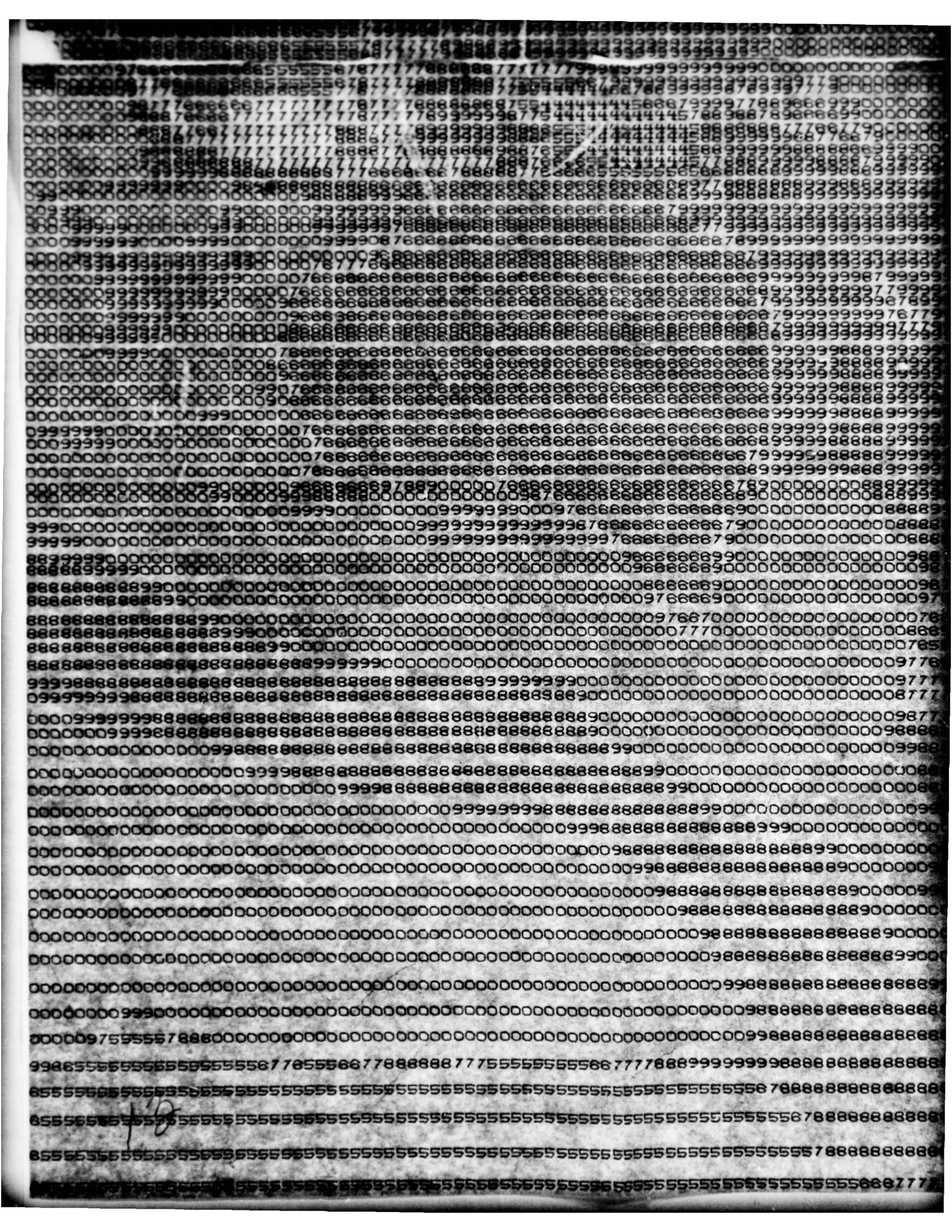

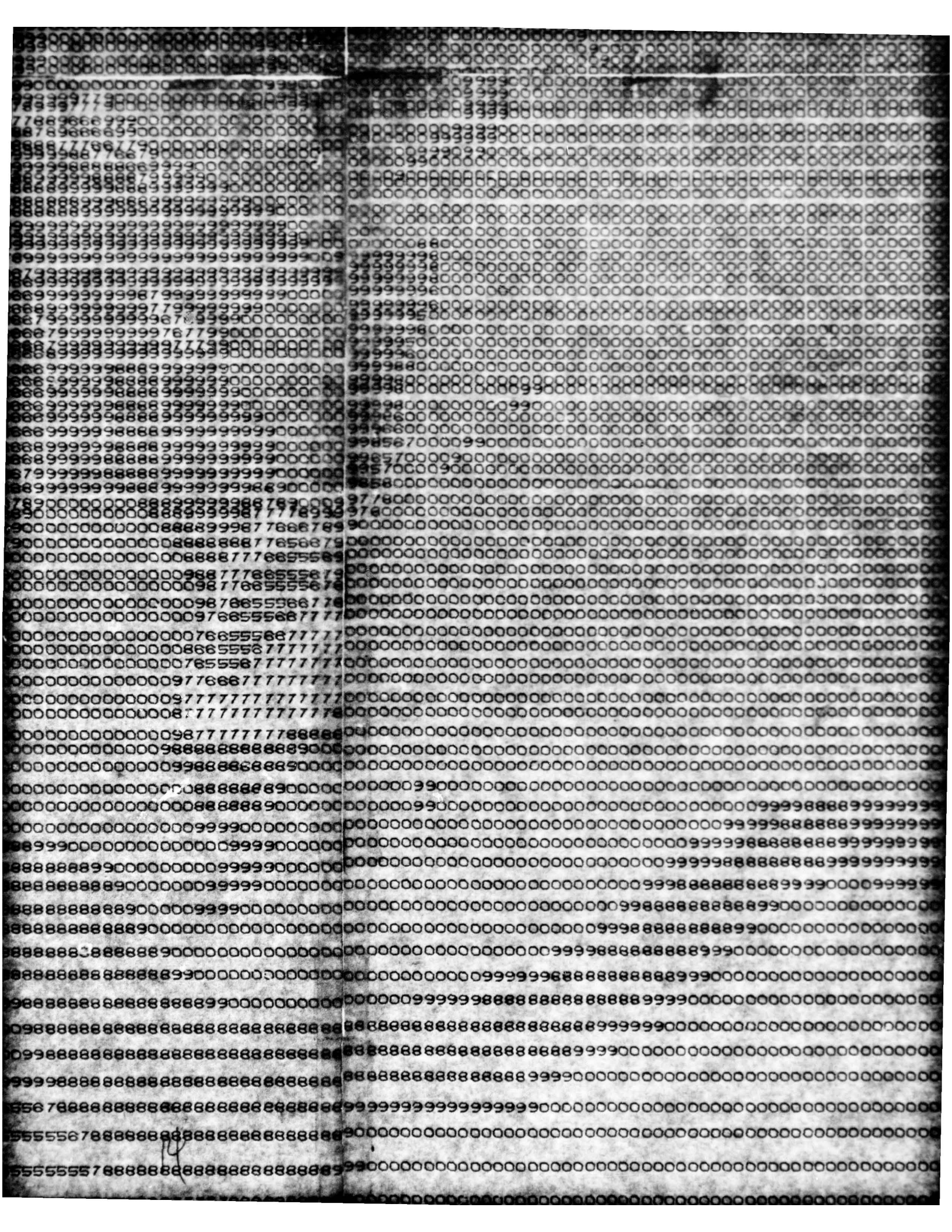

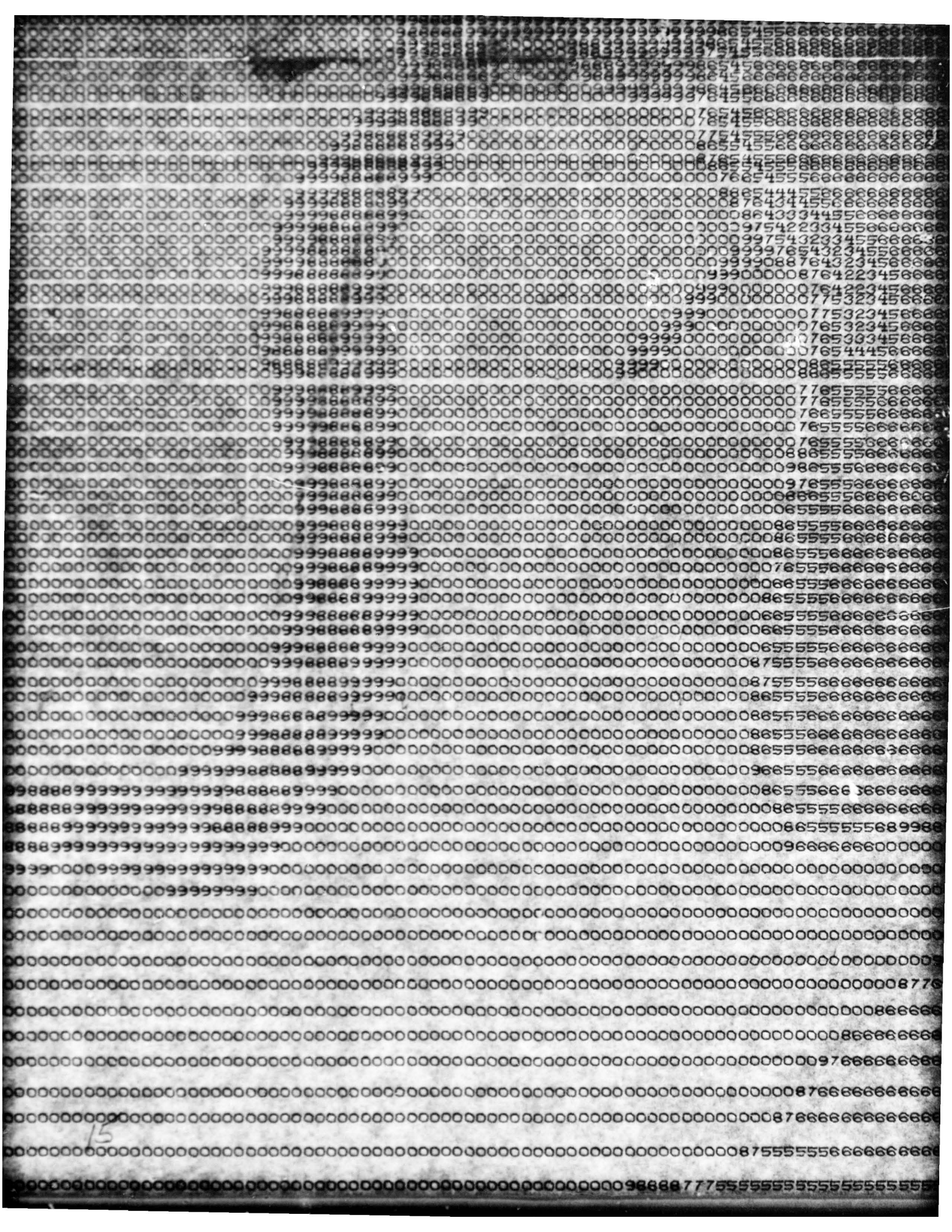

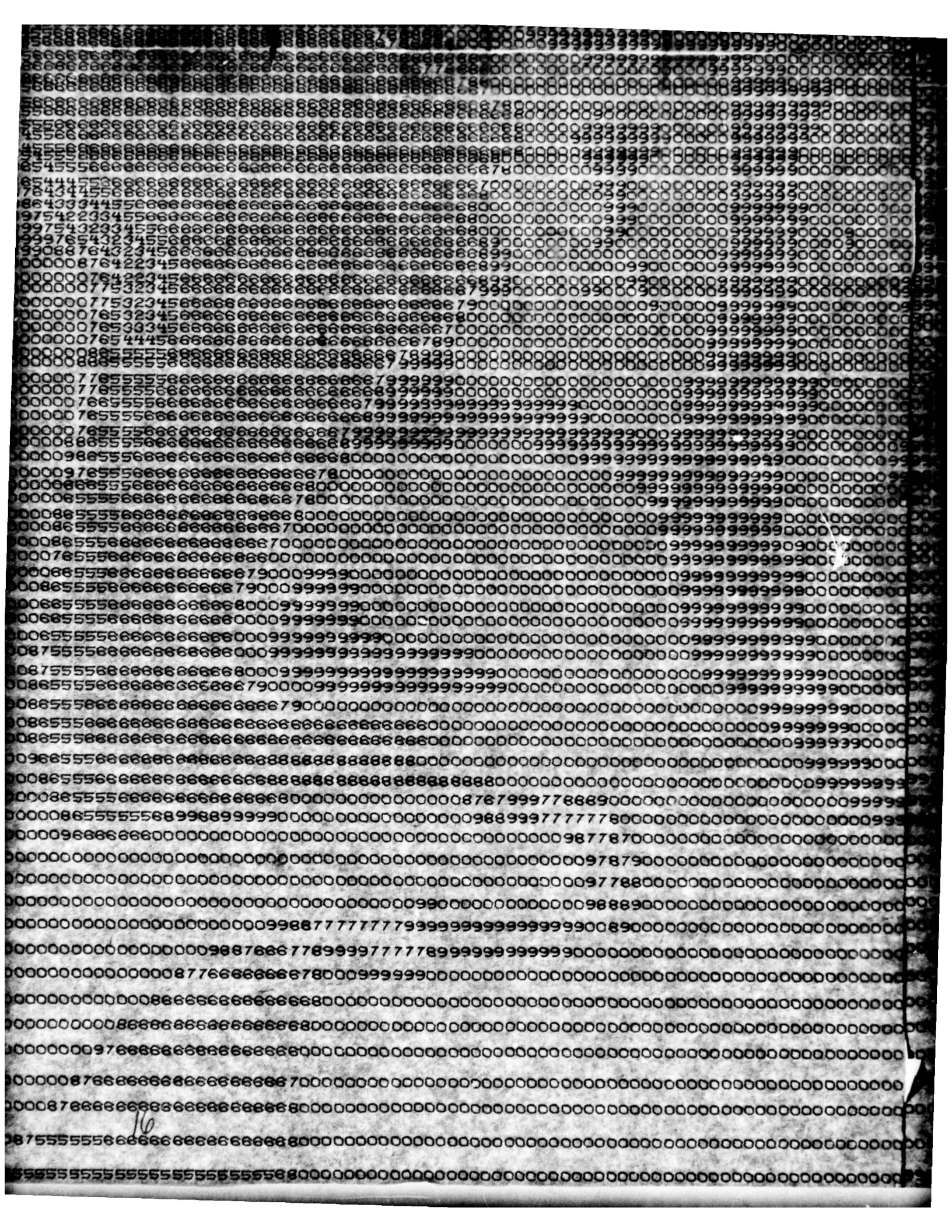

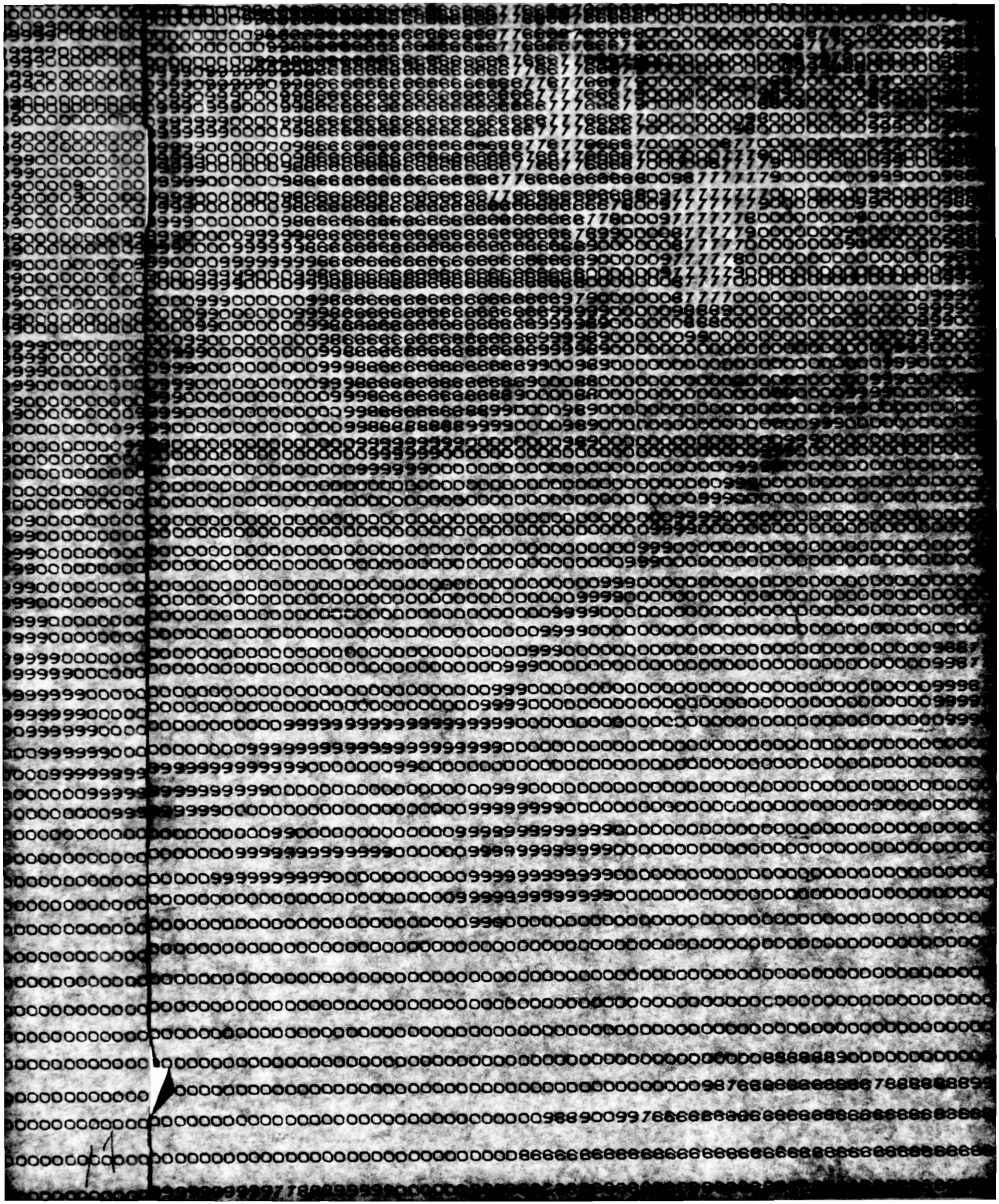

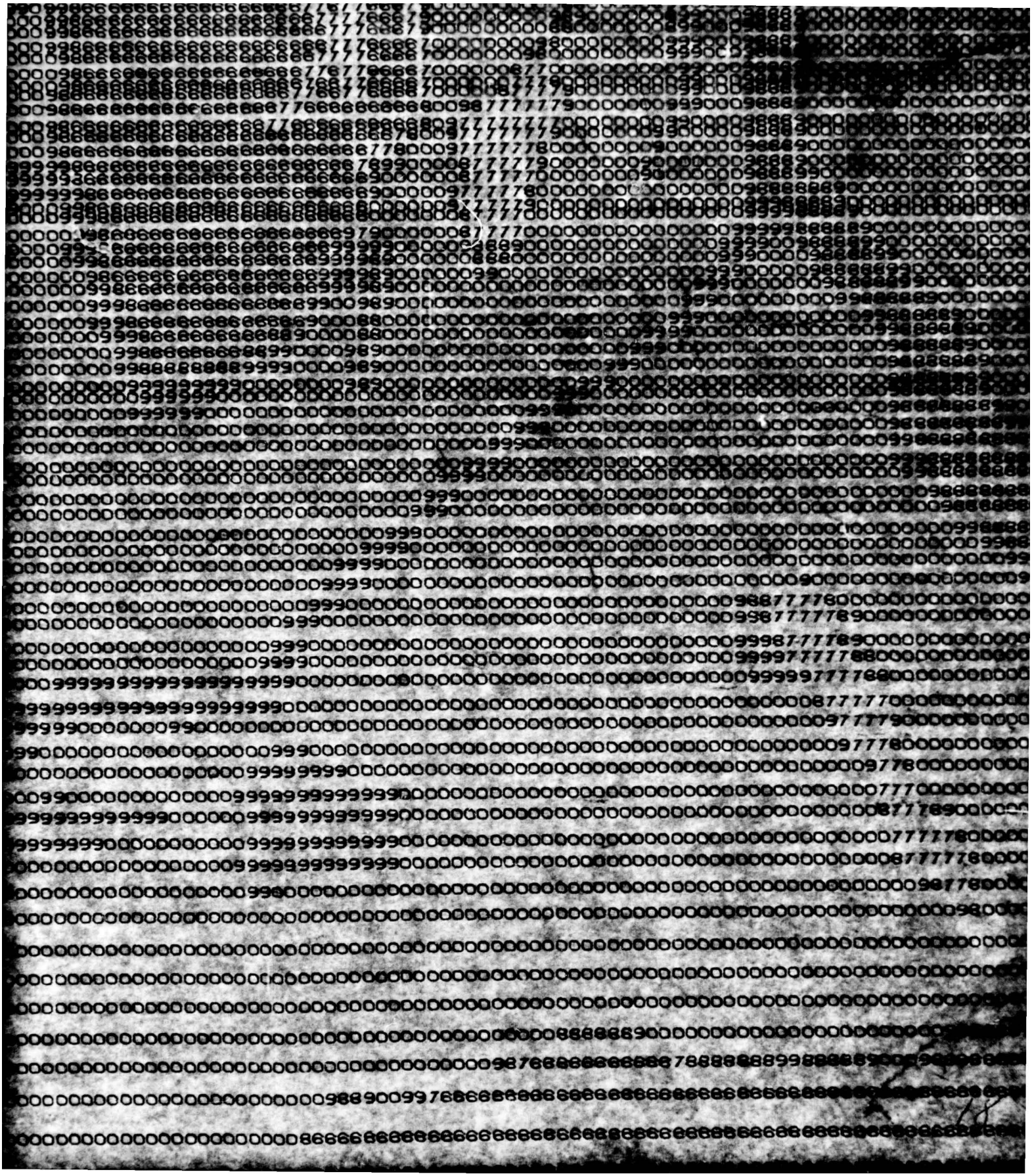

Legend for Figure 5

STATION		A_o	STATION		A_o	STATION		A_o
1	AAE	9.43	51	HLID	34.29	101	PRE	5.22
2	AAM	38.27	52	HLW	3.37	102	PTO	14.79
3	ADE	37.42	53	HNME	111.91	103	QUE	30.19
4	AFI	23.98	54	HNR	55.51	104	QUI	3.36
5	AKU	53.76	55	HVMA	38.93	105	RAB	15.44
6	ALQ	17.00	56	INK	51.77	106	RES	45.16
7	ANP	25.49	57	IST	20.26	107	RGSD	39.42
8	AQU	5.76	58	JCT	61.59	108	RIV	10.14
9	ATL	21.79	59	JER	12.81	109	RKON	49.70
10	ATU	15.34	60	JPAT	107.12	110	SBA	5.09
11	BEC	19.23	61	KBL	6.65	111	SCB	33.18
12	BEFL	36.24	62	KBS	30.61	112	SCH	124.10
13	BHP	1.62	63	KCMO	31.14	113	SCP	80.37
14	BHYK	162.96	64	KEV	9.42	114	SDB	14.55
15	BKS	15.50	65	KIP	14.55	115	SFA	126.75
16	BLA	36.17	66	KJN	30.42	116	SHA	13.17
17	BLC	221.78	67	KNUT	20.18	117	SHI	28.05
18	BMO	40.06	68	KOD	4.43	118	SHK	6.35
19	BOG	36.21	69	KON	6.22	119	SHL	5.47
20	BUL	4.60	70	LCNM	13.59	120	SIBC	50.22
21	CAR	12.68	71	LEM	3.73	121	SJG	13.49
22	CHG	3.02	72	LHC	44.36	122	SJTX	54.06
23	CHMT	300.73	73	LON	21.58	123	SLM	9.46
24	CMC	109.43	74	LOR	47.54	124	SNG	49.11
25	COL	162.76	75	LPA	5.43	125	STJ	176.66
26	COR	54.32	76	LPB	3.04	126	STU	5.78
27	CPCL	29.27	77	LPS	3.56	127	SVQB	413.85
28	CRNB	139.96	78	LUB	13.95	128	SWMA	44.90
29	CTA	15.39	79	LZBV	11.54	129	TAB	27.74
30	DAL	37.07	80	MAL	12.95	130	TAU	14.20
31	DAV	26.38	81	MAT	48.27	131	TEGL	50.86
32	DHNY	227.34	82	MBC	36.57	132	TFCL	28.32
33	DUG	32.51	83	MNNV	21.14	133	TFO	38.95
34	ESK	9.52	84	MSH	14.97	134	TOL	10.47
35	FBC	54.24	85	MUN	6.77	135	TRI	11.11
36	FCC	169.93	86	NAI	5.89	136	TRN	106.37
37	FFC	24.60	87	NAT	13.42	137	TUC	6.09
38	FLBC	88.87	88	NDI	8.50	138	UME	16.35
39	FLO	8.27	89	NNA	2.83	139	VAL	24.24
40	FNWV	35.01	90	NOR	28.83	140	VIC	19.86
41	FSJ	19.10	91	NPNT	92.03	141	WEL	39.71
42	GDH	8.21	92	NUR	35.84	142	WES	95.34
43	GEO	68.52	93	OGD	105.63	143	WHYK	598.77
44	GOL	50.29	94	OTT	209.92	144	WIN	9.33
45	GRM	12.10	95	OXF	12.70	145	WLYK	1189.76
46	GSC	7.51	96	PDA	22.11	146	WMO	27.40
47	GUA	21.37	97	PGBC	32.09	147	WNSD	66.62
48	GVTX	35.85	98	PMG	22.93	148	WSAT	207.24
49	GWC	259.68	99	PNT	11.88	149	YKC	656.50
50	HKC	5.49	100	POO	24.40	150	YRCL	72.22